INVESTIGATION OF THE PROTEIN-PROTEIN AND PROTEIN-LIPID INTERACTIONS OF IPAB FROM *SHIGELLA FLEXNERI*

By

PHILIP ROBERT ADAM

Bachelor of Science in Microbiology
University of Kansas
Lawrence, KS
2009

Submitted to the Faculty of the
Graduate College of the
Oklahoma State University
in partial fulfillment of
the requirements for
the Degree of
DOCTOR OF PHILOSOPHY
May, 2014

INVESTIGATION OF THE PROTEIN-PROTEIN AND PROTEIN-LIPID INTERACTIONS OF IPAB FROM *SHIGELLA FLEXNERI*

Dissertation Approved:

Dr. William Picking

Dissertation Adviser

Dr. Wendy Picking

Dr. Edward Shaw

Dr. Marianna Patrauchan

Dr. Josh Ramsey

ACKNOWLEDGEMENTS

I would first like to thank my research mentors, Dr.'s William and Wendy Picking. Their passion for research sparked my own interest while I was an undergraduate at the University of Kansas. I am forever grateful for their constant support, constructive criticism, grant writing, and especially for forcing me to give talks at conferences. The Pickings pushed me to achieve more than I ever thought was possible, and for that I am thankful.

The people that mentored me throughout my early research career deserve recognition. Christina Wiens and Nathan Smith taught me all of the basic techniques in the lab. I also want to thank Dr. Nick Dickenson for humoring my questions about biophysics and quantum mechanics. Nick was my "in-lab" mentor for many years and helped me become a better scientist. Dr. Chelsea Epler and I worked together for six years, and remains one of my closest friends.

I want to thank the current students in the lab including: Kelly Harrison, Kirk Pendleton, Joshua Encinas, Shyamal Choudhari, Xiaotong Chen, Olivia Arizmendi, and Dr. Francisco Martinez. Thank you for making the long days in the lab seem shorter, all of the laughs we shared, Margarita Thursdays, and for listening to me vent. Thank you for all that you have done for me. I will miss each of you tremendously.

Perhaps most importantly, I also want to thank the people who supported me behind the scenes. Thank you, dad, for always supporting me and encouraging me to do my best. Thank you for coming to visiting Amy and I often and for bringing us a trunk full of gluten-free foods so that Amy could eat a proper meal. You always made it possible for me to chase my dreams, and I will never forget that. Lastly, I want to thank my wife, Amy. She is the one who was most impacted by the long hours required in graduate school. Thank you for doing much more than your share of the work around the house so I could spend more time in the lab. I would not have made it through my prelims without your constant support and encouragement. Thank you for listening to my talks, my complaints, and asking questions about the "theme" of my presentation. I love you and our growing daughter, Arya (I'm going to be her favorite)!

Name: PHILIP ROBERT ADAM

Date of Degree: MAY, 2014

Title of Study: INVESTIGATION OF THE PROTEIN-PROTEIN AND PROTEIN-LIPID INTERACTIONS OF IPAB FROM SHIGELLA FLEXNERI

Major Field: MICROBIOLOGY AND MOLECULAR GENETICS

Abstract: *Shigella* spp. are a major cause of morbidity and mortality in the developing world, causing over 125 million cases of diarrhea annually. Like many Gram-negative pathogens, *Shigella* utilizes a type three secretion system (T3SS) to manipulate its environment. Invasion plasmid antigen B (IpaB) is a hydrophobic translocator protein of the *Shigella* T3SS that is responsible for forming pores in host cell membranes. A recently published crystal structure of the soluble N-terminal domain of IpaB was the first insight into the structure of IpaB and was used as the starting point of this work. We sought to characterize the nature of the interaction of IpaB with other proteins, with model phospholipid membranes, and with itself. In the *Shigella* cytoplasm, IpaB associates with a chaperone, IpgC. Co-expression of IpgC with IpaB is also required for recombinant protein production in *E. coli*. The soluble N-terminal domain of IpaB was used to study the thermodynamics, stoichiometry, and conformational changes that occur as a result of the IpaB-IpgC interaction. Using the N-terminal domain of IpaB overcame the complications encountered when using full-length IpaB, which requires detergents to remain soluble. Förster resonance energy transfer (FRET) was used to demonstrate a conformational change in the IpaB N-terminal domain upon binding to IpgC. The next phase of this work examined the interaction of IpaB with model phospholipid membranes. Fluorescence quenching with potassium iodide was used to probe how the environment of individual residues throughout the IpaB sequence was affected by membrane interaction. These studies revealed that regions outside of the hydrophobic domain are involved in pore formation. Limited proteolysis experiments helped to further determine what regions of IpaB are involved in membrane interaction and several truncated forms of IpaB were generated for recombinant protein expression. Among the most interesting findings was that the C-terminal 85 residues of IpaB are not required for pore formation, and actually may function to regulate pore formation. As a whole, this work was used to develop a model of IpaB's interaction with IpgC and with phospholipid membranes.

TABLE OF CONTENTS

Chapter Page

Chapter Page

LIST OF TABLES

Table Page

LIST OF FIGURES

Figure Page

CHAPTER I

BACKGROUND AND HISTORICAL REVIEW

Shigella species

Bacteria of the genus *Shigella* cause a severe disease in humans that, in the absence of supportive care, can lead to death. *Shigella* infections are spread via the fecal-oral route, usually by consuming contaminated water. Flies have an affinity for fecal matter and are known to land on human food, thus flies have been implicated in the spread of diarrheal disease.[1,2] A study by the Israel Defense Force found that population-control measures against the common housefly (*Musca domestica*) reduced the incidence of shigellosis by 85%.[1] In developing countries, infections with *Shigella* can quickly turn into outbreaks due to the absence of public sanitation and a lack of clean drinking water. Members of this genus are non-motile, Gram-negative bacilli. There are four species within the genus *Shigella*: *dysenteriae* (serogroup A), *flexneri* (serogroup B), *boydii* (serogroup C), and *sonnei* (serogroup D).[3] Serogroup A contains 15 serotypes, B contains 8 serotypes, C contains 19 serotypes, and D contains only one serotype.[3,4] *Shigella* has a remarkably low infectious dose of 10-200 organisms due to its acid-tolerance systems.[5] Once in the large intestine, *Shigella* crosses the epithelial cell barrier, evades the innate immune system

and induces its uptake into colonic epithelial cells from the basolateral side.[6] Once inside the epithelial cell the bacterium escapes its vacuole, begins to multiply and spreads directly to neighboring epithelial cells without entering the extracellular environment.[7] Symptoms occur as a result of inflammation at the site of infection and include fever, severe abdominal cramping, and watery diarrhea.[8] Within two days, the patient will develop bright-red bloody, mucus-laden low volume stools and tenesmus.[9] Disease severity ranges from relatively minor watery diarrhea to complicated, life-threatening dysentery. Dehydration is a life-threatening complication that can result in renal failure and death; however, most healthy adults can recover from the infection. Hemolytic uremic syndrome can develop if an individual is infected with *S. dysenteriae* due to Shiga toxin production by this species.[10]

Clinical laboratories typically use MacConkey agar, Hektoen enteric agar, and xylose lysine deoxycholate agar to isolate *Shigella*.[11] Serological assays are the most reliable means of distinguishing between *Shigella* species. Humans appear to be the natural reservoir for *Shigella*, although intriguing evidence suggests that *Shigella* can live within the amoeba *Acanthamoeba castellanii,* which could serve as an environmental reservoir.[12] *Shigella* has not been found in this living arrangement in the environment, however, and this potential association remains unconfirmed. *Shigella* outbreaks have occurred in non-human primate colonies.[13] Individuals can asymptomatically carry *Shigella*, though the reason for carriage versus disease state is not clear.[14] Nevertheless, this phenomenon may explain why *Shigella* remains endemic in some areas of the world.[14,15] The pathology of *Shigella* in primates is similar to humans and they have been used as animal models in the study of this pathogen. Outside of non-human primates, a reliable model for dysenteric disease has not been developed.

Discovery of *Shigella*

Kiyoshi Shiga isolated *Bacillus dysenteriae* in 1898, which distinguished bacillary dysentery from amoebic dysentery.[16] *Shigella* was initially thought to be a member of a human's natural flora, and that disease occurred when the equilibrium between the host, *Shigella*, and the natural intestinal flora was disrupted.[17] This theory is similar to today's understanding of *Clostridium difficile* induction of disease.[18] The disease produced by *Shigella* was thought to be a result of vascular damage caused by excessive endotoxin release by the pathogen.[17] It was not until the 1950's when the Congress of the International Association of Microbiologists *Shigella* Commission extensively reviewed epidemiological, physiological, and serological reports of bacilli causing dysentery and recommended that the genus be named *Shigella* and established the species subgroups as we know them today.[16] There are over 40 serotypes of *Shigella*; infection provides only homologous serotype protection, so the need for a vaccine is urgent.[16,19]

Epidemiology

The World Health Organization estimates that there are about 1.7 billion cases of diarrheal disease globally each year.[20] Approximately 1.9 million people die each year as a result of diarrheal disease, with about 800,000 of these deaths being in children under five years of age.[20] *Shigella* causes about 125 million cases of diarrhea and ~14,000 deaths annually.[21] Ninety nine percent of all cases of shigellosis occur in the developing world where *S. flexneri* is the species most commonly isolated, while *S. sonnei* is most common in developed countries.[22] In a real-time demonstration of this phenomenon in China, Thailand, South Korea and Taiwan, the prevalence of *S. flexneri* has decreased and *S. sonnei* has increased during the recent economic growth in these countries.[23-26] *S. flexneri* 2a is the most commonly isolated strain. A recently emerged strain, *S. flexneri* 4c, was the second most-common strain in China over the past ten years.[23]

Deaths from shigellosis are rare in developed countries due to greater access to medical care. In the developed world, outbreaks can occur among children in daycare and among inmates at correctional institutions.[27,28] *Shigella* spp. are also known to cause traveler's diarrhea in people who have visited endemic regions of the world.[29] Those returning from North Africa, South and Southeast Asia, and Oceania are at the highest risk.[30]

Recent studies challenge the 1.1 million deaths attributable to *Shigella* reported by Kotloff, et al. in 1999. One such study was limited to cases of shigellosis occurring in Asia, and reported that approximately 125 million cases of shigellosis occur and only 14,000 of these cases are fatal annually.[21] The reason cited for the recent decrease in the number of *Shigella*-related deaths is the improved overall health of children at the onset of infection.[21] The availability of the measles vaccine may have played a role in the decreased number of deaths, because dysentery and measles were often comorbid.[21] Measles exacerbated the diarrhea caused by *Shigella* and other enteric pathogens, leading to increased mortality.[21,31,32]

The global enteric multicenter study (GEMS) paired children experiencing diarrhea with a healthy control individual, and found that *Shigella* spp. were the 4th, 2nd and 1st leading causes of moderate to severe diarrhea in children aged < 12 months, 12-23 months, and 24-59 months, respectively.[33] This study, however, found that *Shigella* spp. were not associated with an increased risk of death relative to the healthy control group.[33] This finding may be misleading, as case-fatality rates of up to 52% have been reported during *S. dysenteriae* outbreaks.[34]

The mortality from diarrheal disease is declining at a rate of ~4% per year, but the prevalence of disease has remained high.[33,35,36] Diarrheal disease is only one aspect of a complicated public health scenario in developing countries. It has an impact on long-term nutritional status that is associated with stunted growth.[37] The risk of pneumonia increases by 1.06% for every day of diarrheal disease in the 4 weeks prior to the onset of pneumonia.[38,39] The

risk of secondary infections can be decreased by promoting hand washing and other personal sanitation techniques.[39] The impact of drinking water quality on diarrheal disease burden is only visible when other factors are satisfied first, namely community and personal sanitation.[40] In very poor countries the sanitary disposal of human excrement is not always possible. Providing the infrastructure to dispose of waste in a more sanitary way is expected to decrease the diarrheal disease burden by 30-40%.[40] Decreasing the burden of fecal coliforms in drinking water by two orders of magnitude would then decrease diarrheal disease incidence by another 40% once community sanitation is improved.[40] Building sewer systems is expensive and not a practical solution for underdeveloped countries. Thus, there is a need for a low-cost vaccine that can be provided by philanthropic organizations.

Emergence of antibiotic resistance

Multi-drug resistance is a problem for many important human pathogens, and *Shigella* is no exception. One study examined 81 *S. flexneri* isolates from India, and found resistance to 21 different antibiotics including many that are considered first line therapy for shigellosis.[41] Almost half of these isolates were resistant to ten or more drugs.[41] Over 70% of the isolates were resistant to second-generation fluoroquinolones (ciprofloxacin, nofloxacin), and 17% were resistant to third generation cephalosporins (cefixime, ceftriaxone).[41] Resistance to tetracycline, chloramphenicols, sulfonamides, and gentamycin was noted.[41] Multi-drug efflux pumps and mutations in DNA gyrase and topoisomerase were also major contributors to multidrug resistant strains.[41]

A review published in 2012 revealed that antibiotic resistance is much more pervasive in Asia and Africa than in Europe and America.[42] For *S. flexneri* and *S. sonnei* in Asia and Africa, resistance to nalidixic acid has risen from 4% in 2000 to 84% in 2009, whereas the rate has remained close to 3% in Europe and America over the same time span.[42] *S. flexneri* isolates are

also rapidly acquiring resistance to ciprofloxacin in Asia and Africa, from 0.3% in 2000 to 13% in 2006.[42]

Shigella isolates acquire their antibiotic resistance genes from mobile genetic elements identified within islands in the bacterial genome such as R plasmids, transposons, and integrins.[43] Class 1 and class 2 integrons have been found within *Shigella* isolates and contain the genes required for resistance to ampicillin, streptomycin, trimethoprim, and streptothricin.[43-45] *S. dysenteriae* type 1 isolates are typically susceptible to nalidixic acid, ciprofloxacin, and ceftriaxone, whereas they are resistant to ampicillin, chloramphenicol, tetracycline, and sulfa drugs.[34]

Recent documented outbreaks in the developed world

A clonal outbreak of *S. sonnei* was reported in Los Angeles, California in May 2012.[46] Forty-three cases of shigellosis were reported among members of a private club aged from 54-98 years.[46] No deaths occurred despite the severity of the illness; the disease severity was attributed to the advanced age of the patients.[46] Most notably, this was the first reported outbreak of *S. sonnei* with decreased susceptibility to azithromycin in the United States.[46]

In North London in 2011 an outbreak of *S. sonnei* was reported among members of the Orthodox Jewish community.[47] The outbreak was caused by a single strain and lasted a total of eight weeks, causing 82 illnesses with no associated mortality.[47] The cases occurred in both children and the parents of young children with daycare centers and schools serving as the conduit for transmission.[47] Genome-level examination of the isolates in this outbreak revealed that the isolates were all very closely related, but the strain accumulated up to 7 single-nucleotide polymorphisms during the outbreak, though no phenotypic differences were evident.[47] The length of this outbreak was attributed to poor communication between public health officials and members of the Orthodox Jewish community.[47]

In the United Kingdom, an outbreak of *S. flexneri* 3a among homosexual men was reported.[48] This outbreak started in 2009 and was detected in 2011, causing 381 confirmed cases.[48] This epidemic is ongoing and causing relatively few cases, only 1-7 per month.[48] The continued low-level transmission is due to poor hygiene during and after sex.[48] A similar outbreak of *S. sonnei* occurred in Tokyo, Japan in late 2011 encompassing five patients; however an epidemiologic investigation was not conducted so there may have been more cases.[49]

Complications

Hemolytic uremic syndrome

S. dysenteriae type 1 is associated with a high incidence of severe gastrointestinal symptoms and hemolytic uremic syndrome (HUS).[34,50] Disease progression to HUS results in mortality rates of up to 52%.[34] HUS caused by *S. dysenteriae* type 1 nearly always occurs in young children and is primarily caused by massive production of Shiga toxin.[51] Lipopolysaccharide (LPS) is another potential mediator of HUS. LPS was detected in the blood of several patients with *Shigella*-mediated HUS and can induce similar damage to the kidneys of rabbits.[34] *Escherichia coli* O157:H7 is also noted for causing HUS, but it does not occur exclusively within one age group.[52] Three standard clinical signs are typical of HUS development: hemolytic anemia, thrombocytopenia (low platelet count), and elevated serum creatinine concentrations.[34] Classically, HUS is known as a blood clotting disorder in which clots preferentially form in the glomeruli of the kidneys.[34] Decreased serum sodium concentrations cause the serum to become hypotonic and may exacerbate hemolysis of red blood cells, especially in young children.[34] Development of HUS is strongly linked to the start of antibiotic therapy four or more days after the onset of symptoms.[34] Furthermore, the choice of antibiotic is important when treating *S. dysenteriae* Type I infections.[53,54] Clinical outcomes of *S. dysenteriae* type 1 treatment with either ampicillin or nalidixic acid were compared, and it was found that HUS

occurred at a much higher frequency in the ampicillin-treated patients than the nalidixic acid-treated patients.[53,54] Anti-motility drugs are contraindicated in the treatment of dysentery because they increase the risk of HUS.[34] The use of appropriate antibiotics early in the onset of disease symptoms is recommended.[34] Resistance to nalidixic acid has led to its replacement with ciprofloxacin as the recommended treatment for shigellosis.[55]

Reactive Arthritis

Reactive arthritis (ReA) is an inflammatory disease of the joints that can be triggered by gastrointestinal pathogens including *Shigella*, *Salmonella*, *Campylobacter*, *Escherichia coli*, *Yersinia* spp. and other gastrointestinal parasites.[56,57] The disease onset is 1-5 weeks post-infection, is usually polyarticular and tends to occur in joints of the legs, but can also manifest outside of the joints as a mucosal, urethral, cutaneous, or ocular inflammation.[57] ReA symptoms have a broad range of severity, ranging from relatively minor and temporary discomfort to chronic, debilitating arthritis.[57] Incidences of ReA due to *Shigella* infection are typically associated with *S. flexneri*, but *S. sonnei* has been implicated as well.[58-61] ReA may occur in up to 7% of individuals who recover from infection with *Shigella* and are uncommon in children.[56] Other reported complications include tendonitis, enthesopathy, and bursitis.[56] Most individuals that develop ReA after enteric infection are HLA-B27 positive.[56,62] Development of irritable bowel syndrome (IBS) has been linked to previous infection with an enteric pathogen, with an incidence ranging anywhere from 4-32%.[63-66] Risk factors for post-infection IBS include young age, stress, high production of TNF-alpha and low production of interluekin-10 (IL-10).[67,68] Clearly, the development of post-infection complications is the result of a complex interplay between the pathogen, host, and a multitude of host-specific factors and is the subject of continuing research.[56,57,68]

Virulence Factors

Type Three Secretion System

S. flexneri has a type three secretion system (T3SS) that is encoded on a 200 kb virulence plasmid composed of ~100 genes.[69-71] T3SS's are used by a diverse array of Gram-negative pathogens to deliver proteins into the extracellular environment or directly into the target cell's cytoplasm. The *Shigella* "entry region" is a conserved 31-kb portion of the virulence plasmid encompassing 34 genes that encode the T3SS and various effector proteins that are required for invasion of host epithelial cells, immune evasion, and intracellular survival.[72-75] These genes are only expressed at 37°C but can be influenced by other environmental factors.[72,76] Transcription of the *mxi-spa* locus and the first set (early) of effectors is activated by exposure to 37°C, thus allowing the bacterium to invade epithelial cells. Secretion of the early effectors frees IpaB and IpaC's chaperone, IpgC.[77] IpgC then binds to MxiE and induces expression of the late effector proteins.[77] The entry region of the virulence plasmid contains four distinct functional groups of genes: proteins that affect host cell function, structural components of the T3SS, transcriptional activators, and chaperones.[72]

Invasion plasmid antigens (Ipa) B, C and D are essential virulence factors secreted by the T3SS. IpaB is necessary for macrophage killing and formation of the translocon pore through which effector proteins are injected into the host cell.[78,79] IpaC induces major actin rearrangements by activating small GTPases and is also thought to participate in translocon pore formation.[78,80] IpaD and IpaB control secretion from the T3SS needle tip, and IpaD also serves as an environmental sensor by binding to bile salts and recruiting IpaB to the needle tip.[81-84] Whether IpaD possesses a host effector function is unclear.

Structural components of the T3SS are encoded by two groups of genes: membrane expression of *ipa* (*mxi*) and surface presentation of *ipa* (*spa*) antigens.[85,86] Genes of the *mxi-spa*

locus are absolutely essential for secretion of all T3SS effector proteins.[78] Two T3SS-transcriptional activators, VirB and MxiE, comprise another distinct group of genes within the entry region.[87,88] These proteins regulate various genes in the entry region and in other loci throughout the virulence plasmid. The four T3SS chaperones comprise the next group of genes within the entry region: IpgA, IpgC, IpgE, and Spa15.[89-91] IpgC and Spa15 are also transcriptional regulators.[92,93] T3SS effectors that are encoded outside of the entry region, such as the outer *Shigella* protein (Osp) and IpaH families of proteins, help shape the immune response by altering host cell transcription.[72] Intracellular motility via actin polymerization is provided by a set of genes located outside of the entry region and, with the exception of VirA, are not secreted by the T3SS.[72]

T3SS's Role in Invasion

Shigella has been proposed to initially interact with host cells by binding to CD44 and $\alpha_5\beta_1$ integrins within cholesterol-rich membrane raft microdomains.[94,95] Adherence of *Shigella* to the host cell triggers aggregation of membrane rafts creating a locally high concentration of receptors and their signaling components, and induces the preliminary cytoskeletal rearrangements necessary for invasion.[96] The T3SS effector proteins IpaC, IpgB1, IpgB2, VirA, IpgD, and IpaA alter the host cell's cytoskeleton to promote bacterial uptake into the host cell. IpaC interacts with small GTPases to form membrane extensions around the bacterium.[80] IpgB1 and IpgB2 destabilize cytoskeletal components by mimicking the actions of small GTPases, whereas VirA acts through its protease activity.[97-99] IpgD is a phophoinositide-4-phosphatase that hydrolyzes membrane components to ultimately separate the membrane from the cytoskeleton.[100] IpaA increases vinculin's affinity for actin, leading to vinculin capping of actin filaments and further disassociation of the cytoskeleton.[101,102]

T3SS's Role in Immune Evasion

Before *Shigella* can invade the host's epithelium, it must first escape the innate immune system. In short, *Shigella* is ingested and passes through the gastrointestinal tract to the large intestine, where it crosses the epithelium via M-cells and is phagocytosed by a macrophage.[103,104] Once inside the macrophage *Shigella* escapes the phagosome[105] and then induces macrophage apoptosis via the T3SS effector IpaB which directly binds to caspase-1.[79,105,106] Macrophage cell death leads to the release of proinflammatory cytokines that trigger the inflammatory response, leading to the symptoms of dysentery.[107] Nonetheless, once freed from the macrophage *Shigella* uses its T3SS to induce its own uptake into host epithelial cells from the basal side.[6]

Shigella uses its T3SS to lyse the phagosome within 15 minutes of bacterial uptake into the epithelial cell.[108] IpaB, IpaC, and IpaD are all important for phagosome escape, but IpaC may play the most pivotal role.[109-111] The late effector IpaH7.8 is also required for efficient phagosome escape, however, its role in the process remains unclear.[112] Within the host epithelial cytoplasm, *Shigella* secretes numerous proteins via its T3SS that interfere with host cell transcription and signaling, thus allowing the bacterium to persist in the epithelial cell cytoplasm and avoid detection by the immune system. IpgD promotes host cell survival by setting off a signaling cascade that activates the serine-threonine kinase Akt.[113] Another unknown T3SS effector also inhibits apoptosis within the epithelial cell.[114] OspF simultaneously interferes with intracellular pathogen detection systems by dephosphorylating MAPK, thus inhibiting MAPK-mediated signaling.[115,116] In the absence of MAPK signaling the transcription of pro-inflammatory genes is greatly reduced.[117] Further down-regulating the inflammatory response, OspG promotes the proteolytic degradation of the transcription factor NF-κB.[118] IpaH9.8 can even act as an ubiquitin ligase, thereby destroying downstream components of the MAPK kinase-dependent pathway.[119] In the cytoplasm, *Shigella* grows, divides and spreads cell-to-cell using actin-based motility.[72] VirA degrades microtubules in front of the bacterium, while the intracellular spread protein (Ics)

A localizes to and nucleates actin from one pole of the bacterium, thus creating an actin tail to propel the bacterium through the cytosol.[120-122] The bacterium creates membrane bulges into neighboring cells at tight junctions, which then endocytose the protrusion leaving the bacterium surrounded by a double membrane.[123] The double membrane is then lysed in a T3SS-dependent manner and the bacteria perpetuate the cycle of intracellular growth and intercellular spread.[111,124]

Toxins

Shiga Toxin

Shiga toxin was first described in *S. dysenteriae* and is the "original" member of the Shiga toxin family.[10] Several homologous toxins, referred to Shiga toxins 1 and 2, are present in various strains of *E. coli*, most notably strain O157:H7.[10,125,126] Shiga toxins are AB_5-type toxins, where the toxic A subunit is enzymatically active and the non-toxic B subunits bind to the target receptors.[10] The A subunit's C-terminus is inserted into the center of the pore formed by the 5 B subunits.[127,128] The B subunit binds to the glycosphingolipid Gb3 resulting in uptake of the toxin complex into target cells.[129] After uptake, the enzymatically active, 27.5 kDa A1 fragment is released upon cleavage by the intracellular protease furin.[130] Eventually the A1 fragment enters the cytosol where it displays single-site RNA *N*-glycosidase activity, thereby inactivating ribosomes through the removal of a single adenosine from the 28S rRNA of the 60S ribosomal subunit.[131] Inhibition of protein synthesis leads to apoptosis of the intoxicated cells.[132] How Shiga toxin reaches the kidneys is poorly understood. The most likely scenario is that the secreted toxin enters the bloodstream from the intestine via the bloody lesions that are the result of shigellosis.[34] Free Shiga toxin has never been found in the blood, but it has been observed to bind with low affinity to polymorphonuclear leukocytes via the A subunit and could reach its target in this way.[133]

Enterotoxins

Four enterotoxins are encoded by *S. flexneri*: ShET1 (*setAB*), ShET2 (*sen*), Pic, and SepA.[134] Collectively, these enterotoxins are thought to cause electrolyte secretion into the small intestine, contributing to the watery diarrhea that often accompanies shigellosis.[134] What advantage *Shigella* would gain by increased fluid level in the small intestine is unclear, but it has been proposed that this may expedite transit to the colon where *Shigella* actually causes disease.[72] ShET1 and Pic are encoded on the bacterial chromosome, whereas ShET2 and SepA are encoded on the *Shigella* virulence plasmid.[134] ShET1 is only found in *S. flexneri* 2a and 2b, whereas ShET2 is found in most serotypes of *S. flexneri* as well as in *S. boydii*, *S. sonnei*, *S. dysenteriae*, and enteroinvasive *Escherichia coli*.[135-137] ShET1 is an A-B type toxin, but the stoichiometry remains undefined.[137] ShET2, also known as OspD3, is secreted via the T3SS.[138] ShET2 is found in 80-90% of all *Shigella* isolates tested that also retained the virulence plasmid.[139] ShET2 increases the amount of the pro-inflammatory cytokine IL-8 secreted post-invasion by cultured epithelial cells.[140] The prevalence of these toxins does not appear to follow any geographical pattern. The molecular mechanism of action of ShET1, ShET2 and SepA is poorly understood; however Pic has been studied in some detail.

Pic (Protease involved in colonization) is a member of the serine protease autotransporters of Enterobacteriaceae (SPATEs) family, class 2 that binds to and cleaves proteins modified with Sialyl Lewis-X (SLeX)-O-glycans.[141] SepA is also a SPATE that contributes to the enterotoxicity of *Shigella*, but its target remains unknown.[134] Pic is involved in colonizing the mucosal epithelium, cleaves mucin and induces mucin release.[141,142] This toxin is only expressed in *S. flexneri* 2a.[141] Pic may be involved in immunomodulation because it cleaves many cell-surface O-linked glycans (*e.g.* CD43) that are involved in leukocyte trafficking.[141]

Deletion of ShET1, ShET2, and Pic resulted in a live-attenuated vaccine that does not cause watery diarrhea, thus solving a problem that has plagued vaccine development.[143] Live-attenuated vaccines are effective at inducing homologous serotype protection, but they are noted for a lack of cross-protection against distinct serotypes. Therefore, the need for a universal vaccine candidate is urgent.[143] An intriguing finding was that this live-attenuated vaccine also generates very high titers to antigens conserved across all *Shigella* species, namely IpaB, IpaC, and IpaD.[143]

CHAPTER II

INVASION PLASMID ANTIGEN B (IpaB) FROM *SHIGELLA FLEXNERI* UNDERGOES A CONFORMATIONAL REARRANGEMENT UPON INTERACTION WITH ITS CHAPERONE IpgC

Introduction

Shigella's ability to invade human cells depends on the insertion of a functional translocon pore into host cell membranes. Pore formation is impossible without the translocators Invasion plasmid antigen B (IpaB) and IpaC. IpaB is a hydrophobic, 62 kDa protein that has been demonstrated to form pores in model membranes.[144] Invasion plasmid gene C (IpgC) is a 17.8 kDa, α-helical chaperone protein that maintains IpaB and IpaC in a soluble, secretion competent state within the bacterial cytoplasm prior to secretion via the T3SS.[91,145-147] IpgC is classified as a class II T3SS chaperone that has a tetratricopeptide repeat (TPR) fold.[145,146] After IpgC releases the translocators, it forms a transcription-activating complex with MxiE, specific for late T3SS effector proteins.[91,92,148] Degradation of IpaB occurs when *ipaB* is expressed in the absence of IpgC and this applies both to expression in *Shigella* or recombinant expression in *Escherichia coli*.[91,144] When in a complex with IpgC, the translocator proteins are unable to interact with membranes.[144]

Others have proposed that IpaB possesses two separate chaperone-binding sites (CBS's) within the N-terminus, where CBS 1 spans residues 16-35 and CBS 2 spans 51-70.[149] The authors

of that work speculated that the presence of two CBS's indicates that two IpgC molecules bind to a single IpaB molecule, thereby forming a heterotrimer.[149] This claim was based on the identification of the two separate CBS's in a co-crystal structure of an IpgC dimer in complex with a 56-residue IpaB peptide encompassing both CBS's.[149] The aforementioned study contributed valuable knowledge to the field, however, the IpaB peptide used represents less than 10% of the total length of IpaB. Furthermore, IpgC binding to IpaB as a dimer conflicts with existing literature demonstrating that IpgC and IpaB interact at a 1:1 stoichiometry.[144]

Full-length IpaB can be recombinantly expressed in large quantities, but in order to maintain solubility it must be co-expressed with its chaperone IpgC.[144] The 6x His-tagged IpaB-IpgC complex can then be purified by immobilized metal affinity chromatography. Mild detergents can be used to irreversibly separate IpaB and IpgC.[144] Separation is irreversible because IpaB requires the presence of detergent to remain soluble, yet the presence of any detergent was not compatible with their reassociation. Attempts to reconstitute the IpaB-IpgC complex after separation with mild detergents failed, at least in part because complete removal of detergents led to precipitation of the IpaB (Adam, P. R. unpublished results). Fortunately, a soluble N-terminal fragment of IpaB was identified by limited proteolysis, which could potentially be used to explore the IpgC-IpaB interaction. This fragment was also used to solve a crystal structure of the IpaB region spanning residues 74-224.[150]

With a stable N-terminal fragment of IpaB in hand, we were thus in a position to carry out a detailed analysis of the interaction between IpaB and IpgC. There have been no previous studies concerning the structural consequences of this important interaction. We first used fluorescence polarization (FP) and isothermal titration calorimetry (ITC) to demonstrate an interaction between the IpaB N-terminal fragments and IpgC. Then we explored the stoichiometry of the IpaB-IpgC interaction by chemical-crosslinking. Finally, we explored the possibility of a conformational rearrangement within the IpaB N-terminal fragment using Förster

Resonance Energy Transfer (FRET). The results from this study contributed to our developing an understanding of one of the most important protein-protein interactions that occurs to allow the process of type III secretion.

Results

Identification of the IpaB N-terminal domain

M. L. Barta et al. used Subtilisin-A to carry out limited proteolysis of the IpaB-IpgC complex (Figure 1.1). Tandem mass spectrometry was then used to identify proteolytically stable bands.[150] IpaB fragments were selected and cloned for recombinant protein expression based on predicted solubility, including $IpaB^{1-226}$, $IpaB^{28-226}$, and $IpaB^{1-94}$.[150] Each of these fragments were stably expressed in the presence of IpgC; however, only the two larger fragments could be stably expressed in the absence of IpgC. $IpaB^{28-226}$ was then used by M. Barta et al. to obtain a crystal structure for the internal fragment $IpaB^{74-224}$ (Figure 1.2).[150] The crystal structure revealed a >100 Å coiled-coil and was structurally homologous to the pore-forming toxins colicins E3 and Ia.[150,152,153]

$IpaB^{1-226}$ and $IpaB^{28-226}$ could be stably expressed in the absence of chaperone or co-expressed with IpgC, indicating that they were excellent candidates for exploring the nature of the interaction between IpaB and IpgC. $IpaB^{28-226}$ separated from IpgC during later chromatographic purification, so no information is presented for this co-purified complex. On the other hand, $IpaB^{1-226}$ and $IpaB^{1-94}$ remained associated with IpgC throughout the entire purification protocol. $IpaB^{1-94}$ was unstable in the absence of IpgC and thus no data concerning this fragment were collected.

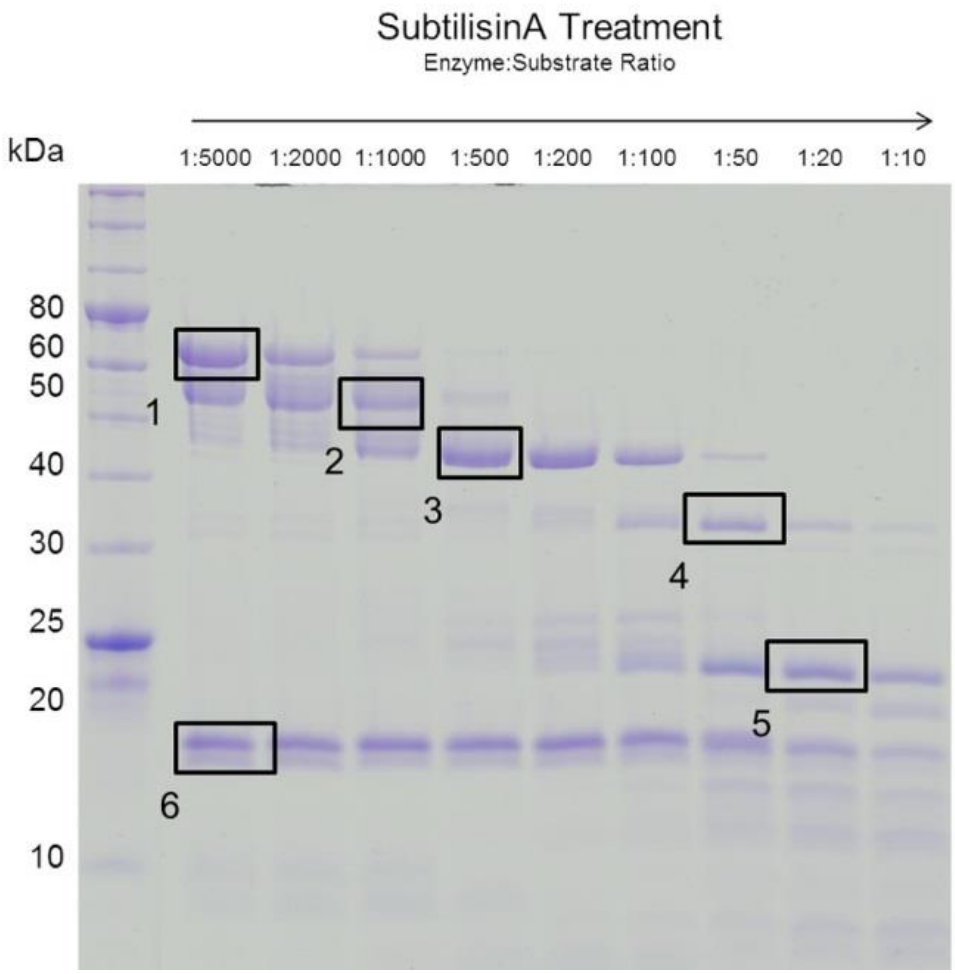

Figure 1.1: Limited Proteolysis of the IpaB-IpgC Complex.[151] Full-length IpaB-IpgC was incubated with increasing concentrations of subtilisin A for 60 min. Band 1: Full-length IpaB. Definite identification of bands 2, 3, and 4 was not possible, but they may represent progressive degradation from the C-terminus of IpaB. Band 5 represented a proteolytically stable domain and was identified by LC-MS/MS as IpaB$^{28\text{-}226}$. Band 6: Full-length IpgC. This work was done by M. L. Barta.[151]

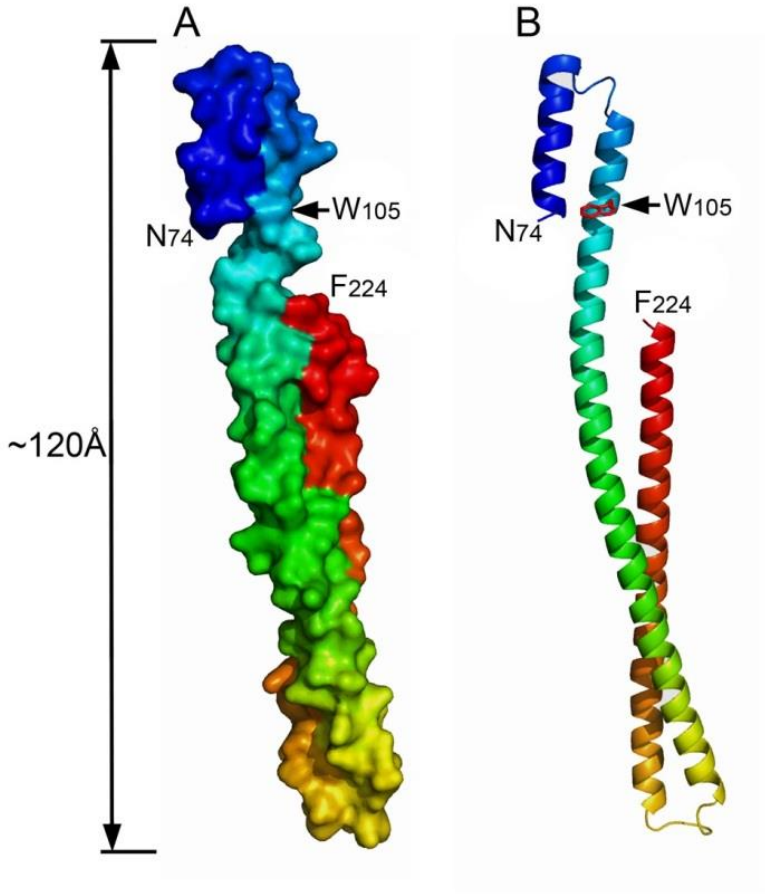

Figure 1.2. Crystal Structure of IpaB$^{74\text{-}224}$.[150,151] Cartoon representation of the crystal structure of IpaB$^{74\text{-}224}$ solved at 2.1 Å resolution. The structure consists of a 120 Å long coiled-coil. W105 is identified in this figure, as are the N- and C-terminal residues. This figure was prepared for Adam et al., 2012[151] according to the crystal structure solved by Barta, et al., 2012.[150]

Secondary structure content and stability analysis

Far-UV circular dichroism (CD) spectroscopy was performed on the highly purified proteins listed in Table 1.1. The spectra of all IpaB fragments and their IpgC complexes possessed strong minima at 222 nm and 208 nm, indicating dominant α-helical secondary structure content (Figure 1.3A).[151] This was in good agreement with the published crystal structure of $IpaB^{74-224}$ (Figure 1.1).[150] CD was also used to examine the thermal stability for the folding of these IpaB fragments (Table 1.1).[151] The CD signal at 222 nm was monitored as a function of temperature to determine if the structural stability of the IpaB N-terminal domain was affected by the presence of IpgC (Figure 1.3B). Transition temperatures ("T_m") were defined as the midpoint of any observed transitions, and indicate the temperature at which the α-helical secondary structure content and disordered structure content are approximately equal. $IpaB^{1-226}$ and $IpaB^{28-226}$ both unfolded at 57.5° C, whereas IpgC unfolded at 45° C. The $IpaB^{1-94}$-IpgC complex had the highest T_m of 62.5° C. The co-purified $IpaB^{1-226}$-IpgC complex displayed two transitions, each near the T_m of the component proteins. This suggests that the dimeric complex dissociated and each protein unfolds independent of the other. This is in contrast to the single elevated T_m observed for $IpaB^{1-94}$-IpgC where the proteins may lend structural support to each other.

In Vitro Interaction between IpgC and N-terminal IpaB fragments:

Since the isolated IpaB N-terminal domain co-purified with IpgC following recombinant expression in *E. coli*, the *in vitro* interaction between these proteins was explored. Fluorescence polarization (FP) is a technique that can indicate changes in the molecular volume of a fluorescent species which influences the rotational diffusion (how quickly a molecule is rotating) of that molecule.[154] The rate of rotational diffusion is inversely related to the size of the molecule, with small molecules rotating quickly and large molecules rotating more slowly. This

Table 1.1. Molecular Weights and Thermal Stability of Proteins Used in this Chapter.

Protein	Molecular Mass (kDa)	T_m (°C)[151]
$IpaB^{1-226}$	25.1 (50.2)[a]	57.5
$IpaB^{28-226}$	22.3 (44.6)[a]	57.5
IpgC	17.8 (35.6)[a]	45.0
$IpaB^{1-226}$-IpgC	42.9	45.0/60.0
$IpaB^{28-226}$-IpgC	40.1	ND[b]
$IpaB^{1-94}$-IpgC	27.7	62.5

Theoretical molecular masses (kDa) and thermal stability of the proteins and protein complexes used in this study. [a]Mass of the homodimeric complex is shown in parentheses. [b]The $IpaB^{28-226}$-IpgC complex dissociated during purification, thus no thermal stability data are available.

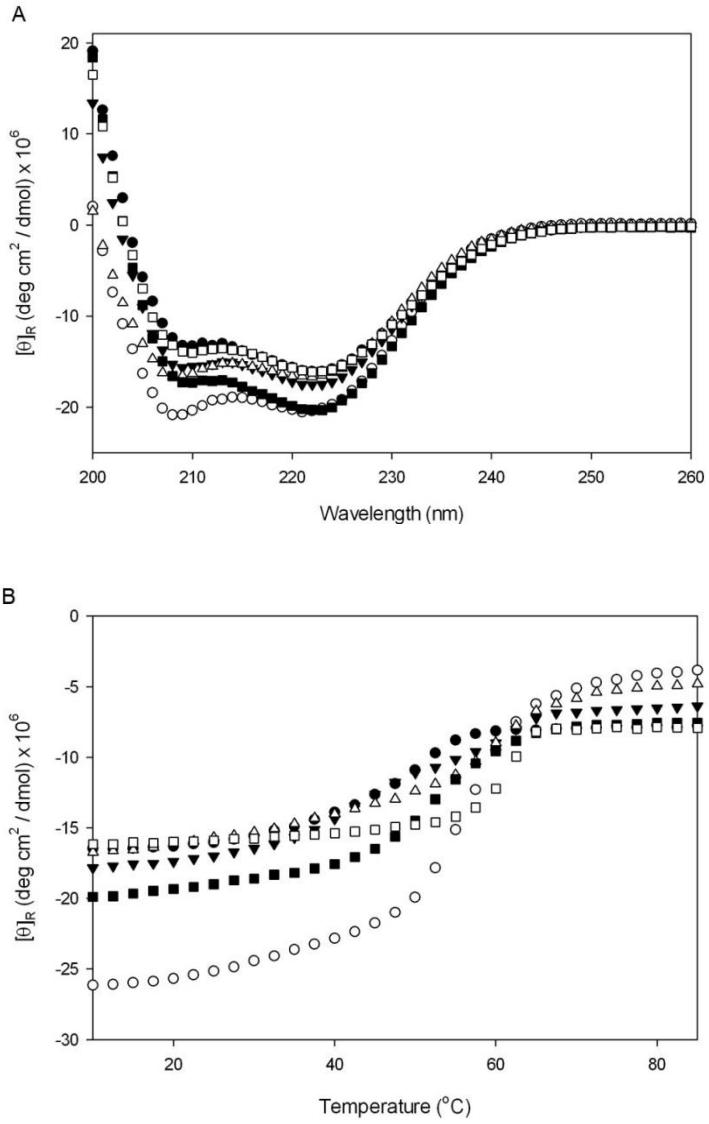

Figure 1.3. CD Spectra and Thermal Unfolding.[151] Proteins were dialyzed against citrate-phosphate buffer, containing 150 mM NaCl, pH 7.0. Panel A: CD spectra were collected from 200-260 nm following the parameters in materials and methods. Panel B: The CD signal at 222 nm was monitored as a function of temperature (10 to 85° C) using the parameters in materials and methods. Both panels: IpgC (closed circles); IpaB$^{1-226}$ (open circles); IpaB$^{1-226}$-IpgC (closed triangles); IpaB$^{28-226}$ (open triangles); IpaB$^{28-226}$-IpgC (closed squares); IpaB$^{1-94}$-IpgC (open squares).

phenomenon can be harnessed to explore protein-protein interactions. We expressed and purified IpaB$^{1\text{-}226}$ and IpaB$^{28\text{-}226}$ with an N or C-terminal Cys residue (designated by the N or C in front of the residue numbers in each fragment name) to allow for fluorescent labeling at a single site using the sulfhydryl-reactive dye fluorescein-maleimide (FM). FM-IpaB$^{N1\text{-}226}$, FM-IpaB$^{C1\text{-}226}$, FM-IpaB$^{N28\text{-}226}$, and FM-IpaB$^{C28\text{-}226}$ were incubated with increasing concentrations of unlabeled IpgC (Figure 1.4). The milli-polarization (mP) values were plotted as a function of IpgC concentration and analyzed with SigmaPlot (Systat Software Inc., San Jose, CA), which also calculated the dissociation constant (K_d; Table 1.2). The correlation coefficient (R^2) was ≥ 0.94 for each plot. The K_d's for FM-IpaB$^{N1\text{-}226}$ and FM-IpaB$^{C1\text{-}226}$ were 199 nM and 60 nM, respectively. Conversely, the K_d's for FM-IpaB$^{N28\text{-}226}$ and FM-IpaB$^{C28\text{-}226}$ were 411 nM and 501 nM, respectively. These data indicated that IpaB$^{1\text{-}226}$ interacts with IpgC more strongly than does IpaB$^{28\text{-}226}$. This relationship was not altered by the location of FM on the N- or C-terminus (Figure 1.4). These data are consistent with the previous report that IpaB's N-terminal 25 residues contain a CBS that is distinct from a CBS located C-terminal of residue 28.[149] The presence of both chaperone binding sites is not necessary for IpaB-IpgC interaction, but the interaction is strongest when both sites are present within a single polypeptide.

To explore the thermodynamic parameters of the IpaB-IpgC interaction, isothermal titration calorimetry (ITC) was used in the laboratory of Dr. Brian Geisbrecht in parallel with our fluorescence polarization data (Table 1.3). ITC is fluorophore-independent and can be used to calculate the K_d, ΔH, ΔS and stoichiometry of interaction (N). The K_d's in Table 1.3 agree well with those derived from FP experiments, where IpaB$^{1\text{-}226}$ was shown to have greater affinity for IpgC than IpaB$^{28\text{-}226}$. The ITC and FP data indicate a 14-fold and a 2 to 8-fold stronger affinity of IpaB for IpgC when both CBS are present, respectively. ΔH and ΔS are positive in both cases indicating that these interactions are endothermic and entropic (Table 1.3). Interestingly, the ITC

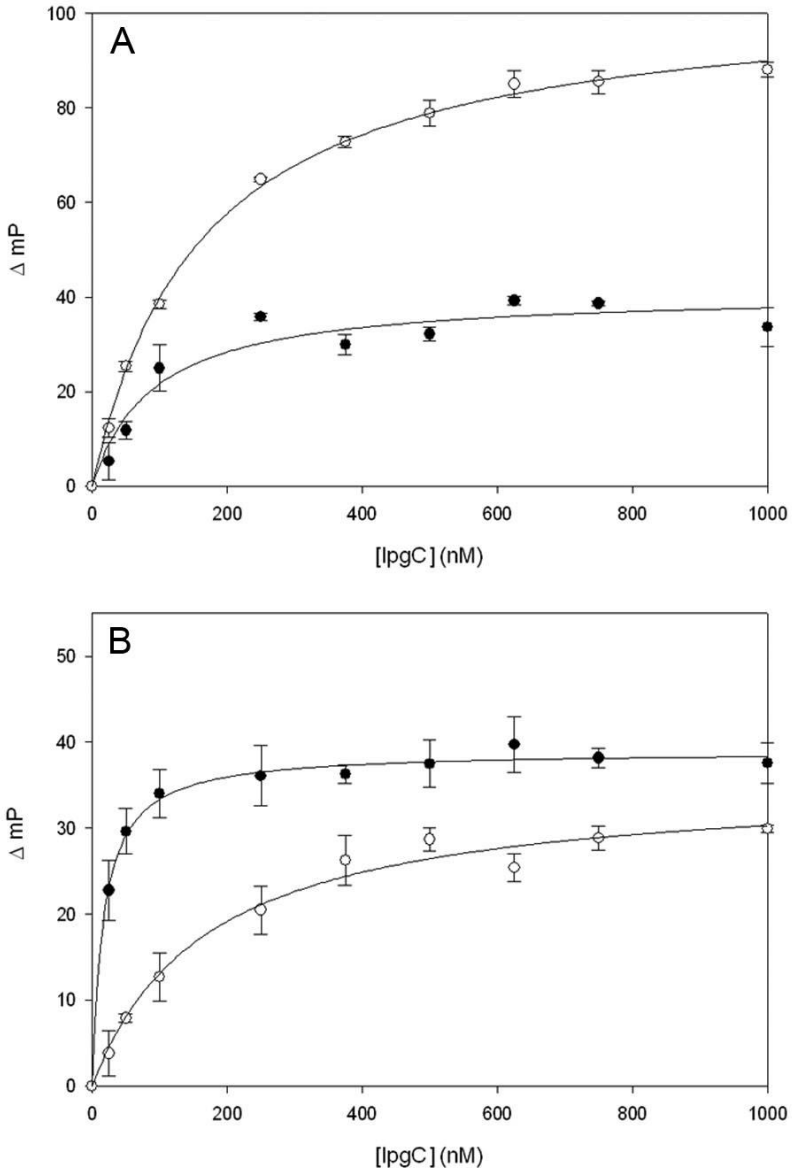

Figure 1.4. FP with IpaB fragments.[151] Panel A: FM-IpaB$^{N28-226}$ (open circles, $R^2 = 0.99$) and FM-IpaB^{N1-226} (solid circles; $R^2 = 0.94$). Panel B: FM-IpaB$^{C28-226}$ (open circles; $R^2 = 0.99$) and FM-IpaB^{C1-226} (solid circles; $R^2 = 0.99$). 80 nM solutions of the FM-labeled IpaB fragments were prepared with increasing concentrations (0 to 1 μM) of unlabeled IpgC. SigmaPlot was used to fit a single-site saturation binding curve to the data. Error bars = standard deviation.

Table 1.2. Fluorescence Polarization Derived Dissociation Constants for the IpaB N-terminal Domain and IpgC.[151]

Protein	K_d (nM)
$IpaB^{N1-226}$	199.4 ± 62.6
$IpaB^{C1-226}$	59.5 ± 5.6
$IpaB^{N28-226}$	410.9 ± 14.2
$IpaB^{C28-226}$	500.7 ± 77.1

IpaB fragments labeled at either the N- or C-terminus were prepared at 80 nM while unlabeled IpgC was titrated up to a concentration of 1 μM. Data were plotted as an (x,y) scatter and fit to a single-site saturation ligand binding equation using SigmaPlot (Figure 1.4). Dissociation constants (K_d) were derived from the equation.

Table 1.3. Isothermal Titration Calorimetry Reveals Thermodynamic Properties of Interaction Between IpaB N-terminal Domain and IpgC[151]

Parameter	**IpaB$^{1-226}$**	**IpaB$^{28-226}$**
N	1.03 ± 0.01	0.88 ± 0.02
ΔH (kcal / mol)	8.68 ± 0.14	3.55 ± 0.11
ΔS (J/K)	59.7	37.2
K_d (nM)	210 ± 50	2960 ± 530

The thermodynamic properties of IpaB-IpgC interaction were monitored by isothermal titration calorimetry in the laboratory of our collaborator Dr. Brian Geisbrecht. Stock solutions of IpaB$^{1-226}$ (600 µM) and IpaB$^{28-226}$ (1.569 mM) were injected 6 µl at a time into 1.456 ml IpgC (30 µM and 48 µM, respectively). N = stoichiometry of the interaction; ΔH = change in enthalpy; ΔS = change in entropy (Joules / Kelvin); K_d = calculated dissociation constant. Errors represent standard deviations of three independent measurements.

data suggested a 1:1 stoichiometry between IpaB and IpgC, which fits with the original observations of Birket et al.[144]

Stoichiometry of the IpaB-IpgC Interaction

IpgC is known to form homodimers in solution[146] and this is consistent with the structure of other class II T3SS chaperones, such as SycD from *Yersinia enterocolitica*.[155] This structure did differ somewhat from another report on the dimeric structure of a truncated form of IpgC, however, the latter structure included a small fragment of IpaB as part of the structure.[145] The work by Lunelli et al. provided conflicting evidence as to whether IpgC remains a dimer while complexed with IpaB.[144,145,149] To examine this translocator-chaperone complex more closely, the stoichiometric relationship between the IpaB N-terminal domain and IpgC was investigated by using the homobifunctional cross-linking agent dithiobis[succinimidyl propionate] DSP. First, co-purified IpaB$^{1-94}$-IpgC and IpaB$^{1-226}$-IpgC were cross-linked (Figure 1.5A).[151] Co-purified IpaB$^{1-226}$-IpgC formed a cross-linked product of approximately 40 kDa, which agrees well with the expected mass of 42.9 kDa for an IpaB$^{1-226}$-IpgC heterodimer (See Table 1.1 for molecular masses).[151] Co-purified IpaB$^{1-94}$-IpgC formed a cross-linking product of 25 kDa, also indicative of heterodimer formation.[151]

As a control in these cross-linking experiments, each protein was incubated alone with cross-linking agent. When this was done, we found that each protein formed complexes having a mass that is consistent with homodimer formation (Table 1.1 and Figure 1.5B & C).[151] It should be noted that in all cases, the sizes of the observed homodimers and heterodimers were sufficiently different to distinguish them by SDS-PAGE. Because of this and the suggestion by others that IpaB may interact with IpgC at a 1:2 ratio, the IpaB fragments (except for IpaB$^{1-94}$) were mixed with IpgC at a 1:2 molar ratio (IpaB:IpgC) and then incubated with DSP.[151] A two-

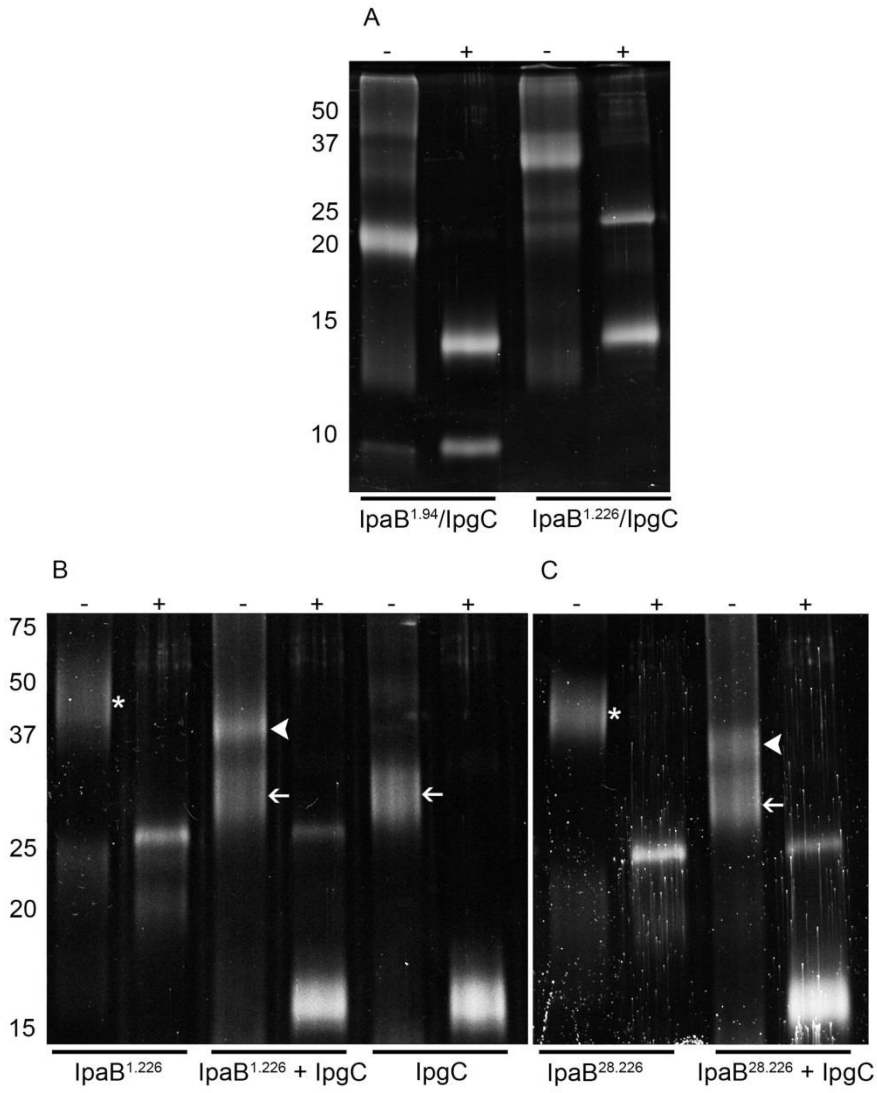

Figure 1.5. Crosslinking of IpaB N-terminal fragments and IpgC.[151] Proteins were chemically cross-linked using the disulfide-containing agent DSP. DSP cross-linking can be reversed by using reducing agents. Panel A represents co-purified IpaB$^{1\text{-}94}$-IpgC and IpaB$^{1\text{-}226}$-IpgC. Dithiotheritol (DTT) was used to reverse cross-linking and its presence is indicated at the top of each panel. Panel B (IpaB$^{1\text{-}226}$) and Panel C (IpaB$^{28\text{-}226}$) depict cross-linking using independently purified IpaB$^{1\text{-}226}$ or IpaB$^{28\text{-}226}$ and IpgC. These proteins were mixed at a molar ratio of 1:2 (IpaB:IpgC). The left- and right-most lanes in Panel B depict cross-linking of individual proteins as labeled. Panel C is similar to B, except IpaB$^{28\text{-}226}$ was used. Asterisks = IpaB homodimers;

Continued (Figure 1.5 legend)

arrowheads = IpaB-IpgC heterodimer; thin arrows = IpgC homodimers. The numbers on the left side of each panel indicate the molecular weights (in kDa).

fold molar excess of IpgC was used to ensure that IpgC could still form a dimer in case the addition of IpaB disrupted IpgC homodimer formation. SDS-PAGE analysis revealed that IpaB$^{1-226}$ and IpaB$^{28-226}$ co-incubated with IpgC formed 40 kDa and 38 kDa complexes, respectively (Figure 1.5B & C).[151] These masses were once again consistent with heterodimer formation. Interestingly, a 35 kDa cross-linked product was present in both conditions, which is consistent with the continued presence of IpgC homodimers following formation of the IpaB-IpgC heterodimer.[151] No IpaB homodimeric products were detected in any of the samples, indicating that all of the IpaB molecules had formed heterodimeric complexes with IpgC.[151] Since IpgC was present at a twofold molar excess, the consistency by which IpgC homodimers formed suggested that IpaB and IpgC form a heterodimer.[151] Taken together with the cross-linking analyses of co-purified full length IpaB-IpgC,[144] the data suggest that IpaB forms a 1:1 heterodimer with IpgC *in vitro* and *in vivo*.

The heterodimeric complexes formed by IpaB and IpgC are smaller than the IpaB N-terminal domain homodimers, yet paradoxically there was a rise in mP values observed when IpgC was added to the IpaB samples (Figure 1.4). Decreases in molecular volume generally lead to decreases in mP values, however, the flexibility within the region to which the fluorophore is attached can have a significant impact on the observed mP value. Decreased flexibility of the termini as a result of IpgC binding would readily explain the rise in mP values seen upon heterodimer formation. To explore this, FP experiments were performed using IpaB's native Trp at position 105 (Figure 1.6). It is unlikely that the region surrounding W105 is flexible since it is located within the long coiled-coil of IpaB. When IpgC was titrated into non-fluorescent IpaB$^{28-226}$, a decrease in polarization values was observed, with the smallest FP values observed at an eqimolar concentration of these proteins. Taken together, the FP, ITC, and cross-linking data presented here strongly support our proposal that an interaction occurs between the IpaB N-terminal domain and IpgC and that this interaction gives rise to a heterodimer.

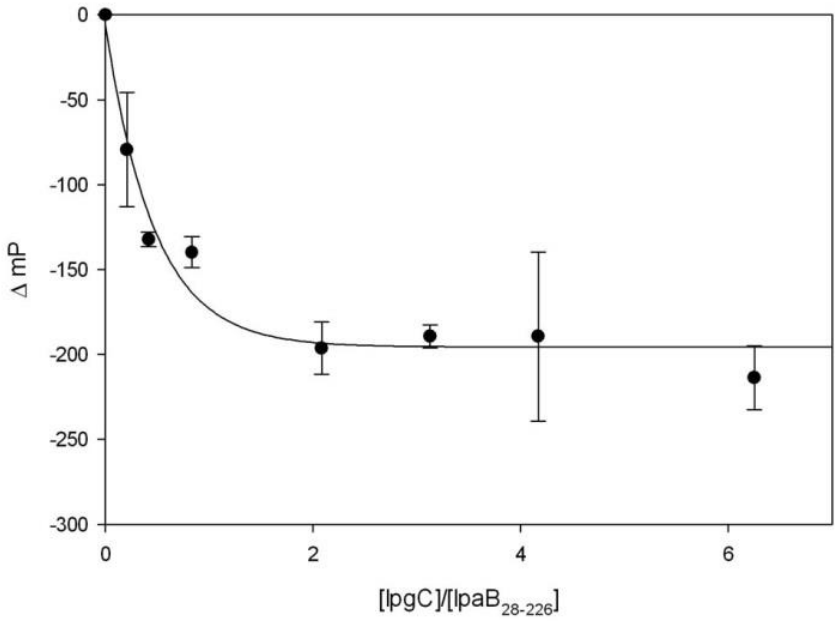

Figure 1.6. Fluorescence Polarization (FP) using Native Trp Within the Coiled-Coil of IpaB$^{28\text{-}226}$.[151] FP measurements obtained during titration of IpgC into IpaB$^{28\text{-}226}$ were obtained using IpaB's intrinsic W105 as the fluorophore. IpgC does not contain any Trp residues and thus did not interfere with the measurements. 3 μM IpaB$^{28\text{-}226}$ was required to obtain a reliable fluorescence signal. The X-axis is shown as the molar ratio of IpgC:IpaB. Samples were excited with plane-polarized 295 nm light and emission was monitored at 340 nm.

Förster resonance energy transfer (FRET)

FRET is a technique that allows distance determinations within macromolecules with precision approaching the Angstrom level. It is a molecular ruler that relies upon using two different fluorophores, a fluorescence donor and a fluorescence acceptor. The donor's emission spectrum must overlap with the acceptor's absorption spectrum, which allows the donor's excitation energy to be directly transferred non-radiatively to the acceptor fluorophore.[154] This results in quenching of the donor's emission. The extent of this quenching depends upon the spectral properties of both probes and with an efficiency that is inversely proportional to the distance between the donor and the acceptor.[154] In our application, we used FRET to determine if conformational changes occur in the IpaB N-terminal domain upon binding to IpgC. The donor fluorophore used was the native tryptophan residue (W105) located within the N-terminal region of IpaB and the acceptor was an extrinsic dye, Alexa Fluor 350 (Alexa350) covalently linked to the sulfhydryl moiety of the N- and C-terminal Cys residues alluded to above. It should be noted that there are no interfering Trp residues within IpgC. This FRET pair has an R_o of 21 Å.[156] R_o is the distance between the probes' dipoles at which 50% energy transfer would be expected to occur, and it depends upon the spectral overlap and absorption properties of the donor, along with the assumption of random orientation of the dipoles.[154] $IpaB^{N1-226}$, $IpaB^{C1-226}$, $IpaB^{N28-226}$, and $IpaB^{C28-226}$ were labeled with Alexa350-maleimide. $IpaB^{C1-226}$ became unstable when labeled with Alexa350, which precluded collection of fluorescence spectra for this protein. Alexa350-labeled IpaB fragments were incubated with or without 1 µM IpgC. To calculate the FRET efficiency in each case, the spectrum of the donor only sample (IpaB lacking the Alexa350 label) was collected with and without IpgC. The donor only spectrum was then compared to the spectrum for Alexa350-labeled IpaB with and without IpgC. Representative fluorescence spectra for the unlabeled and Alexa350-labeled IpaB fragments alone and in the presence of IpgC are shown in

Figure 1.7. Maximum donor emission was determined based on these spectra and used to calculate the FRET efficiency (Table 1.4) as described in the Materials and Methods section.

The fact that these IpaB N-terminal fragments form homodimers complicated the confidence in the calculation of distances. In a homodimer of IpaB, there would be two Trp's and two Alexa350 moieties for the donor plus acceptor samples, thus making it difficult to distinguish intermolecular FRET from intramolecular FRET within the homodimer as long as it remains intact. Nevertheless, we calculated distances based on the fluorescence measurements with this caveat in mind. The results of the FRET calculations are shown in Table 1.4. Based on the crystal structure for $IpaB^{74.224}$ (PDB entry 3U0C),[150] the distance between W105 and A224 is ~18 Å, which agrees well with the calculated FRET distance in $IpaB^{C28\text{-}226}$ of 17 Å in the absence of IpgC. We were unable to determine a precise distance between W105 and the N-terminus of IpaB in the crystal structure because the extreme N-terminus of IpaB was not resolved.[150]

The data for $IpaB^{N1\text{-}226}$ indicated that a large decrease in FRET efficiency occurred after the addition of IpgC, which resulted in an approximate 10 Å increase in distance between the donor and acceptor probes. Addition of IpgC to $IpaB^{N28\text{-}226}$ did not result in a significant change FRET efficiency. When IpgC was added to $IpaB^{C28\text{-}226}$, a measureable decrease in FRET efficiency occurred, resulting in a modest 4 Å increase in distance. Because of homodimer formation, the FRET data cannot unequivocally demonstrate that a conformational change occurs within the IpaB N-terminal domain upon IpgC binding; however, when taken together with the FP data, a strong argument can be made for a conformational rearrangement occurring in IpaB upon chaperone binding.

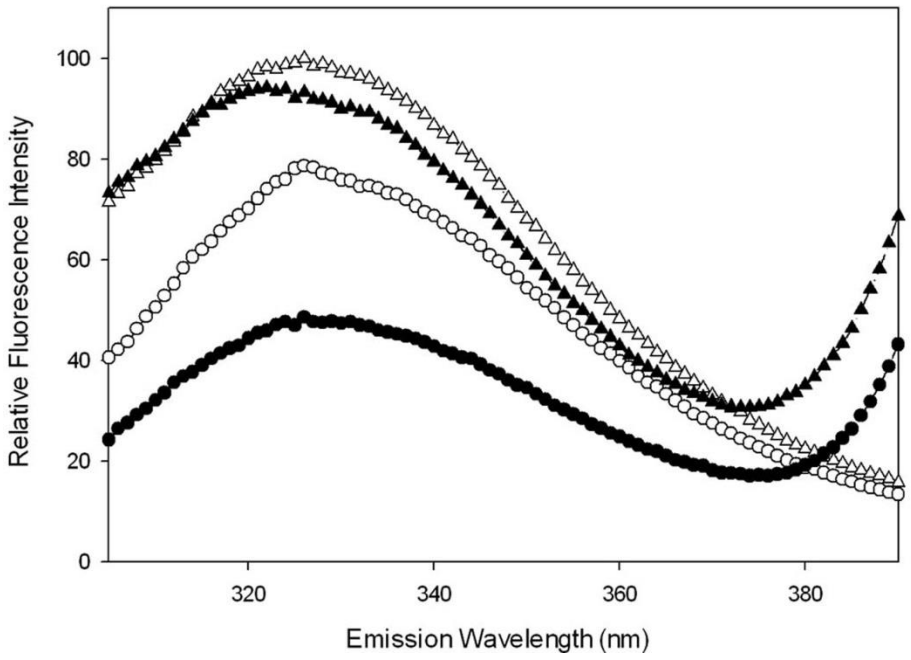

Figure 1.7. Representative Fluorescence Emission Spectra used to Calculate Intramolecular Distances by FRET.[151] The Trp residue within unlabeled IpaB^{N1-226} (Donor only, D) or Alexa350-labeled IpaB^{N1-226} (Donor/Acceptor, D/A) was excited at 295 nm and the resulting spectra are shown above. Spectra were collected in the presence and absence of 1 μM IpgC. Unlabeled IpaB^{N1-226} with and without IpgC (dark and open circles, respectively); Alexa350-IpaB^{N1-226} with and without IpgC (dark and open circles, respectively). Spectra were normalized to IpaB^{N1-226} + IpgC.

Table 1.4. Förster Resonance Energy Transfer (FRET) Efficiencies and Calculated Distances.[151]

	0 µM IpgC		1 µM IpgC	
Protein	**FRET Efficiency**[a]	**Distance**[b]	**FRET Efficiency**[a]	**Distance**[b]
$IpaB^{N1-226}$	37.6 ± 3.3	22.8	6.5 ± 3.6	32.8
$IpaB^{N28-226}$	47.1 ± 3.2	21.4	37.9 ± 14.8	22.8
$IpaB^{C28-226}$	74.5 ± 5.9	17.6	46.1 ± 6.8	21.6

[a]FRET efficiencies (%) were calculated using Equation 1 (see Materials and Methods section) after determination of the quenching of the Trp (donor) emission in the presence of Alexa350. [b]The apparent distance was then calculated based on Equation 2 (see Materials and Methods) and it is given here in Angstroms.

Conclusions

Previous studies identified a highly soluble domain (the "N-terminal" domain) of IpaB that was used to solve a structure from residues 74-224.[150] Because this soluble N-terminal domain contained the proposed sites required for IpaB binding to its chaperone (IpgC), it was used to study the interaction between IpaB and IpgC. This has been previously impossible because the stable expression of full-length IpaB requires co-expression with IpgC, thus yielding an IpaB-IpgC complex that cannot be reconstituted after dissociation. The continued presence of the detergent used to separate IpaB and IpgC is necessary to maintain IpaB as soluble and makes the reassembly of the complex impossible. Studying all aspects of the structural features of IpaB is important for identifying methods for blocking its function, especially since recent findings have suggested that IpaB exists in many functional oligomeric and conformational states that may be relevant to function during infection.[157,158] This chapter features three main findings. First, the N-terminus of IpaB interacts strongly with IpgC and the strength of this interaction is affected in an additive manner by the presence of both chaperone binding sites (CBS's). Secondly, IpaB and IpgC are in a homodimeric state that is dissociated in favor of the more energetically favorable heterodimer when the two are mixed. Finally, the N-terminal domain of IpaB appears to undergo a conformational change upon binding to IpgC, and it is presumed that this change is related to how IpgC is able to maintain full-length IpaB in a membrane-inactive and soluble state prior to IpaB secretion.

Building off of the partial crystal structure described by Barta et al.,[150] we expressed and purified the soluble fragments $IpaB^{1-94}$, $IpaB^{1-226}$ and $IpaB^{28-226}$.[151] These fragments, except for $IpaB^{1-94}$, do not require IpgC for stable expression, however, they can be co-purified with IpgC. The $IpaB^{28-226}$-IpgC complex dissociated during the purification process, perhaps because of the high ionic strength conditions used in some of the later purification steps, though it is unclear why the complex remained intact after the high salt conditions used in the IMAC chromatography

process but separated during size-exclusion chromatography (P.R. Adam and M. L. Barta, personal communication).[151] Nevertheless, the IpaB$^{1-94}$-IpgC and IpaB$^{1-226}$-IpgC complexes remained intact throughout all purification steps and were analyzed by CD spectroscopy, as were individually purified proteins except for IpaB$^{1-94}$. All of the proteins were highly α-helical. The IpaB$^{1-226}$-IpgC complex appeared to separate prior to unfolding due to the presence of two transitions. In contrast, the single transition of the IpaB$^{1-94}$-IpgC complex suggests that this complex remained intact until both proteins unfolded simultaneously. IpaB$^{1-94}$ may have a stabilizing effect on the secondary structure of IpgC. This may be due to an alternate conformation adopted by IpaB$^{1-94}$ that increases the affinity of these two proteins for one another.

As stated above, IpaB$^{28-226}$-IpgC separated during purification, whereas IpaB$^{1-226}$-IpgC remained intact, implying a stronger interaction exists between IpaB$^{1-226}$-IpgC than between IpaB$^{28-226}$-IpgC. IpaB's N-terminal domain was proposed to contain two CBS's (CBS 1 = residues 16-35, CBS 2 = 51-70),[149] so a stronger interaction may exist when both CBS's are present. Thus, we investigated whether the IpaB N-terminal domain could interact with IpgC *in vitro* using complementary techniques: fluorescence polarization (FP) and isothermal titration calorimetry (ITC). For the FP experiments, we genetically introduced a single Cys at either the N- or C-terminus of IpaB$^{1-226}$ and IpaB$^{28-226}$ and fluorescently labeled the proteins with the sulhydryl-reactive dye fluorescein maleimide (FM). FP experiments suggested an interaction between IpaB's N-terminal domain and IpgC, so we further investigated that interaction using ITC with the help of our collaborators in the laboratory of Dr. Brian Geisbrecht. Data from both techniques indicated that IpaB$^{1-226}$ had a lower K_d than IpaB$^{28-226}$ for IpgC interaction, indicating that IpaB had a higher affinity for IpgC when both CBS's were present. IpaB$^{28-226}$ contains only one complete CBS and does not interact as strongly with IpgC, supporting the two CBS hypothesis. In the case of the ITC data, a 14-fold higher affinity was observed when both IpgC binding sites were present, versus a 2 to 8-fold increase based on the FP experiments. ITC data also indicated

that this interaction was energetically favorable and suggested a 1:1 stoichiometry between IpaB and IpgC. Based on these findings, we investigated the stoichiometry of binding in more detail.

Using chemical cross-linking, the Picking laboratory previously demonstrated that the two translocator proteins (IpaB and IpaC) interact with IpgC at a 1:1 stoichiometry.[144] Another group later proposed that there are two separate CBS's in IpaB and speculated that two IpgC molecules bind to one IpaB molecule.[149] We sought to address these conflicting findings, and thus designed chemical cross-linking experiments using purified IpaB fragments, IpgC, and the co-purified $IpaB^{1-94}$-IpgC and $IpaB^{1-226}$-IpgC complexes. These data agreed with previous findings from the Picking laboratory and strongly suggested a 1:1 stoichiometry between IpaB and IpgC. $IpaB^{1-226}$, $IpaB^{28-226}$, and IpgC all formed homodimers when purified independently, which agrees well with independent crystallographic studies where IpaB's N-terminus and IpgC each crystallized as homodimers.[145,146,149] Furthermore, we incubated $IpaB^{1-226}$ (possessing both CBS's) and $IpaB^{28-226}$ (possessing only one CBS) with a two-fold molar excess of IpgC and found that the products consistently had the molecular mass of the expected IpaB-IpgC heterodimer, and that the excess IpgC remained as a homodimeric complex. These data indicate that in the presence of both CBS's each IpaB molecule binds only one IpgC molecule. The thermodynamic parameters derived from the ITC experiments indicated that these heterodimers formed spontaneously via an endothermic process. The heterodimers formed are smaller in mass than the homodimers, yet an increase in FP values occurred upon IpgC addition to IpaB's N-terminal domain. The formation of a heterodimer may lend some structural rigidity to the N and C-termini of the IpaB fragments which is reflected in the FP values of the probes located at these sites. This structural rigidity would account for an increase in FP values despite formation of a product with a smaller molecular mass. What we may have observed was a decrease in the "propeller effect,"[154] which refers to the artificially low FP values observed when a fluorescent molecule is linked to a highly flexible entity. Flexibility within the termini of these fragments is likely the reason that they were

not resolved in the crystal structure of IpaB$^{74-224}$.[150] We utilized FRET to determine if a conformational rearrangement occurred within the IpaB N-terminal domain upon binding to IpgC by taking advantage of the Cys residues placed at the N- and C-termini of IpaB$^{1-226}$ and IpaB$^{28-226}$. A dramatic increase in distance between W105 and the N-terminus of IpaB^{N1-226} was observed upon IpgC addition, indicating that IpaB may adopt a more extended conformation in the region containing CBS 1 following association with IpgC.

Within the bacterial cytoplasm, IpaB remains bound to IpgC within a stable heterodimeric complex. The ATPase at the base of the T3SS provides the input of energy required to overcome the IpaB-IpgC interaction,[159] perhaps through some conformational change in one or both proteins. The data in this chapter show that IpaB and IpgC form heterodimeric complexes and, as a result, IpaB undergoes a conformational change. This is an important observation that helps to explain a poorly understood step between the construction of the nascent T3SS and the recruitment of IpaB to the T3SS needle tip.

CHAPTER III

INFLUENCE OF OLIGOMERIC STATE ON THE INTERACTION OF IPAB WITH PHOSPHOLIPID MEMBRANES

Introduction

Invasion plasmid antigen B (IpaB) is the first hydrophobic translocator protein secreted by the *Shigella* T3SS. Studies by our group have demonstrated that recombinant IpaB can exist in two distinct oligomeric states.[157] Oligomeric IpaB is co-expressed with its cognate chaperone, IpgC to maintain IpaB in a soluble state.[91,144] The translocator-chaperone complex is dissociated using either of the mild detergents N,N-dimethyldodecylamine N-oxide (LDAO) or n-octyl-oligo-oxyethylene (OPOE).[144,157] IpaB exists primarily as a monomer when prepared in LDAO, whereas it exists primarily as a tetramer when prepared in OPOE.[157] Both oligomeric states of IpaB can interact with liposomes, however, only the tetrameric state is capable of forming pores in liposomes.[157] Other groups have shown that higher-order IpaB oligomers induce pyropotosis in macrophages by forming cation-selective channels.[158] IpaB has also been shown to activate the caspase-1 mediated apoptotic pathway.[79] IpaB may be capable of existing in distinct oligomeric states depending on the stage of infection.[157]

IpaB has a hydrophobic region stretching from approximately residue 310 to 420.[160] This prediction is based on bioinformatic sequence analysis and has never been experimentally tested. To better understand the nature of IpaB's interaction with host cell membranes, we introduced

several single Cys substitution mutations throughout the length of the protein. We then purified each of these point mutants in its monomeric or tetrameric state. The Cys residues allowed for site-specific labeling with the fluorescent probe fluorescein-maleimide (FM). The modified proteins were used in fluorescence quenching experiments to determine how the solvent accessibility of each residue was affected by the oligomeric state of IpaB and by membrane interaction. Our experiments provide evidence that the membrane-interacting domain of IpaB is larger than the predicted hydrophobic region, and suggest sequences outside of the hydrophobic region of IpaB are important for oligomer formation. Interestingly, we found that the hydrophobic domain was more exposed in the soluble tetrameric state, which is capable of pore formation after membrane association. The hydrophobic region was also the most protected from quenching following liposome interaction, suggesting that the hydrophobic region does, in fact, drive membrane interaction. We also found that residues outside of the hydrophobic region are involved in pore formation.

We then sought to determine if there is a minimum part of IpaB's hydrophobic domain required for membrane interaction or pore formation. Limited proteolysis was used to reveal structural differences between the monomer and tetramer, as well as their respective membrane-associated states. We used the proteolytic products of IpaB in liposome flotation analysis and found that certain products were enriched in the liposome-containing fraction. Next, fragments with unique proteolytic termini were cloned, recombinantly expressed, and purified. These truncated forms of IpaB were evaluated for their ability to interact with and form pores in liposomes. We found that $IpaB^{11\text{-}495}$ was capable of forming pores in model membranes in both its monomeric and tetrameric states, whereas full-length IpaB can only form pores as a tetramer. The observation that $IpaB^{11\text{-}495}$ was capable of forming pores even when it was prepared as a monomer could indicate the C-terminal 85 residues regulate pore formation through an unknown mechanism.

Results

Cys mutations do not abolish IpaB activity in vivo

IpaB contains a single native Cys at position 309. This residue was mutated to Ser, and the resulting ΔCys plasmid was used as the template for generating the other Cys mutations. We generated IpaB S58C, S107C, S149C, S237C, A254C, A353C, S486C, and S519C using inverse PCR. Plasmids containing the *ipaB* variants were transformed into the *ipaB*-null strain, SF620, to determine the *in vivo* impact of the *ipaB* mutations on *Shigella* in contact-mediated hemolysis, and invasion assays. Contact-mediated hemolysis was used to determine if the Cys mutations affected *Shigella*'s ability to insert a functional translocon pore into cells (Table 2.1). The Cys mutations did not negatively affect the hemolytic ability of *Shigella* beyond modest 15% and 17% decreases for IpaB S149C and S519C, respectively. We also performed gentamycin-protection assays to measure the ability for *Shigella* expressing IpaB Cys variants to invade cultured HeLa cells (Table 2.1). This assay is a more sensitive measure of protein function within the T3SS. IpaB S107C, S149C, A254C and A353C were approximately 50% less invasive than the positive control, which is still indicative of efficient entry into cultured cells. Because these proteins did not dramatically attenuate the virulence functions of *Shigella*, we were able to confidently continue with our studies.

IpaB Cys mutants retain the previously described functions of the wild-type protein in vitro

We co-expressed IpaB S58C, S107C, S149C, S237C, A254C, A353C, S486C, and S519C, as well as the wild-type IpaB which contains a Cys at 309 in *E. coli* with IpgC. IpaB was then separated from IpgC using the mild detergents LDAO and OPOE, giving rise to a monomeric or tetrameric state of the protein, respectively. As an indicator of protein function, the capacity for IpaB to form pores *in vitro* was measured by a liposome disruption assay (Figure 2.1). In this assay, defined liposomes containing 100 mM sulforhodamine-B (SRB) are prepared.

Table 2.1. Contact-Hemolysis and Invasion by *Shigella* Expressing *ipaB* variants.

Shigella strain	Hemolysis[a]	Relative Invasion[b]
SF620	3.2 ± 0.2	0.7 ± 0.6
SF620 + WT *ipaB*	100 ± 11.8	100.0 ± 8.8
SF620 + S58C	114.5 ± 4.0	88.7 ± 23.0
SF620 + S107C	94.4 ± 1.9	43.3 ± 8.3
SF620 + S149C	85.2 ± 3.4	43.5 ± 12.3
SF620 + S237C	112.0 ± 4.0	93.3 ± 8.4
SF620 + S254C	93.1 ± 8.3	52.4 ± 6.1
SF620 + A353C	94.4 ± 5.2	45.7 ± 6.1
SF620 + S486C	97.8 ± 1.8	80.8 ± 7.9
SF620 + S519C	83.2 ± 3.4	103.1 ± 21.4

[a]Contact-mediated hemolysis using sheep red blood cells was performed to determine the impact of individual Cys mutations on IpaB's ability to be delivered into target cell membranes by *Shigella*.[161] [b]A gentamycin-protection assay using HeLa cells was performed to determine the impact of single Cys mutations on *Shigella*'s invasive capacity. The positive control was SF620 transformed with native *ipaB* (100% relative invasion). The values shown are an average (n = 3) from a representative experiment ± standard deviation. WT = Wild-type.

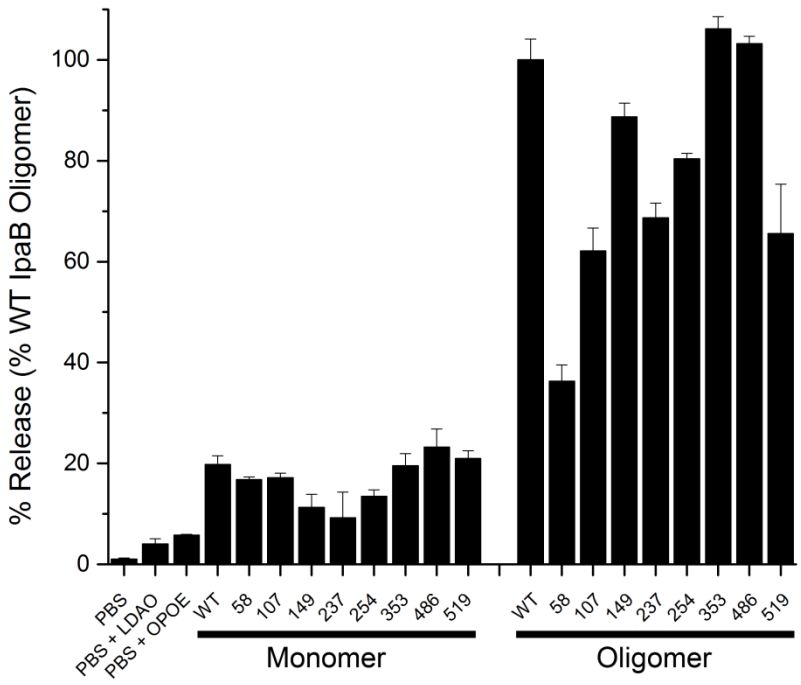

Figure 2.1 Fluorophore release by IpaB Cys variants. Recombinant IpaB mutants were evaluated for their ability to cause release of SRB from liposomes as detailed in experimental procedures. Error bars represent standard deviations (n = 3). Tetrameric wild-type IpaB (WT) prepared in OPOE was used as a positive control and all values shown are relative to this level of SRB release. Addition of buffer alone (PBS) was used as a negative control.

Due to the high concentration of SRB within the liposomes, SRB is autoquenched. When SRB is released from the liposomes an increase in fluorescence emission signal is observed as the autoquenching is relieved.[162] Previous studies demonstrated that the monomeric IpaB does not lead to a substantial release of SRB from liposomes, indicating that the monomeric protein is incapable of forming a pore. Tetrameric IpaB, on the other hand, is capable of forming pores and leads to a substantial release of fluorophore. Thus, we used this assay to evaluate the *in vitro* ability for the IpaB Cys variants to form pores in liposomes (Fig 2.1). We found that the monomeric IpaB Cys variants did not lead to substantial release of fluorophore, whereas the tetrameric form of each protein did promote pore formation. IpaB S58C had a reduced ability to form pores, which is interesting since this mutant was fully hemolytic when tested *in vivo*. The rest of the IpaB Cys variants were at least 60% as effective as the wild-type protein. Therefore, we were confident that the Cys mutations did not abrogate the *in vitro* function of IpaB.

Impact of oligomerization on the accessibility of various regions of IpaB

Monomeric and tetrameric IpaB Cys variants were labeled with fluorescein-maleimide (FM) and used in fluorescence quenching experiments. Potassium iodide (KI) was used as the quenching agent. The resulting data were plotted using the Stern-Volmer equation and fit to a linear regression (Equation 3). The slope of the linear regression represents the Stern-Volmer quenching constant (K_{SV}, Table 2.2). The K_{SV} is a measure of the accessibility of a fluorophore to a quenching agent. To aid in data interpretation, we calculated a protection index (PI, Equation 4) for each position, in this case using the oligomeric state of IpaB as the variable (Figure 2.2). A PI = 1 indicates no change in the solvent accessibility of a particular residue, whereas a PI > 1 or PI < 1 indicates that the fluorophore was less available or more available for quenching relative to the variable condition, respectively.[163] In Figure 2.2, residues 58 and 519 were the most protected positions in the tetramer relative to the monomeric state. This means that the K_{SV} of the tetramer was lower than the K_{SV} for the monomer, resulting in a numerical (PI) value > 1. The solvent

Table 2.2. K_{SV} Values for the Quenching of IpaB by Iodide.

	K_{SV}			
	- Liposomes		+ Liposomes	
Mutant	**Monomer**	**Tetramer**	**Monomer**	**Tetramer**
S58C	6.68 ± 0.11	4.81 ± 0.02	6.62 ± 0.11	4.41 ± 0.02
S107C	5.26 ± 0.19	5.21 ± 0.01	3.98 ± 0.04	3.94 ± 0.02
S149C	7.26 ± 0.18	6.39 ± 0.09	6.22 ± 0.13	5.99 ± 0.07
S237C	5.29 ± 0.06	4.63 ± 0.02	4.01 ± 0.05	4.16 ± 0.02
A254C	7.07 ± 0.24	6.53 ± 0.16	5.66 ± 0.18	5.94 ± 0.13
WT (309C)	4.91 ± 0.05	5.24 ± 0.11	3.96 ± 0.06	3.41 ± 0.04
A353C	4.79 ± 0.02	7.08 ± 0.08	3.29 ± 0.02	3.97 ± 0.02
S486C	5.23 ± 0.07	5.57 ± 0.03	4.62 ± 0.06	4.24 ± 0.02
S519C	5.84 ± 0.04	4.82 ± 0.06	4.71 ± 0.04	4.28 ± 0.03
Carboxyfluorescein (CF)	10.83 ± 0.42		10.69 ± 0.38	

100 nM FM-labeled IpaB was subjected to fluorescence quenching using KI as described in Experimental procedures. Shown here are representative K_{SV} values with standard errors (n = 3). WT = wild-type.

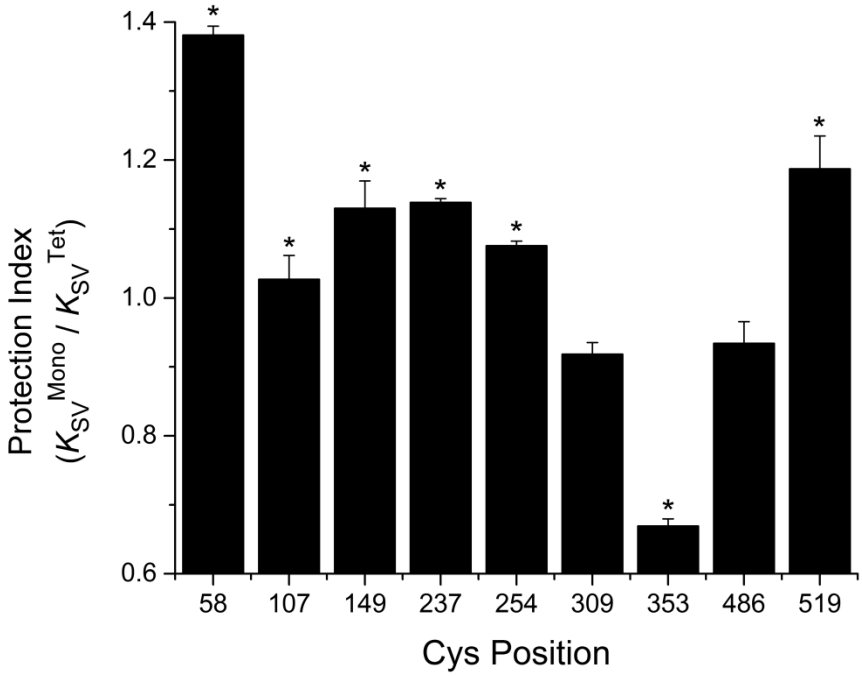

Figure 2.2 Oligomeric state affects the accessibility of quenching agent to the hydrophobic region of IpaB. FM-IpaB (100 nM) prepared in LDAO (monomeric) and OPOE (oligomeric) was quenched by titration of KI in the absence of liposomes. The protection index (PI) for oligomer formation was calculated using K_{SV}^{Mono} / K_{SV}^{Tet} as described in Materials and Methods. Error bars represent standard deviation of the PI's derived from at least three independent experiments performed in triplicate. Statistically significant differences are indicated by *, $P <$ 0.02 when tested against the native Cys (309) using the *t* test.

accessibility of residue 107 was unaffected by the change in oligomeric states, indicating that it exists in a similar environment in the monomer and tetramer. The data reflect relatively small increases in the protection of residues 149, 237, and 254 in the tetrameric form of IpaB relative to the monomer.

The most striking result here is the low PI value for residue 353. The low PI indicates that this residue was actually more exposed to solvent than in the monomeric state. This is surprising because residue 353 is located in the heart of the hydrophobic domain. The nearest residues, 309 and 486, were also slightly less protected in the tetrameric form of IpaB. Residue 486 lies outside of the predicted hydrophobic region (residues 310-420). Taken together, these data may reveal protein-protein contacts important for IpaB's organization as a tetramer are located outside of the hydrophobic region and that the hydrophobic region of IpaB is most exposed to solvent in the tetrameric complex.

The hydrophobic domain is protected by liposome interaction.

Above it was shown that all of the IpaB Cys mutants interacted with liposomes *in vitro* and that the monomer and tetramer interact with liposomes in different ways, *i.e.* interaction vs. pore insertion (Figure 2.1). Therefore, we sought to determine the impact of liposome interaction on the accessibility of the FM probes conjugated to each of the IpaB Cys residues to the polar quenching agent KI (Figure 2.3). Each FM-IpaB variant was incubated with liposomes, and then KI was titrated into the samples to progressively quench the FM fluorescence. We used these data to calculate the K_{SV} for each Cys position and then determined the PI caused by interaction with the liposomes (Equation 5). Carboxyfluorescein, a water-soluble fluorescein derivative, was used as a control for the impact of liposomes on the emission properties of fluorescein.

The K_{SV} changes seen following liposome addition gave rise to an interesting observation for the FM at residue 353. This residue is within the hydrophobic domain of IpaB and was the

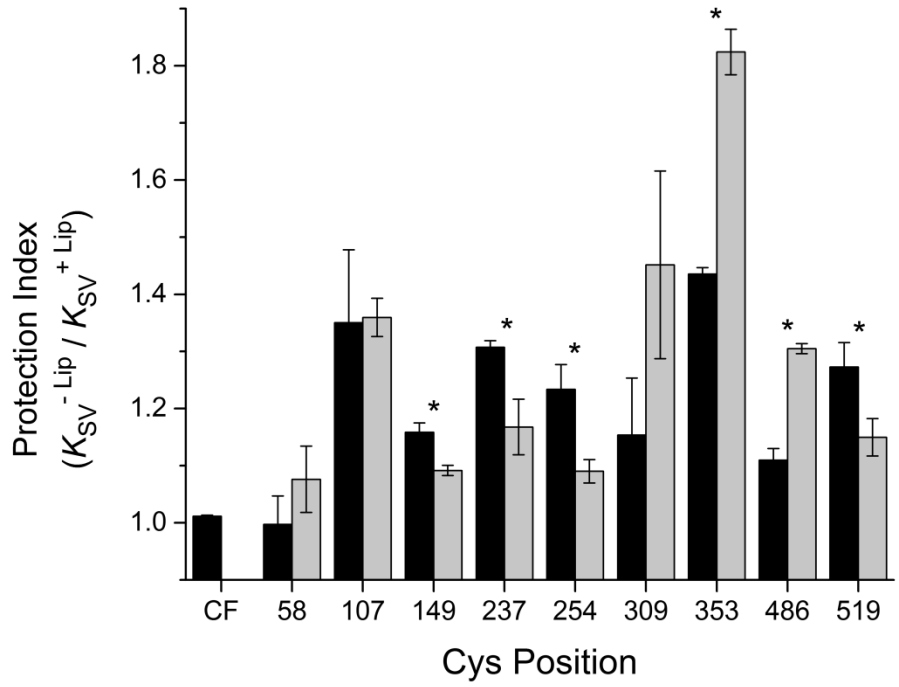

Figure 2.3 Protection of FM-labeled IpaB mutants from KI quenching by liposome association. Monomeric and oligomeric FM-IpaB (100 nM) was subjected to quenching in the absence or presence of liposomes composed of 1,2-dioleoyl-sn-glycero-3-phosphocholine (DOPC), 1,2-dioleoyl-sn-glycero-3-[phosphor-rac-(1-glycerol)] (DOPG), and cholesterol. The protection index (PI) for liposome association was calculated using K_{SV}^{-Lip} / K_{SV}^{+Lip} for each FM-labeled IpaB point mutant in both the monomeric (black bars) and tetrameric (shaded bars) states. Carboxyfluorescein (CF) was used as a control to demonstrate that the addition of liposomes does not arbitrarily affect the quenching of fully exposed fluorescein. Error bars represent standard deviation of the PI's derived from three independent experiments performed in triplicate. Statistically significant differences between the monomer and tetramer for each IpaB variant are indicated by *, $P < 0.05$ using the *t* test.

most solvent exposed residue for the IpaB tetramer (Figure 2.2), however, it showed the greatest PI increase of all samples tested upon incubation with liposomes. Monomeric IpaB A353C also showed a substantial PI increase upon liposome addition, but not to the extent of that seen for the tetramer. Residue 309 and 486 were also significantly more protected by liposomes for the tetramers relative to the monomeric forms of IpaB. Collectively, the data suggest that residues 309, 353, and 486 are involved in membrane penetration and this is especially clear for the IpaB tetramers.

It is worth noting that residues 149, 237, 254, and 519 were more protected from quenching agent by liposomes for monomeric IpaB than for the tetramer. The significance of this observation is not clear, but it may reflect differences in the modes of liposome interaction of monomeric IpaB vs. tetrameric IpaB. IpaB S107C was not differentially protected depending on its oligomeric state, which agrees well with the protection by oligomerization PI = 1 (Figure 2.2), however, it was protected by liposome interaction. This residue lies within IpaB's highly soluble N-terminal domain, so it would seem unlikely that this region of IpaB actually initiates membrane interaction and liposome flotation experiments with $IpaB^{28-226}$ indicated that it does not interact with liposomes.[157] Also, none of the nearby Cys residues were substantially protected from quenching by liposomes, supporting the notion that residue 107 is not driving membrane interaction. Residue 58 was not protected by liposomes, consistent with being in a highly soluble region of IpaB.

Limited Proteolysis reveals structural differences between monomeric and tetrameric IpaB

We hypothesized that structural differences exist between monomeric and tetrameric IpaB, and that membrane interaction could cause changes in IpaB's conformation. Samples containing wild-type monomeric and tetrameric IpaB were prepared in the presence or absence of

liposomes, after which the samples were exposed to subtilisin-A, a serine-protease, for a defined period of time.

Monomeric IpaB was more resistant to proteolysis than tetrameric IpaB as indicated by the persistence of higher-mass products in Figure 2.4. Incubation with liposomes, however, led to rapid degradation of monomeric IpaB to a 40 kDa product and a pattern that was similar to that observed for tetrameric IpaB. This suggests that the protease cleavage sites are readily available in the membrane-inserted condition. Tetrameric IpaB was rapidly degraded to a 40-kDa product regardless of whether the liposomes were present, and this degradation was slightly expedited in the presence of liposomes. It is possible that LDAO impacts the activity of subtilisin-A. To address this, a T3SS protein that does not interact with liposomes, IpaD, was used as a control to determine if LDAO was impacting subtilisin-A activity (Figure 2.5). IpaD was degraded to a similar extent in the presence of LDAO or OPOE. Therefore, the detergents did not influence the proteolytic activity of subtilisin-A.

Identification of IpaB fragments that retain liposome interaction activity

To better define what regions of IpaB interact with liposomes, we designed limited proteolysis experiments. Monomeric IpaB was digested with subtilisin-A and the reaction was stopped by adding the protease inhibitor AEBSF. The resulting IpaB peptides were incubated with liposomes that were then floated over a sucrose density gradient to isolate peptides able to interact with liposomes. After separation of the bottom and top fractions of the gradient, the proteins were concentrated by trichloroacetic acid precipitation. SDS-PAGE analysis of the precipitated proteins revealed three distinct bands of 40 kDa, 37 kDa, and 30 kDa that co-migrated with the liposomes (Figure 2.6). These three bands were also found in the bottom of the gradient with an additional band at 25 kDa. Samples were submitted for mass spectrometric (MS)

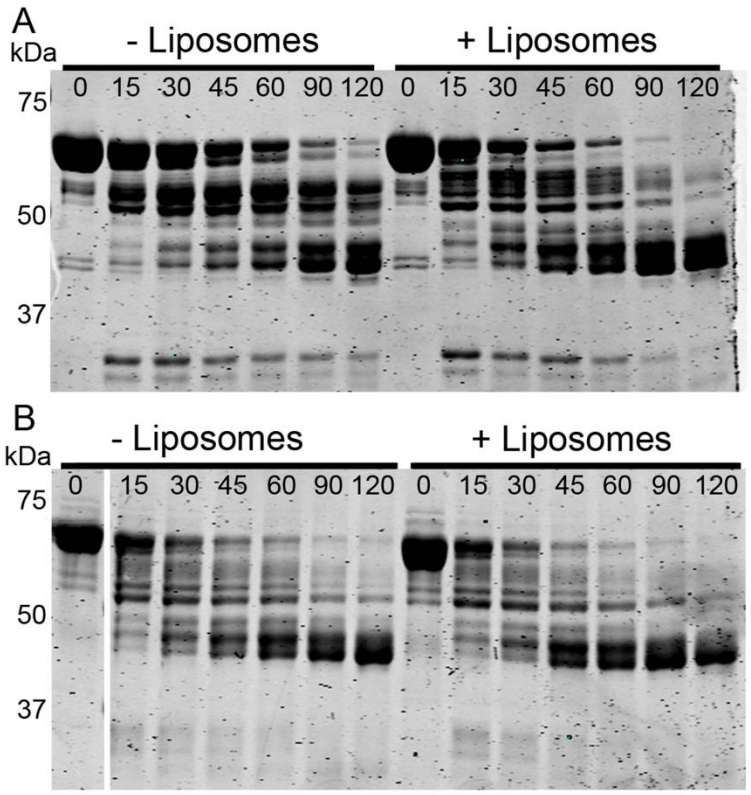

Figure 2.4. Susceptibility of IpaB to proteolysis is influenced by oligomeric state and liposome interaction. Monomeric (A) or tetrameric (B) IpaB was subjected to proteolysis by subiltisin-A in the absence or presence of liposomes, as indicated above the gel images. Samples were analyzed on 12% SDS-PAGE gels. Time points (in seconds) are indicated above each lane in the gels. Gels were stained with Coomassie blue R250 and imaged on an Odyssey infrared imager (LI-COR, Lincoln, NE) to detect low-abundance products.

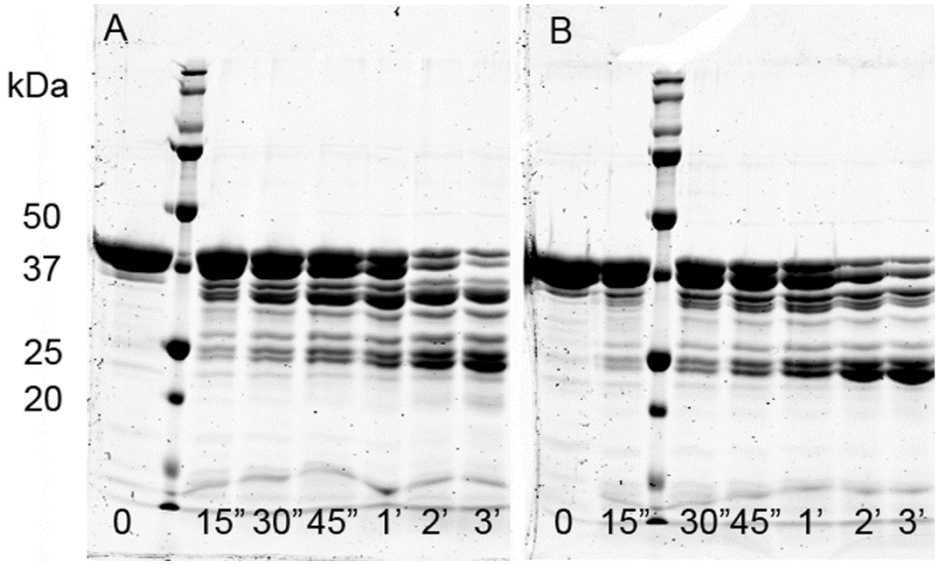

Figure 2.5. Limited proteolysis of IpaD. IpaD in (A) PBS + 0.05% LDAO or (B) PBS + 0.5% OPOE was diluted to 0.4 mg/ml. Subtilisin-A was added at a final dilution of 1:160,000 (relative to the subtilisin-A stock). Aliquots were removed from the digestion and placed into 99° C 3x SDS-PAGE sample buffer at the time points indicated below each lane. Samples were analyzed on 12% SDS-PAGE gels. Gels were stained with Coomassie blue R250 and imaged on an Odyssey infrared imager (LI-COR, Lincoln, NE) to detect low-abundance products. Molecular masses in kDa are indicated on the left.

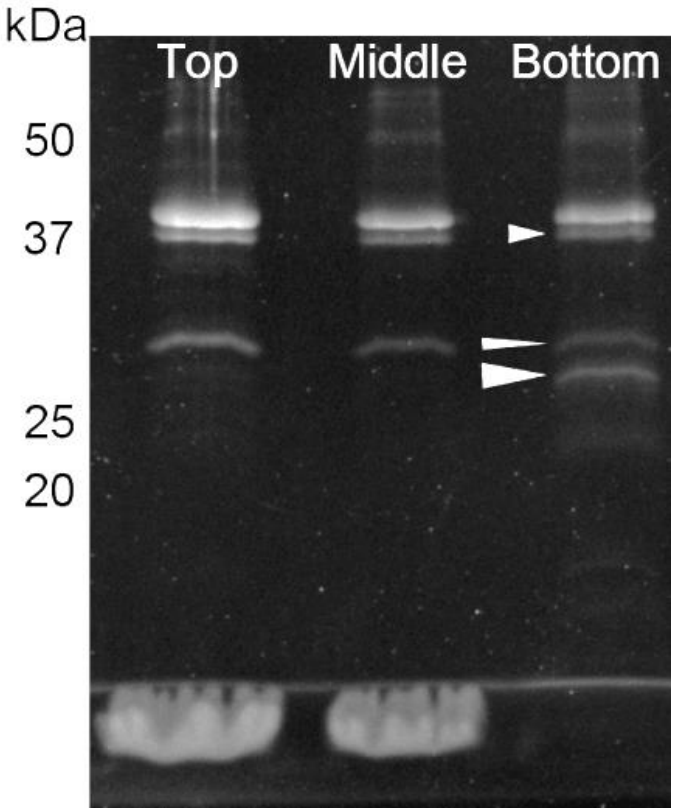

Figure 2.6 Flotation following limited proteolysis of IpaB. IpaB was exposed to subtilisin-A for 30 seconds and placed on ice after the addition of 20 mM AEBSF. Top, middle, and bottom fractions were collected from the gradient. Fractions were analyzed by SDS-PAGE. The gel was stained with Oriole fluorescent gel stain (Biorad). The large, diffuse band at the bottom of the two leftmost wells is liposomes. Molecular mass is indicated on the left, in kDa. Small arrowhead = 37 kDa band; thin arrowhead = 30 kDa band; large arrowhead = 25 kDa band.

analysis, which identified several IpaB peptides with unique cleavage sites. Unfortunately, there was overlap among the bands, which prevented confident identification of each band. The MS analysis, while not conclusive, did highlight peptides that warranted further investigation. Thus, we generated recombinant IpaB$^{11\text{-}312}$, IpaB$^{11\text{-}357}$, IpaB$^{11\text{-}390}$, and IpaB$^{11\text{-}495}$. The truncated proteins were used for co-expression with IpgC in *E. coli* Tuner (DE3) and all of them could be co-expressed successfully with IpgC, except for IpaB$^{11\text{-}495}$. To generate IpaB$^{11\text{-}495}$, we introduced a tobacco etch virus (TEV) protease site into IpaB$^{11\text{-}580}$ (IpaB$^{11\text{-}580\ \text{TEV}\ 495}$). The resulting gene was co-expressed with IpgC as before, purified, and then the IpaB$^{11\text{-}580\ \text{TEV}\ 495}$- IpgC complex was digested with TEV protease to generate an IpaB$^{11\text{-}495}$-IpgC complex. The truncated forms of IpaB were purified as IpaB-IpgC complexes and were then separated from the chaperone using LDAO or OPOE, which for the full-length protein gives rise to monomeric and tetrameric states of IpaB, respectively. Both detergents were used separately to determine if the truncated proteins behaved differently in the two detergents. Each protein was analyzed by liposome flotation, and it was found that all of the proteins interacted with liposomes as indicated by their presence in the liposome-rich "top" fraction (Figure 2.7). IpaB$^{11\text{-}312}$ had a reduced affinity for liposomes, which is likely because it lacks a substantial part of the hydrophobic region. IpaB$^{11\text{-}357}$, IpaB$^{11\text{-}390}$, and IpaB$^{11\text{-}495}$ interacted with liposomes to an extent similar to that of wild-type IpaB.

The truncated forms of IpaB were next analyzed by chemical crosslinking to determine if they were capable of oligomer formation. The fluorescence quenching data presented above suggest that the termini of IpaB are implicated in IpaB oligomerization (Figure 2.2), so we used these truncated forms of IpaB to explore that possibility. Other *in vivo* studies have implicated the extreme C-terminus of IpaB in forming the interactions necessary to maintain IpaB on the needle tip.[164] IpaB$^{11\text{-}312}$ formed mostly monomers with and a minor population of dimers, whereas IpaB$^{11\text{-}357}$ formed mostly dimers with a minor population of monomers in both LDAO and OPOE (Figure 2.8A). IpaB$^{11\text{-}390}$ formed dimers and formed tetramers (Figure 2.8B). IpaB$^{11\text{-}495}$ behaved

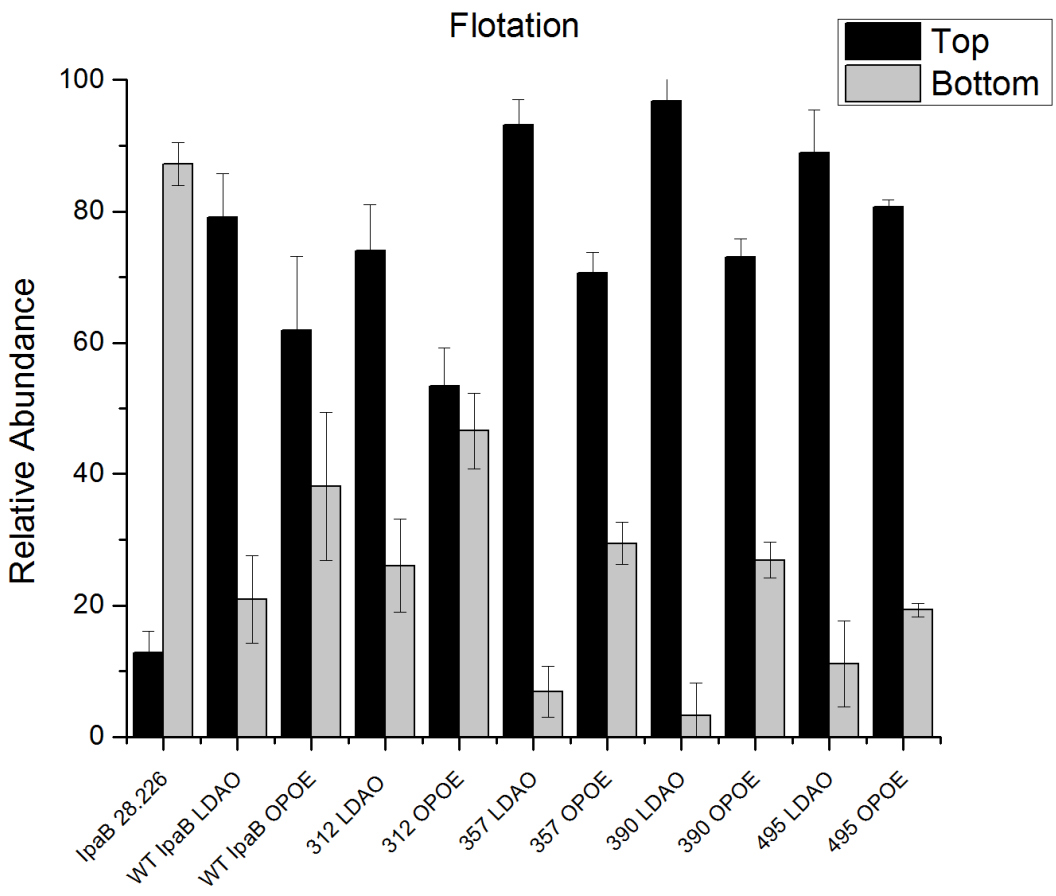

Figure 2.7 Floatation analysis of truncated forms of IpaB. Truncated forms of IpaB were used at a final concentration of 3 µM and were incubated with 4.4 mg/ml liposomes followed by separation on a sucrose density gradient. Top and bottom fractions were collected and analyzed by SDS-PAGE. Gels were stained with Oriole fluorescent gel dye (Biorad) and quantified by densitometry. Data are presented as averages of at least three independent experiments. Error bars represent standard deviations (n = 3).

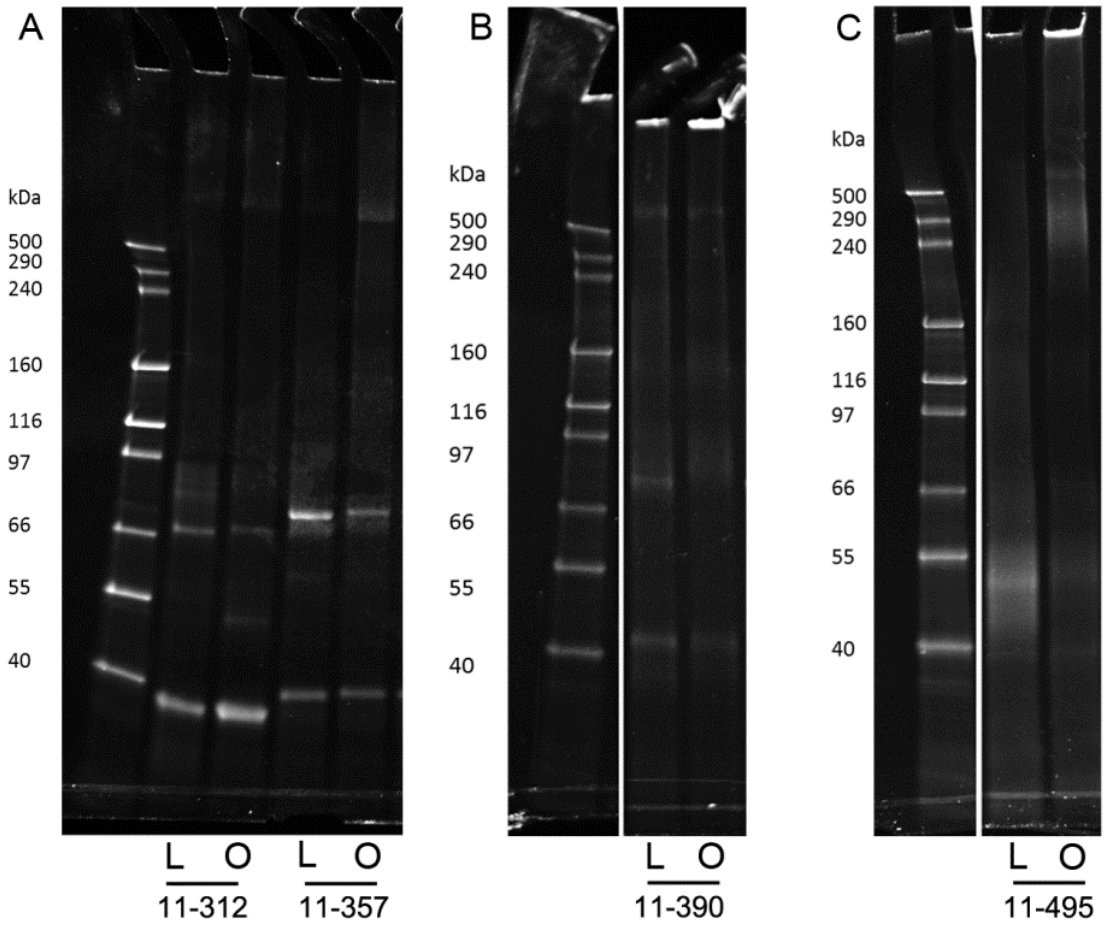

Figure 2.8 Cross-linking of truncated forms of IpaB. IpaB$^{11\text{-}312}$ and IpaB$^{11\text{-}357}$ (Panel A),IpaB$^{11\text{-}390}$ (Panel B), and IpaB$^{11\text{-}495}$ (Panel C) were separated from IpgC with either LDAO (L) or OPOE (O). 5 μM protein was cross-linked with DSP and separated on a 4-20% gel and stained with Oriole fluoresecent gel stain (Biorad). Molecular masses are indicated on the left hand side of each panel.

much like wild-type IpaB,[157] where in LDAO it formed mostly monomers and in OPOE it formed mostly tetrameric complexes (Figure 2.8C). IpaB$^{11\text{-}495}$ and IpaB$^{11\text{-}390}$ in OPOE formed aggregates too large to enter the gel, but not when prepared in LDAO, perhaps reflective of the tendency for LDAO to prevent aggregation of IpaB.[157] These data suggest that the C-terminal 85 residues are not necessary for oligomerization. Next the truncated forms of IpaB were evaluated for their capacity to form pores in liposomes (Figure 2.9). We found that IpaB$^{11\text{-}495}$ promoted release of SRB, whereas the other truncated forms of IpaB did not. IpaB$^{11\text{-}312}$ in OPOE may promote release of fluorophore, but this activity varies as indicated by the large error bars. We expected that tetrameric IpaB$^{11\text{-}495}$ would form pores since full-length IpaB behaves in this way, however, we found that monomeric IpaB$^{11\text{-}495}$ also released nearly 60% of the total fluorophore. Full-length, monomeric IpaB does not release substantial amounts of fluorophore. This could indicate that the C-terminal 85 residues of IpaB play a role in regulating pore formation.

Incubation with liposomes imposes ordered oligomerization on IpaB

To determine if liposome interaction affected the oligomeric state of IpaB, monomeric or tetrameric IpaB$^{11\text{-}495}$ and full-length IpaB were incubated with liposomes and cross-linked with the chemical cross-linking agent Bis[sulfosuccinimidyl] suberate (BS3). BS3 was chosen because it is polar and does not cross lipid membranes. When monomeric IpaB was cross-linked without liposomes, it remained mostly monomeric, with a small amount of dimer (Figure 2.10 A). When incubated with liposomes, the monomer transitioned to products with masses consistent with tetramers and octomers. These data suggest that monomeric IpaB is capable of self-organizing within a lipid membrane to form a higher-order oligomer.

IpaB prepared in OPOE forms primarily tetramers when cross-linked with DSP.[157] Oligomeric IpaB cross-linked with BS3 in the absence of liposomes, however, formed mostly tetramers and octomers, along with complexes too large to enter the gel. Interestingly, when

oligomeric IpaB was incubated with liposomes, it formed monomers, dimers, tetramers, and octomers. Only small amounts of immeasurable products were formed. These data suggest that liposome interaction maintains IpaB as a tetramer or octomer. However, the large proportion of monomer in the presence of liposomes suggests the possibility that liposome interaction may interfere with the cross-linking of the tetramer via steric shielding of reactive residues.

IpaB$^{11\text{-}495}$ behaved in a similar way to full-length IpaB. IpaB$^{11\text{-}495}$ prepared with LDAO forms a monomer in solution, but when incubated with liposomes it forms a series of oligomers, some consistent with dimers, tetramers, and octomers (Figure 2.11). When prepared with OPOE, IpaB$^{11\text{-}495}$ forms tetrameric complexes and higher-order aggregates. Oligomeric IpaB$^{11\text{-}495}$ becomes more ordered when incubated with liposomes, where it does not form a large number of higher ordered aggregates (Figure 2.11).

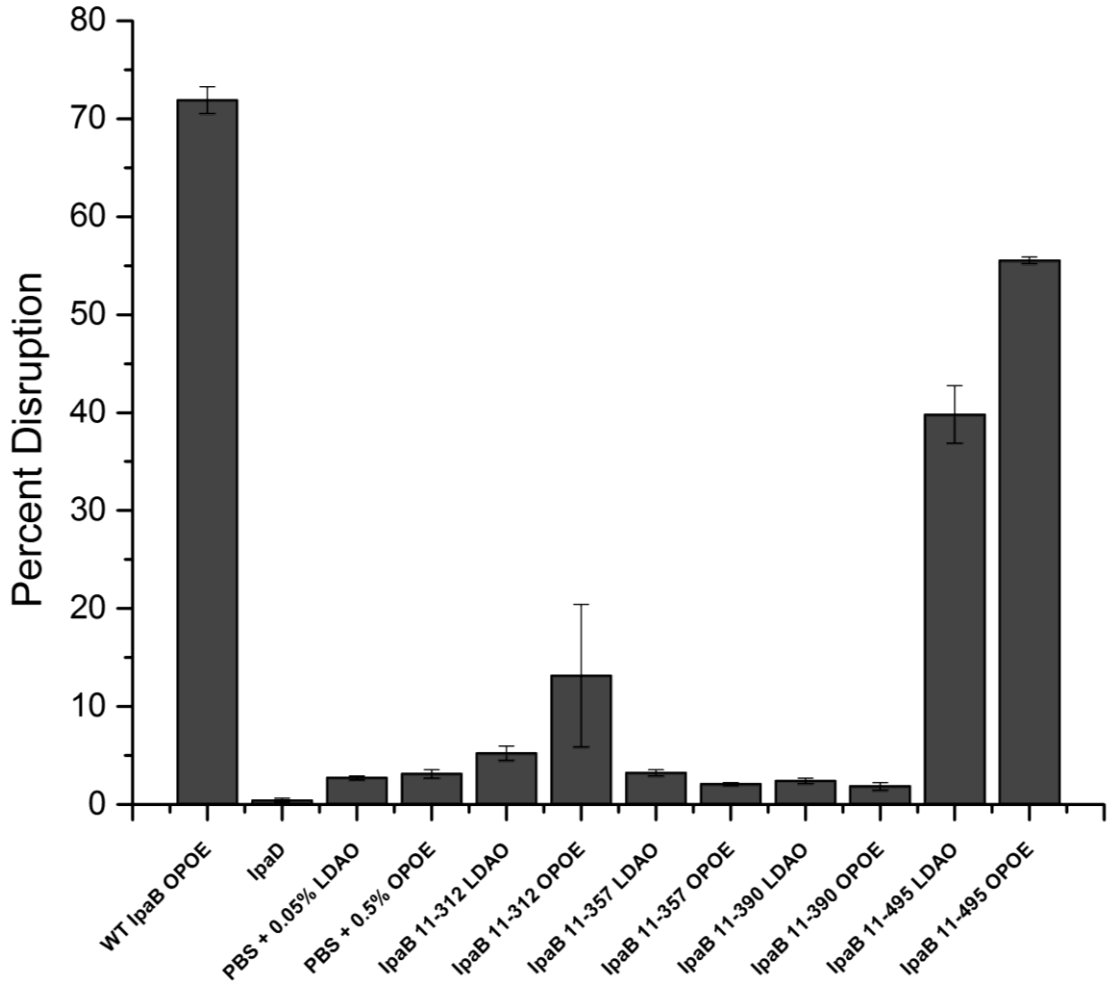

Figure 2.9 Liposome disruption experiments using the truncated forms of IpaB. 100 nM truncated forms of IpaB were added to liposomes containing 100 mM sulforhodamine-B (SRB). SRB release was monitored for 4 min, after which all dye was released by the addition of 0.1% Triton X-100. Percent release was calculated by dividing the fluorescence intensity after Triton addition by the fluorescence intensity immediately prior to Triton addition, multiplied by 100. Results presented are the average of at least three independent experiments (n = 3). Error bars indicate the standard deviation.

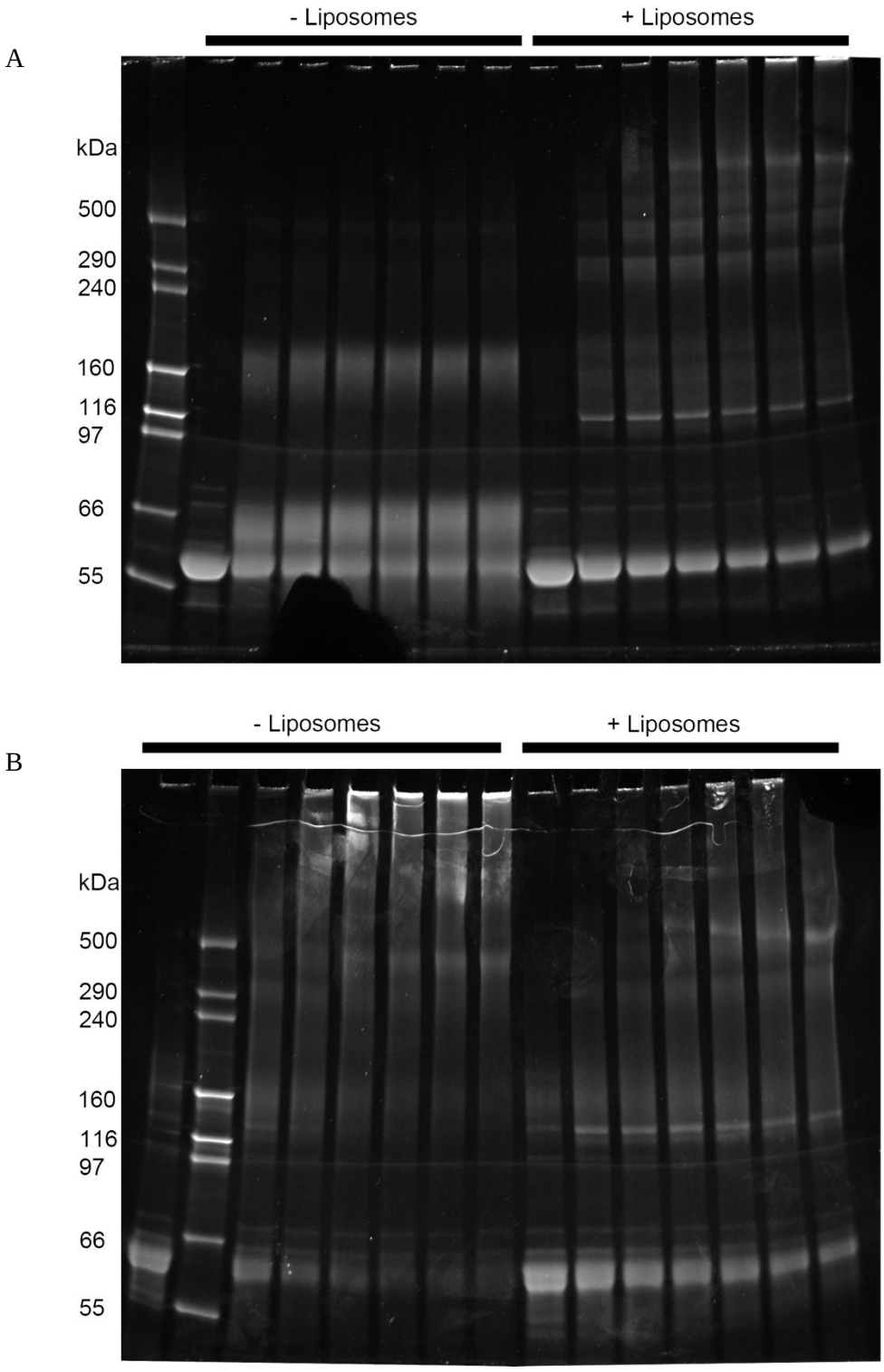

Figure 2.10 Impact of liposome association on the oligomeric state of IpaB. 5 μM monomeric (A) and tetrameric (B) were incubated for ten minutes with or without 7.0 mg/ml

Continued (Figure 2.10 legend)

liposomes. Then the chemical cross-linking agent BS3 was added to a final concentration of 200 μM. Samples were removed every five minutes and placed in 3x SDS-PAGE sample buffer to quench the reaction. Cross-linked products were separated on a 4-20% TGX gradient gel (Bio-Rad). From left to right, the lanes represent samples taken at 0 (before cross-linking), 5, 10, 15, 20, 25, and 30 min. The gel was stained with Oriole fluorescent gel stain (Biorad). Molecular masses are indicated by the ladder in the first or second lane of each gel in kDa.

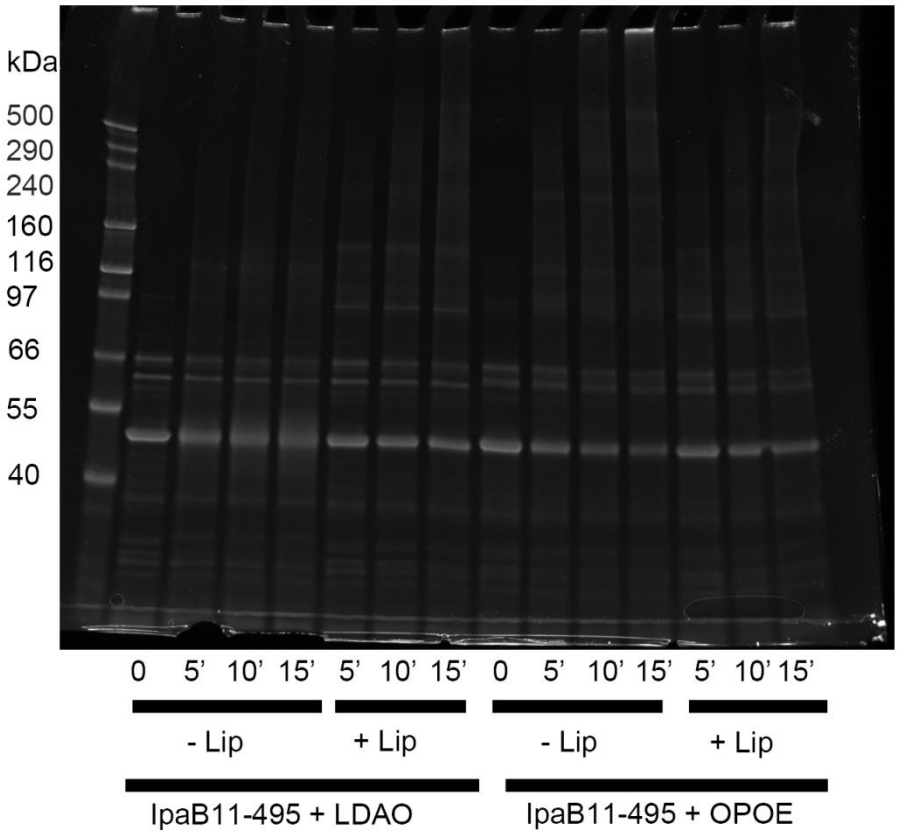

Figure 2.11. Cross-linking IpaB$^{11\text{-}495}$ reveals similarities to full-length IpaB. IpaB$^{11\text{-}495}$ prepared in either 0.05% LDAO or 0.5% OPOE was incubated in the absence or presence of liposomes and then cross-linked with BS3. Cross-linked products were separated on a 4-20% TGX gradient gel (Bio-Rad). The time points are indicated across the bottom of the gel. Molecular masses (in kDa) are indicated on the left. – Lip = no liposomes; + Lip = + liposomes.

Conclusions

The data presented in this chapter illuminated some aspects of IpaB's interaction with itself and with lipid membranes. The quenching data suggested that the oligomeric state affects the extent to which residues within the hydrophobic domain interact with membranes. The hydrophobic domain is critical to protein structure because deleting nearly any part of this region leads to loss of invasion function.[160] Quenching and proteolytic data suggest that IpaB regions in addition to the described hydrophobic domain are involved with membrane interactions. C-terminally truncated forms of IpaB also suggested a novel role for the C-terminal 85 residues in controlling pore function. Collectively, these data were used to provide an updated model of IpaB's interaction with itself and with membranes (Figure 2.12).

The hydrophobic domain is more solvent exposed upon IpaB oligomerization than it is for the monomer, whereas the termini are less exposed. This suggested that IpaB oligomerization could be due to specific protein-protein interactions within the hydrophilic termini instead of nonspecific hydrophobic collapse. However, we found that $IpaB^{11-495}$ could oligomerize in OPOE, suggesting that the C-terminal 85 residues are dispensable for oligomer formation. The relative size of the full-length IpaB tetrameric complex and ability to form pores is consistent with this complex being the one observed at the T3SS needle tip. IpaD is a pentamer at the T3SS needle tip[165] and it is predicted that an IpaB tetramer would fit on top of the IpaD pentamer based on computations that account for molecular mass and the predicted structure of IpaB (Epler, C.R. and Bullit, E., unpublished observations). This is speculative and this hypothesis is currently being tested. The experimental data here lead one to speculate that exposure of a hydrophobic region to solvent, an energetically unfavorable event, may occur at the T3SS needle tip in preparation for host cell contact. This is further supported because the increased solvent accessibility of the hydrophobic region is lost upon liposome interaction. Collectively, these data suggest that the hydrophobic domain plays a central role in IpaB translocon pore formation.

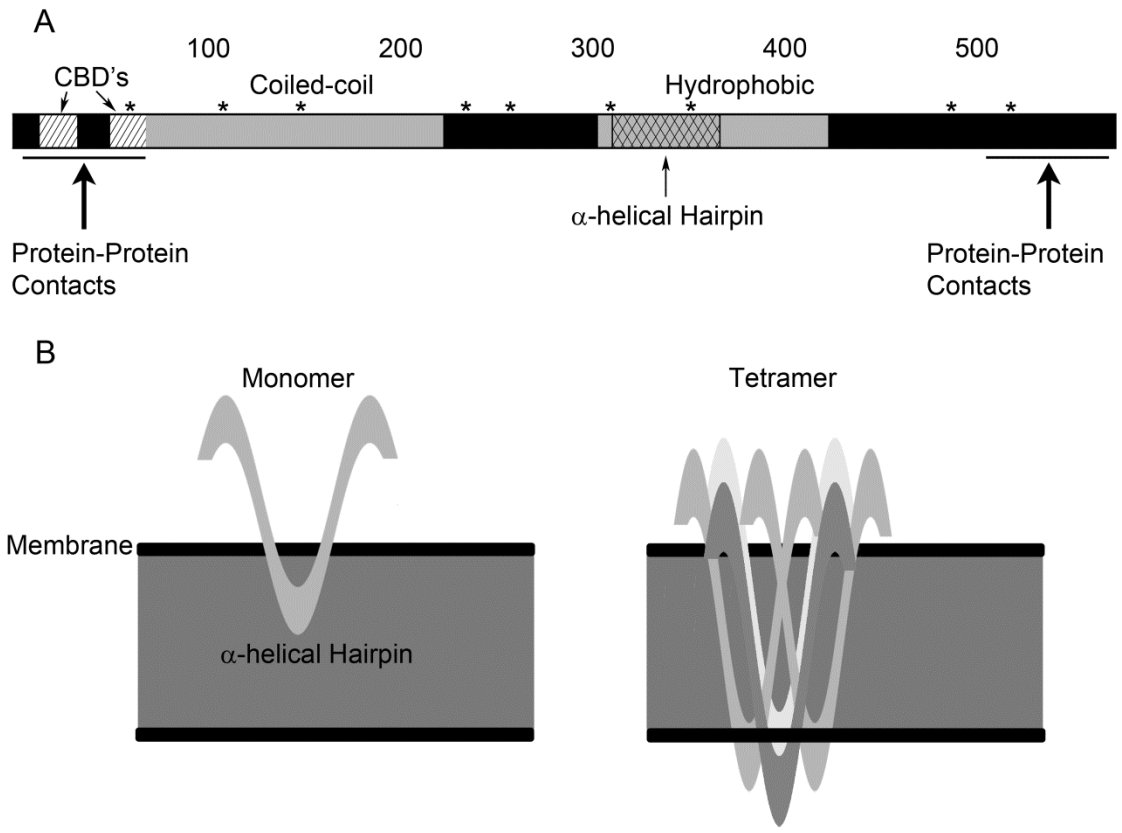

Figure 2.12. Functional organization of IpaB with regard to oligomerization, chaperone binding and membrane association. (A) IpaB is shown as a single bar with regions believed to be involved in specific macromolecular interactions. Residue numbers (100, 200, etc.) are indicated above the bar. Chaperone-binding domains (CBD's) based on experiments performed using a soluble IpaB fragment are indicated near the N-terminus. This region and sequences near the C-terminus may also be involved in protein-protein contacts (large arrows). A coiled-coil domain for which a crystal structure has been solved is also located in the N-terminal half of IpaB. Less is known about the structure of the C-terminal half of IpaB which contains a prominent hydrophobic region. It is in this region that IpaB may possess a hydrophobic α-helical hairpin (indicated) similar to what has been observed in colicins. (B) A closer look at the possible position of monomeric (left) and tetrameric (right) IpaB within the eukaryotic membrane.

Continued (Figure 2.12 legend)

Initial contact may occur via the immediate region surrounding residue 353 with the oligomeric arrangement of the protein then allowing a more intimate interaction with the hydrophobic core of the membrane.

The recent crystal structure of IpaB$^{74-224}$ indicates that the N-terminal domain of IpaB is a long coiled-coil and a similar finding was made for the IpaB homolog from *Salmonella*, SipB residues 82-226.[150] When queried against a structural homology search engine, both IpaB's and SipB's N-terminal domain shared a high degree of structural homology with the corresponding coiled-coil region of colicin Ia, a bacterial pore-forming toxin.[150] Upon further analysis, it was found that regions within the highly-conserved hydrophobic domains[160,166] of each protein, residues 310-370 of IpaB and 320-380 of SipB, shared sequence homology with an α-helical hairpin in the pore-forming domain of colicin Ia. The α-helical hairpin serves to anchor colicin Ia in the target membrane.[167] IpaB residue 353 lies within the predicted α-helical hairpin motif. Residue 353 was the most protected residue by liposome interaction for both the monomeric and tetrameric states. Residues 309 and 486 also appeared to be important for pore formation. Similar to IpaB, colicin Ia oligomerizes prior to forming a pore.[168] One could speculate that the α-helical hairpin plays a similar role in IpaB, which is supported by the high PI of IpaB A353C. The similarities between IpaB and colicin Ia are striking.

Limited proteolysis was used because the quenching experiments suggested structural differences between the monomer and tetramer. Structural differences between the two states were supported by the proteolysis data. Surprisingly, the tetramer was more sensitive to proteolytic degradation than the monomer. The monomer may adopt a more compact structure that protects the hydrophobic region, rendering it less susceptible to proteolysis. In contrast, the proteolytic pattern of the monomer was substantially altered after incubation with liposomes. The proteolytic pattern of tetrameric IpaB was not significantly impacted by liposome interaction, suggesting that the subtilisin recognition sites are not masked by liposomes and no conformational change was detectable.

To further define what parts of IpaB interact with liposomes, we generated the following truncated forms of IpaB: IpaB$^{11-312}$, IpaB$^{11-357}$, IpaB$^{11-390}$ and IpaB$^{11-495}$. All of these proteins

interacted with liposomes, however, the protein with the smallest portion of the hydrophobic domain, IpaB$^{11-312}$, had a decreased ability to do so. IpaB$^{11-390}$ and IpaB$^{11-495}$ were capable of forming oligomeric species when prepared in OPOE. Cross-linking analysis revealed that IpaB$^{11-495}$ in LDAO or OPOE formed almost exclusively monomers or tetramers, respectively. Interestingly, IpaB$^{11-495}$ formed pores even when prepared as a monomer, which is attributable to the formation of oligomers when incubated with liposomes. This stands in contrast to monomeric full-length IpaB, which forms oligomers in liposomes, but is unable to form functional pores. This suggests that the cross-linking could be an artifact of locally higher protein concentration caused by localization of proteins to the liposome surface. If this were the case, however, one would expect the rapid formation of aggregates instead of discrete species. We also observed that IpaB prepared in OPOE formed discrete tetramers and octomers in liposomes without the formation of higher-order aggregates. This may be due to a slight conformational change, or conformational flexibility, that is required for IpaB to insert into liposomes.[157] The resulting membrane- inserted tetramer/octomer may be impermissive to formation of higher-order structures, thus explaining the absence of higher-order aggregates from our data.

The question remains as to why monomeric IpaB$^{11-495}$ forms a pore and full-length IpaB does not, yet both proteins form higher-order oligomers when incubated with liposomes. The C-terminal 85 residues of IpaB appear to be important in the control of pore function. Without these residues, IpaB$^{11-495}$ generally behaves as full-length IpaB, except for this pore-forming phenomenon. These 85 residues are important for stable recombinant IpaB expression, since we had to generate this protein by inserting a TEV protease site and specifically cleaving the final 85 residues from IpaB.

As a whole, the data presented here suggest that regions in addition to the hydrophobic domain of IpaB are involved in membrane association and that the C-terminal domain plays a role in controlling IpaB's pore forming function. The quenching data suggest that residues 309,

353 and 486 contribute to pore formation. They also indicated that the region surrounding residue 353, a predicted α-helical hairpin, plays a central role in membrane interaction. Deletion of the entire C-terminal region (residues 410-580) of IpaB partially attenuates the invasion function of *Shigella*, and eliminates the ability to bind to caspase-1.[160] We found that the C-terminal 85 residues of IpaB may have a role in controlling pore function, and are not required for oligomer formation. $IpaB^{28-226}$ does not interact with liposomes, so the N-terminal boundary of the membrane-interaction domain is somewhere between residues 226 and 309. $IpaB^{28-226}$ was identified as a stable proteolytic product (see Ch. I) which suggests that residue 226 is near a boundary between the two more structured regions. The quenching data suggest that the region encompassing 237 and 254 may play a role in peripheral membrane interaction, especially for monomeric IpaB. Others have shown that deletion of 247-277 abrogates IpaB function in *Shigella*,[160] so this region may possess some under-appreciated function. Collectively these data suggest that the entire hydrophobic domain is required for pore formation but not for simple liposome interaction. It will next be important to determine the relationship between the structural forms we observe for recombinant IpaB and the IpaB complex that exists at the tip of the type III secretion of *S. flexneri in vivo*.

CHAPTER IV

SIDE PROJECTS

Pore-forming Harpins of the Type III Secretion System of *Pseudomonas syringae*

Introduction

Pseudomonas syringae is a Gram-negative plant pathogen that, like *Shigella*, uses a T3SS to deliver host-altering effector proteins into target eukaryotic cells.[169] *P. syringae* consists of many pathovars specific to particular plant species, and can destroy crops such as tomatoes and soybeans.[169] Secretion of effector proteins via the T3SS is required for *P. syringae* to infect and grow in plants.[170] *P. syringae* is an important model organism because it is easily genetically manipulated with a fully sequenced and well-annotated genome.[169,171]

Harpins are a class of T3SS effectors that are unique to plant pathogens and are thought to contribute to the translocation of T3SS effectors.[172] The hypersensitive response (HR) and pathogenicity (Hrp)[169] and Hrp outer proteins (Hop) are so named because they are translocated by the *hrp/hrc* (hypersensitive response and pathogencity/conserved) T3SS.[173] The HR is a type of programmed cell death that occurs in plants in response to infection and injury.[172] Harpins also invoke the HR.[172] HrpZ1 and HrpW1 are harpins secreted by *P. syringae*, and are conserved across several pathovars.[174-176] HrpZ1 is a lipid-binding and pore-forming protein.[177] HrpW1

consists of a harpin domain and a putative pectate lyase domain within the N- and C-terminal halves of the protein, respectively.[172,174] Additional harpins were recently identified and named HrpK1 and HopAK1.[172] Like other harpins, HrpK1 and HopAK1 are capable of inducing the HR.[172] When all four harpin genes are knocked out, *P. syringae* is unable to translocate bacterial effectors into plant cells, but it still secretes proteins into the medium.[172] In the quadruple knockout strain, each of these harpins is capable of restoring the translocation function of the T3SS.[172]

HopP1 is a lytic transglycosylase that is translocated into plant cells by the *hrp/hrc* T3SS.[178] Lytic transglycoslyases are thought to degrade the peptidoglycan layer of Gram-negative pathogens in a controlled fashion to allow the deployment of extracellular appendages, such as those of T3SSs.[179] HopP1 has recently been demonstrated to play a role in suppressing PAMP-triggered immunity (PTI) of plants.[179] Suppression of PTI is a necessary first step in evading the HR response, thus promoting pathogenesis.[179] We evaluated the aforementioned Hrp and Hop proteins for their ability to form pores in liposomes.

Results and Conclusions

Using a fluorophore release assay,[144] we evaluated the harpins for their ability to form pores in liposome vesicles (Figure 3.1). The liposomes consisted of 20% DOPG and 80% DOPC and contained 100 mM sulforhodamine-B (SRB). The *Shigella* proteins IpaB and IpaD were used as positive and negative controls, respectively. HrpK1 released 32% of the total SRB, and HrpZ1 released 55%, indicating that HrpK1 and HrpZ1 were able to disrupt the liposomes. HopP1 promoted the release of more SRB than did the negative control, however HopP1 was not particularly efficient in SRB release. HopAK1 and HrpW1 did not promote a significant amount of SRB release (only about 5% each).

HrpW1, HopP1, and HopAK1 each contain a putative pectin lyase domain and a harpin domain.[172,174] Thus, these proteins are probably not translocator proteins since they were unable to complement a translocation deficient strain of *P. syringae*.[172] While HrpW1, HopP1, and HopAK1 do not appear to be important for lipid bilayer penetration, as secreted effectors they may serve to degrade the plant cell wall to allow the T3SS to gain access to the cell membrane where the translocator proteins HrpK1 and HrpZ1 would be capable of forming the translocon pore. It has also been speculated that HrpW1 and HopAK1 could serve as a scaffold at the T3SA needle tip for the assembly of the translocon complex, much like the low-calcium response protein V (LcrV) in *Yersinia*[172] or IpaD in *Shigella*.[180] Recent findings suggest that HopP1 is a lytic transglycosylase that assists in the assembly of the T3SS machinery by enlarging the pores in the peptidoglycan layer of Gram-negative bacteria to allow the machinery to protrude from the cell.[178]

HrpK1 and HrpZ1 have been shown to be necessary for the translocation of T3SS effector proteins, but not for secretion.[172] A role in translocation is supported by our data which suggest that both HrpK1 and HrpZ1 form pores in phospholipid membranes. These proteins promoted the release of SRB from liposomes, but at a level lower than the positive control protein, IpaB. This could be because the Hrp's are optimized for plant pathogenesis where they must span the cell wall in addition to the plasma membrane of plants, whereas IpaB only needs to span a single lipid bilayer to infect mammalian cells.

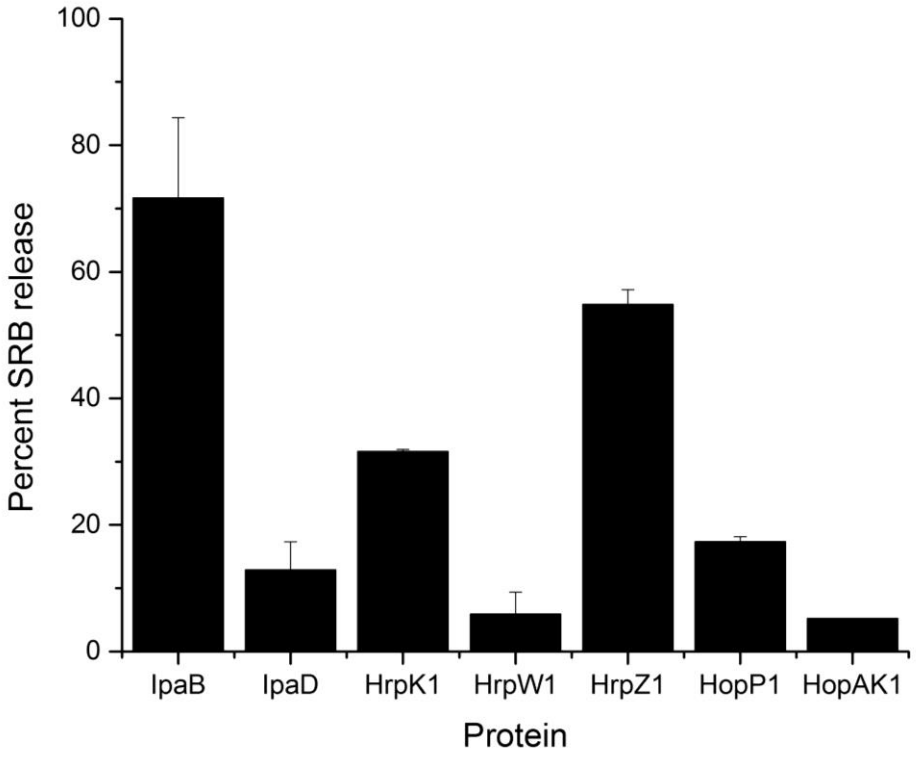

Figure 3.1. Evaluation of the liposome-disrupting capacity of *P. syringae* T3SS translocator candidates. See materials and methods for assay details. Tetrameric IpaB (prepared in the detergent OPOE) was used as a positive control for liposome disruption and IpaD was used as a negative control. Each bar represents the average of three independent experiments. Error bars represent the standard deviation (n=3) of at least three independent measurements.

Evaluation of the bacterial lytic capacity of P60-domain containing enzymes from *Mycobacterium avium* subsp. *paratuberculosis* K-10

Introduction

Mycobacterium avium subspecies *paratuberculosis* (MAP) is the etiologic agent of Johne's disease in animals of agricultural significance, such as goats and cattle.[181] Johne's disease is a chronic enteritis that leads to malnourishment of the affected animals and can have a severe economic impact on the farm industry.[182,183] MAP1204 and MAP1272c are major, surface-exposed antigens of this bacterium and both contain a P60 domain and a membrane-anchoring domain.[181] P60 domains impart enzymatic activity to their constituent proteins, including the ability to hydrolyze peptidoglycan.[181,184] The function of prokaryotic P60 domains may be to modify the cell wall of bacteria to allow the extension of extracellular appendages.[181] MAP1272c is poorly conserved across *Mycobacterium* species, and the protein encoded by the strain used in this study lacks a catalytic residue and is not expected to be enzymatically active.[181] Thus, MAP1272c was used as a negative control in this study. Other MAP strains possess a form of MAP1272c with a putative Cys-His-His catalytic triad.[184] MAP1272c may be erroneously annotated in the genomes of other MAP strains.[181] The physiological role played by an inactive peptidase is unclear.

To determine if MAP1204 enzymatically degraded peptidoglycan, its impact on the survival of the Gram-positive bacterium *Bacillus subtilis* was evaluated. MAP1204 is hypothesized to have a Cys-His-His catalytic triad similar to that proposed for other permutations of MAP1272c.[184] Thus, a Cys to Ser mutation (MAP1204 C155S) of the predicted catalytic residue was generated. Understanding the function of MAP1204 and MAP1272c may lead to the development of novel therapeutic compounds that could interfere with the deployment of bacterial extracellular appendages.

Results and Conclusions

Bacterial survival assays were employed to determine if the putative enzymes from MAP were capable of degrading peptidoglycan. Degradation of the peptidoglycan layer should lead to a decrease in bacterial survival. A laboratory strain of *B. subtilis* was selected for use in the bacterial survival assays as a representative Gram-positive organism. *B. subtilis* was incubated with increasing concentrations of the predicted peptidases (Figure 3.2). The bacteria were diluted in 0.1x PBS prior to the addition of MAP enzymes. In this case, the use of a hypotonic solution was necessary to observe a reduction in survival, perhaps because isotonic PBS did not force the exposed cytoplasmic membrane to rupture. As expected, MAP1272c was unable to reduce bacterial survival (Figure 3.2). This protein is catalytically inactive because it contains an alanine residue at the catalytic position. Incubating *B. subtilis* with MAP1204 reduced bacterial survival in a dose-dependent fashion (Figure 3.2). MAP1204 C155S reduced bacterial survival, though less efficiently, indicating that the mutation affected the ability for the enzyme to hydrolyze peptidoglycan but did not completely abrogate it. This mutation was not predicted to alter the structure of the protein, so the decreased activity was not likely due to protein unfolding. Ser-His-His triads are common, and possess a similar relative orientation to the novel Cys-His-His.[184] It is possible that since the predicted Cys-His-His catalytic triad is a novel active site arrangement, that it is relatively uncommon and may not compose the active site of MAP1204. Alternatively, C155S may be a tolerable mutation because Ser-His-His catalytic triads possess a similar relative orientation to Cys-containing triads.[184] Whether or not this is the active site of the enzyme cannot be determined from the data presented here.

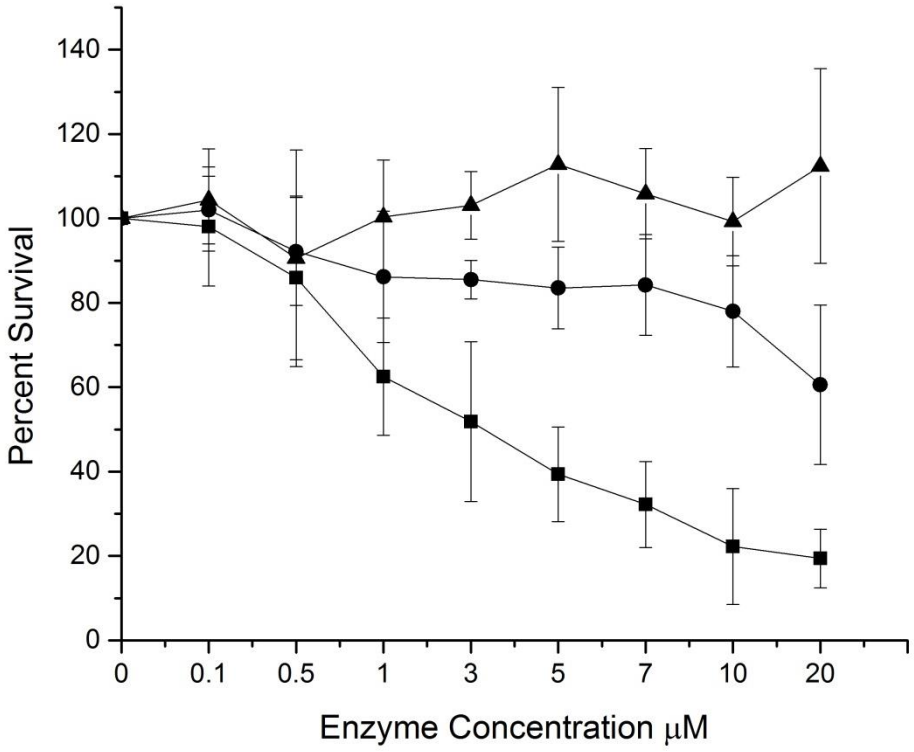

Figure 3.2. Impact of co-incubation of suspected peptidases from *Mycobacterium avium* subsp. *paratuberculosis* K-10 on the survival of *B. subtilis*. *B. subtilis* was incubated for one hr. in the presence of Hen egg white lysozyme (HEWL), MAP1204, MAP1204 C155S, or MAP1272c, plated onto LB agar plates and incubated overnight at 37° C. HEWL was used as a positive control, and is not shown here because *B. subtilis* survival was always 0% for this enzyme. Percent survival was normalized to the "no enzyme" condition for each series. Error bars represent the standard deviation of at least four independent experiments. Squares = MAP1204 WT; circles = MAP1204 C155S; triangles = MAP1272c.

The Effect of Bile Salts on the Invasive Capacity of *Salmonella enterica* serovar Typhimurium

Introduction

Salmonella enterica serovar Typhimurium (*S.* Typhimurium) causes diarrheal disease in humans and livestock worldwide.[185] This pathogen is transmitted via the fecal-oral route. *S. enterica* servars Typhimurium, Typhi, and Enteritidis have been shown to form chronic carrier states in humans through the establishment of biofilms on gallstones.[186] *Salmonella* uses two different T3SSs encoded by two separate genetic islands depending on the stage of infection.[187] T3SS-1 is required for initial invasion of host tissues and is encoded by *Salmonella* pathogenicity island 1 (SPI-1). A SPI-2 encoded T3SS then mediates intracellular survival of the bacterium.[188] After invasion, *Salmonella* can disseminate systemically following invasion of macrophages and uses SPI-2 to maintain the bacteria-containing vacuole.[189]

Bile consists of several detergents that help in the digestion of fats. Like other detergents, bile can damage bacterial cell membranes, however, enteric bacteria possess a variety of mechanisms that minimize the impact of bile on the cell membrane.[190] In fact, some enteric pathogens use bile as an environmental signal.[83,190] *Salmonella* encounters high concentrations of bile in the intestines of humans, however, it has been shown that overnight growth in 3% bile almost completely represses the invasive capacity of *Salmonella* because of repression of SPI-1 gene expression.[191] It was shown that incubation with 3% bile for as little as 30 min reduced the transcription of invasion genes.[192] The aforementioned study, however, did not determine the impact of shorter incubation times on bacterial invasion. Thus, we sought to more closely examine the effect of bile on *Salmonella* invasion.

Results and Conclusions

S. Typhimurium SB241 is isogenic to SL1344, except that SB241 is null for the T3SS effector protein SipD.[193] SipD is essential for the invasion function of *Salmonella*.[193] We grew SL1344 in LB + 3% oxgall, a desiccated bovine bile preparation. We exposed SL1344 to oxgall for 15, 30 or 60 min. during normal growth. It had been shown previously that bile eliminates the ability for *Salmonella* to invade cultured cells when exposed overnight.[191] On the other hand, the bile salt deoxycholate (DOC) primes the T3SS by recruiting IpaB to the T3SS needle tip and thereby enhances the invasion of intestinal cells by *Shigella*.[83,194]

The results of the gentamycin-protection assay are shown in Figure 3.3. SB241 was non-invasive, as expected. SL1344 were grown in the presence of 3% oxgall for 15, 30 or 60 min prior to incubation with HeLa cells. The reduction in invasiveness was not statistically different among the time points, but invasion was decreased by ~50% relative to the control grown without 3% oxgall (Figure 3.3). The OD_{600} of each culture was closely monitored, and thus these data are not reflective of a difference in multiplicity of infection.

These data reflect a ~50% decrease in invasiveness. Previous studies demonstrated that overnight growth in 3% oxgall completely inhibits the invasion function of *Salmonella* through transcriptional regulation.[192] It has been shown that bile represses the expression of genes in the invasion pathway in as little as 30 min, but that study did not test the impact of bile on invasiveness at this time point.[192] It is possible that the decreased invasion observed here was also due to transcriptional regulation, though it is unlikely that preexisting virulence machinery was degraded within this time period. These data suggest that it may take some time for the invasion function to be completely turned-off, perhaps due to the cytoplasmic pool of effector proteins that is hypothesized to accumulate in enteric pathogens.[72] Thus, the selected time points were such that the SPI-1 T3SS may be transcriptionally deactivated, but the cytoplasmic pool of effector proteins[72] was still available for secretion and therefore allowed invasion.

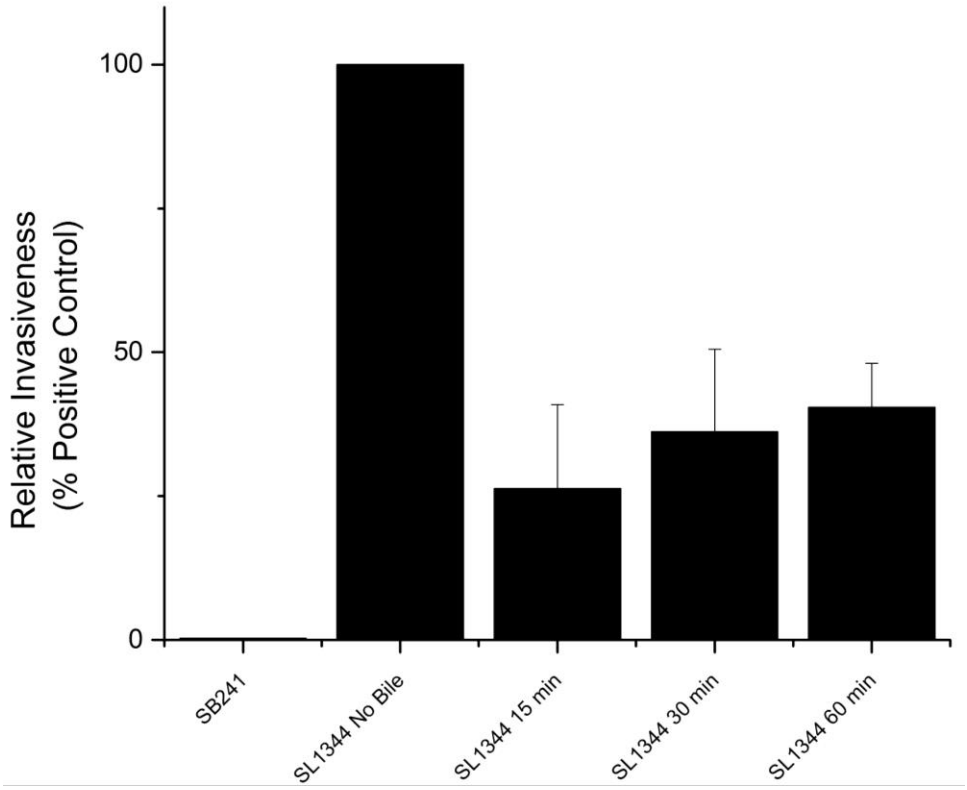

Figure 3.3 Standard gentamycin-protection assay using *S*. Typhimurium in the presence of 3% oxgall. *S*. Typhimurium SL1344 was grown in the presence of 3% oxgall for the indicated times prior to incubation with semi-confluent HeLa cells. *S*. Typhimurium SB241, a strain lacking the T3SS effector SipD, was used as a negative control. Error bars represent standard deviation of three independent experiments.

Impact of inserting of a tetracysteine-pocket into IpaD

Introduction

Invasion plasmid antigen D (IpaD) is the secretion-controlling tip protein of *Shigella*'s T3SS.[180] IpaD also serves as an environmental sensor by binding to bile salts.[83] Multiple crystal structures for this highly soluble, 37 kDa protein have been published.[195,196] Structural analysis reveals a long, central coiled-coil domain with two globular domains at either end of the coiled-coil, resembling a dumbbell.[195] The DOC binding site on IpaD is located at the interface of helices α3 and α7, as determined by a crystal structure of IpaD in complex with DOC.[196] This observation agrees reasonably well with the previously established distance between the DOC binding site and the C-terminus of IpaD.[83] IpaD contains two distinct, independently folding domains. The N-terminal 120 residues comprise a domain that serves as a self-chaperone for IpaD.[197] The remainder of the protein is required for controlling type III secretion, especially what is termed the "distal domain."[165] Binding to bile salts induces a conformational change in IpaD,[198] leading to IpaB docking on the T3SS needle tip.[84] Growth in the presence of bile salts also causes *Shigella* to become about four times more invasive.[194] This section will briefly discuss contributions made to a project exploring the subtle conformational changes that occur in IpaD upon binding to the bile salt deoxycholate (DOC).[198]

Results and Conclusions

Tertiary structure analysis of IpaD containing tetracysteine pockets

Recombinant IpaD constructs were made to contain tetracysteine (TC) pockets (residues CCGPCC) that are specifically recognized by a fluorescin deriviative, 4′,5′-bis(1,3,2,-dithioarsolan-2-yl) fluorescein (FlAsH-EDT_2; Molecular Probes, Eugene, OR) for site-specific labeling.[198] The TC pockets were inserted into unstructured regions of IpaD.[198] Prior to performing the planned *in vitro* assays using these mutant proteins, they were tested for structural

defects using intrinsic tryptophan fluorescence. Trp is an environmentally-sensitive fluorophore that undergoes a blue-shift upon entering a more hydrophobic environment or a red-shift upon entering a hydrophilic environment.[154] Therefore, Trp fluorescence is useful as an indicator of protein folding. IpaD contains four Trp residues, so this technique cannot supply information about the environment of a single a Trp, however, changes in protein structure or aggregation state are reflected by altered peak emission wavelengths.

TC pockets were introduced into IpaD following residues 68, 184, 231, and 264 (TC68, TC184, TC231, and TC264, respectively). Wild-type IpaD (WT-IpaD) and TC-containing IpaD mutants TC68, TC184, TC231, and TC264 were purified as previously described.[199] It was found that the tertiary structure of IpaD was not greatly impacted by the addition of TC pockets (Figure 3.4). WT-IpaD and the TC pocket containing proteins had similar transition temperatures near 65°C, defined as the midpoint of the transitions seen in Figure 3.4. TC184 had the most dramatic red-shift at the end of the experiment, finishing at 346 nm. TC231 has a transition midpoint of 65°C and demonstrated a more intense red-shift at 65 and 72.5° C than the other proteins, and the final peak wavelength was 3 nm longer than WT-IpaD (345 nm vs 342 nm). TC264 followed a trend similar to TC231, but the final peak wavelength was only 1 nm longer than WT-IpaD. Interestingly, TC231 and TC264 were both located in the distal domain. One could speculate that these slightly red-shifted data points indicate a structural perturbation in these proteins, however, due to the very similar transition temperatures it is unlikely that any major tertiary structural changes occurred as a result of TC-pocket insertion. These proteins were used in downstream experiments at room temperature, and the peak emission wavelengths were very similar across 10-40°C. Therefore, the addition of TC pockets to IpaD did not alter the tertiary structure.

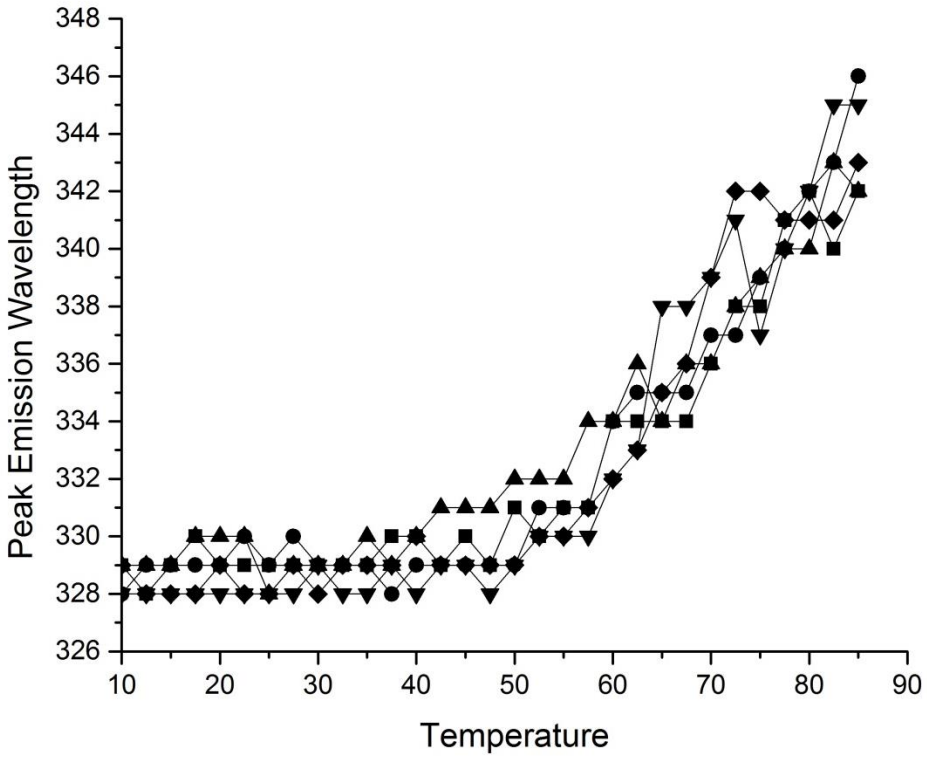

Figure 3.4. Thermal stability of the tertiary structure of IpaD tetracysteine (TC) pocket-containing mutants. Wild-type IpaD (squares), IpaD TC68 (upward triangles), IpaD TC184 (circles), IpaD TC231 (downward triangles), and IpaD TC264 (diamonds) were excited at 295 nm and monitored for changes in peak emission wavelength as a function of temperature. The Y-axis is the peak emission wavelength in nanometers, the X-axis is the temperature in degrees C.

CHAPTER V

DISCUSSION

The purpose of this work was to examine the protein-protein and protein-lipid interactions that IpaB participates in within the T3SS. This study encompassed mostly *in vitro* biochemical approaches, including: fluorescence spectroscopy, chemical cross-linking, mutagenesis, and limited proteolysis. Data from this work contributed to the growing body of knowledge on the enigmatic and multifaceted role of IpaB.

Recombinant expression of IpaB requires IpgC.[144] The major hurdle to investigating the IpaB-IpgC interaction is that the continued presence of detergents is required to maintain IpaB's solubility.[144] The detergents also prevent the reassembly of the translocator-chaperone complex (P. R. Adam, unpublished results). Our collaborator Dr. Brian Geisbrecht and his former student Dr. Michael Barta solved a partial crystal structure of IpaB, spanning residues 74-224 of the 580-residue protein.[150] They identified the soluble N-terminal domain of IpaB, which was used for further study. The N-terminus of IpaB has been shown to contain two separate chaperone binding sites (CBS) and the secretion signal.[149,200] IpaB's crystal structure was highly homologous to an extended coiled-coil in colicin Ia, a pore-forming toxin.[150] The same study identified a predicted α-helical hairpin motif spanning residues 310-370 within the hydrophobic domain of IpaB.[150] An α-helical hairpin motif in colicin Ia serves as a membrane anchor.[152] Our laboratory was the first

to examine the structural consequences of the interaction between IpaB and the chaperone, IpgC.[151]

Studies with the soluble N-terminal domain were first directed at determining if it could in fact interact with IpgC. Fluorescence polarization, isothermal titration calorimetry, and cross-linking data strongly suggested that the N-terminal domain does interact with IpgC.[151] Further, the data supported the proposal by others that two separate CBS's exist within the N-terminal 75 residues.[151] The data showed that IpaB undergoes a conformational change upon binding to IpgC.[151] The exact nature of this conformational change remains unclear, but appears to affect regions of IpaB well outside of the CBS.[151] A possibility is that the N-terminal domain of IpaB adopts a more elongated structure upon binding to IpgC.[151] IpgC prevents IpaB from associating with phospholipid membranes[144,157] and thus, IpgC may hold IpaB in a conformation that does not permit membrane interaction. Later work by our lab revealed that IpaB (without IpgC) requires structural flexibility to insert into liposomes.[157] Thus, IpgC binding prevents IpaB from inserting into membranes due to a conformational change in IpaB, a lack of structural flexibility, or a combination of these factors.

The next series of experiments explored the nature of the IpaB-membrane interaction by probing the microenvironment of several residues within full-length IpaB. The Picking lab has previously reported that IpaB can exist as either a monomer or a tetramer, depending on the detergent used to separate IpaB from IpgC after recombinant expression.[157] Furthermore, both of these oligomeric states are capable of interacting with lipid membranes, but differ in one key feature: tetrameric IpaB forms pores in lipid membranes, whereas monomeric IpaB does not.[157]

The hydrophobic domain was predicted to span residues 310-420.[160] Guichon et al. found that deleting short segments (307-316, and 410-419) within the predicted transmembrane helices of IpaB resulted in an invasion-null phenotype in *Shigella*.[160] Using both monomeric and

oligomeric IpaB, fluorescence quenching was used to examine how the surface topography of IpaB differed with regard to oligomeric state. The hydrophobic domain of tetrameric IpaB was much more solvent-exposed relative to the monomer. The hydrophobic domain was the most protected by membrane interaction, independent of oligomeric state. The data suggest that the pore-forming domain of IpaB may extend as far as residue 486, well beyond the predicted segment. Other studies have predicted that a tetramer of IpaB is recruited to the T3SS needle tip after exposure to bile salts.[165] The recombinant IpaB tetramer may be structurally similar to the arrangement of the putative IpaB tetramer at the T3SS needle tip, although detailed structural analysis is needed to confirm this. Perhaps most importantly, the α-helical motif within IpaB appears to drive membrane interaction. The α-helical motif in IpaB thus represents an attractive target for novel antimicrobials and clearly warrants further study.

We next explored how large C-terminal truncations affected IpaB's ability to interact with liposomes. Previous work found that deletions of residues 311-580 and 401-580 eliminated and reduced the invasiveness of *Shigella*, respectively.[160] We found that very little of the predicted hydrophobic domain is needed for membrane interaction, because $IpaB^{11-312}$ interacted with liposomes. However, complete absence of the hydrophobic domain ($IpaB^{28-226}$) precludes membrane interaction.[157] Of the truncated forms of IpaB, the most fascinating protein was $IpaB^{11-495}$. This protein preserved almost all of the characteristics of the full-length protein, with one major difference. $IpaB^{11-495}$ formed pores in liposomes when prepared as a monomer in solution. Therefore, since all previous data suggested that pore formation by IpaB depended on the oligomeric state, we explored if $IpaB^{11-495}$ formed oligomers after it was introduced to liposomes. We found that full-length IpaB and $IpaB^{11-495}$, when prepared as monomers, formed tetramers after incubation with liposomes. This suggests that the C-terminal 85 residues of IpaB play a role in the regulation of pore-formation.

The presence of a C-terminal peptide, IpaB$^{418-580}$, prevents *Shigella* from invading cells.[166] A similar observation was made for the IpaB homolog from *Salmonella*, SipB.[201] More recently, it was shown that the deletion of as few as three residues from IpaB's C-terminus can disrupt the ability of IpaB to associate with the T3SS needle tip.[164] From our data and other studies, it is clear that the C-terminal residues of IpaB are functionally diverse and important. These residues appear to be necessary for regulating pore formation *in vitro*, and may be structurally important.

This work studied several aspects of IpaB and provided the first evidence that IpaB undergoes a conformational rearrangement upon interaction with the chaperone, IpgC. IpgC may hold IpaB in a conformation that prevents membrane interaction. The first detailed analysis of IpaB's structural topology with regard to oligomeric state and membrane interaction was also provided. Initial membrane interaction may be localized to an α-helical hairpin region within the heart of the hydrophobic domain in the context of the full-length protein. Finally, we showed that the C-terminal 85 residues of IpaB are involved in regulating pore formation. One could speculate that these 85 residues form a "plug," that is displaced by tetramer formation prior to membrane association. Further studies examining the hydrophobic region and C-terminus of IpaB should reveal the subtle structural changes within IpaB that lead to pore formation.

CHAPTER VI

MATERIALS AND METHODS

Materials: All reagent-grade chemicals were purchased from Thermo-Fisher Scientific (Waltham, MA) or Sigma-Aldrich (St. Louis, MO), unless otherwise indicated.

Buffers and Reagents: See Appendix A for buffer compositions, media and other recipes.

Bacterial strains, media, and growth conditions (Chapters I, II, and III). Antibiotic concentrations for both liquid and solid media growth were 100 µg/ml ampicillin (to select for pHS2, pWPsf4, and pET-series constructs) and 34 µg/ml chloramphenicol (to select for pACYC constructs). Growth of liquid cultures was at 37°C with shaking at 200 RPM for *Shigella* and *Escherichia coli*, shaking was 100 RPM for *Salmonella*. *Shigella* were grown on tryptic soy agar plates containing 0.025% congo red. Congo red is used as an indicator dye because it is known to bind to cells with an active T3SS, and is thus used as an indicator of virulence plasmid retention.[202] *E. coli* and *Salmonella* were grown on LB plates. All solid media were incubated at 37°C.

Growth and recombinant expression of IpaB/IpgC complexes. *ipaB*/pET15b was co-transformed with *ipgC*/pACYC into Tuner (DE3) competent *E. coli* cells and grown on a Luria-Bertani (LB) plate containing ampicillin and chloramphenicol and incubated overnight. A single colony was grown in 10 ml LB containing ampicillin and chloramphenicol to generate a permanent stock (200 µl 50% glycerol plus 1 ml broth culture) which was stored at -80° C. This permanent stock was used to start an overnight 10 ml culture in minimal media, and 1-2 ml of the overnight culture was used to inoculate each liter of Terrific Broth (TB; see Appendix A). One liter cultures were grown to an OD_{600} of 0.6-1.0 and moved to a pre-chilled 17°C shaking incubator for 45 min to cool down. Protein expression was induced by the addition of 2 ml of 0.5M Isopropyl-β-D-thiogalactopyranoside (IPTG) and grown overnight (~16 hr) at 17°C with shaking at 200 RPM.

Chemical Crosslinking (Chapters I and II). Chemical cross-linking experiments were used to examine the stoichiometry of IpaB-IpgC complex formation (Chapter I) and the oligomeric state of IpaB (Chapter II). In chapter I, the homobifunctional thiol-cleavable crosslinking reagent Dithiobis[succinimidyl propionate] (DSP; Thermo-Fisher, Rockford, IL) was used for the crosslinking experiments in Chapter I. A 12.3 mM working stock of DSP was prepared by dissolving 1 mg of DSP in 200 µl dimethylformamide (DMF). Protein concentrations were 10 µM in the experiments with $IpaB^{28.226}$, $IpaB^{1.226}$ and IpgC.[151] Protein and cross-linker concentrations were optimized for individual proteins, but these conditions provided a good starting point. Samples (50 µl) of 10 µM $IpaB^{1.94}$/IpgC, $IpaB^{1.226}$, $IpaB^{28.226}$ and IpgC were prepared. To determine if IpaB and IpgC formed a discrete complex *in vitro*, samples were made to contain IpaB and IpgC at a molar ratio of 1:2. DSP (0.68 µl aliquot of 12.3 mM stock) was added to the 50 µl samples, mixed, and incubated at room temperature for 30 min. 25 µl of 3x SDS-PAGE sample buffer was added to quench the crosslinking reaction. Reactions were split into two aliquots and dithiothreitol (DTT) was added at a final concentration of 50 mM to one

aliquot of each reaction to reverse the cross-linking reaction. Samples were separated on a 4-20% TGX gradient gel (Biorad, Hercules, CA) and stained with Oriole fluorescent gel stain (Biorad) for 90 min. After staining, gels were soaked in pure water for 45 min. to remove excess stain. The proteins used for the above experiments were expressed recombinantly in pT7HMT, which encodes a 6x-His-tag on the N-terminus of the protein.[203] pT7HMT encodes a Tobacco etch virus (TEV) protease site immediately downstream of the His-tag. The 6x-His-tag was removed using TEV protease prior to cross-linking.

In Chapter II, full-length IpaB and truncated forms of IpaB were cross-linked with the water-soluble, homobifunctional, non-cleavable cross-linking agent bis[sulfosuccinimidyl] suberate (BS3) was used. BS3 was selected because it does not diffuse across lipid bilayers. A 10 mM working stock of BS3 was prepared in 1x PBS. Proteins were diluted to 5 µM in PBS with or without 4.4 mg/ml of liposomes and incubated for 10 min. at room temperature. After BS3 was added (final concentration = 84 µM) the reactions were incubated 10 min. at room temperature. The reaction was stopped by the addition of 3x SDS-PAGE sample buffer and 50 mM DTT. Samples were boiled, run on 4-20% SDS-PAGE gels and stained with Oriole fluorescent gel stain (Biorad) as above.

Förster Resonance Energy Transfer (FRET) (Chapter I).

FRET was used to detect conformational changes in IpaB's N-terminal domain. The two fluorophores used were tryptophan and Alexa350. This dye pair has an Ro of 22 Å.[204] IpaB's N-terminal domain has a native Trp residue at position 105 (W105). W105 was used as the donor fluorophore, and Alexa350 was used as the acceptor. Alexa350-C5-maleimide was used to label $IpaB^{28.226}$ and $IpaB^{1.226}$ that were modified to have a Cys residue at either the N or C-terminus ($IpaB^{C28\text{-}226}$, $IpaB^{N28\text{-}226}$, $IpaB^{C1\text{-}226}$, and $IpaB^{N1\text{-}226}$). Alexa350-labeled proteins were called "donor-acceptor" (DA), and proteins lacking the extrinsic label were called "donor" (D).

Fluorescence spectra were collected with a Jobin-Yvon FluoroMax-4 spectrofluorometer. Samples were excited at 295 nm. Fluorescence emission spectra were collected from 300-400 nm using a signal integration time of 1 sec. Both sets of slits were adjusted to 2.5 nm. Samples containing 1 μM of D or DA were prepared in the presence and absence of 1 μM IpgC to determine if IpgC altered the FRET efficiency (*E*) as calculated by:

Equation 1: $E = 1 - F_{DA} / F_{D}$

Where F_{DA} is the peak W105 fluorescence intensity of DA samples, and F_{D} is the peak W105 fluorescence intensity of D samples. Distances between the donor probe and acceptor probe were calculated using:

Equation 2: $r = R_0((1 / E) - 1)^{1/6}$

Where *r* is the calculated distance separating the donor and acceptor probes, *E* is the FRET efficiency, and R_0 is the distance unique to this FRET pair at which 50% FRET occurs, which is 21 Å.[204]

Generation of IpaB Mutants (Chapters I and II).

Generation of IpaB Cys mutants for expression in S.flexneri SF620 and E. coli Tuner (DE3) (Chapter II). Primers containing GAGAGAGAG and a BsrGI restriction site were designed to generate the following point mutations (for primer sequences see Appendix B): S19C, S58C, S107C, S149C, S237C, A254C, A353C, A420C, S486C, A502C, and S519C. S107C and S149C required the use of BssHII and AflII, respectively. The mutations were generated by inverse PCR using *ipaB*/pHS2 as a template, followed by digestion with the enzyme indicated above. The linear plasmids were then ligated using Clonables 2X ligation premix (EMD-Millipore, Darmstadt, Germany) and used to transform Nova Blue *E. coli* cells (EMD-Millipore). Nucleotide sequences of purified plasmids were verified by sequencing at the Oklahoma State

University Biochemistry and Molecular Biology Recombinant DNA and Protein Core Facility (Stillwater, OK). *ipaB* mutants in pHS2 were introduced into the *ipaB* null strain SF620 by electroporation. Transformed *Shigella* were plated on trypitcase soy agar containing 0.025% congo red and 100 µg/µl ampicillin. Congo red is used to differentiate between colonies that have retained the virulence plasmid and those that have not.[202] pHS2 contains a beta-lactamase cassette which allowed selection of only those cells that harbored the desired plasmid.

ipaB mutants were subcloned from pHS2 into pET15b for recombinant protein expression. *ipaB* mutants in pHS2 were digested with NdeI and BamHI and then separated from the vector on a 1% agarose gel. Bands corresponding to *ipaB* were cut out and purified from the gel using the Qiagen gel-extraction kit (Venlo, The Netherlands). The gel-purified, NdeI/BamHI digested *ipaB* genes were then ligated into NdeI/BamHI-digested pET15b using Clonables 2x ligation premix (EMD Millipore) according to the manufacturer's protocol, used to transform NovaBlue *E. coli* cells, and grown on LB agar with 100 µg/ml ampicillin. Selected transformants were screened for insertion of a gene by colony PCR using T7 promoter and T7 terminator vector primers. Colonies that screened positive were sequence-verified as above to ensure that no mutations occurred during subcloning.

Generation of truncated forms of ipaB mutants for expression in Tuner (DE3). 5'-phosphorylated primer pairs were designed to generate IpaB$^{11\text{-}312}$, IpaB$^{11\text{-}357}$, and IpaB$^{11\text{-}390}$. An additional *ipaB* mutant covering residues 11-580 included a TEV recognition site after residue 495 (IpaB$^{11\text{-}580\ TEV\ 495}$), because expression of IpaB$^{11\text{-}495}$ was not possible. IpaB$^{11\text{-}580\ TEV\ 495}$ was generated via two-steps. First, IpaB$^{11\text{-}580}$ was generated. The TEV site was introduced using primers encoding the TEV site, with the forward primer encoding the first four residues of the TEV recognition sequence and the reverse primer encoding the final three residues (for primer sequences see Appendix B). The resulting pWPSF4 constructs were verified by sequencing. *ipaB* was then

subcloned from pWPSF4 into pET15b, and along with *ipgC*/pACYC, was used to co-transform *E. coli* Tuner (DE3) for protein expression.

Limited proteolysis. Subtilisin A was purchased from Sigma (Cat # P5459; CAS #: 9014-01-1; EC #: 3.4.21.62). A working stock of 1:1000 protease was generated by serial 1:10 dilutions in phosphate-buffered saline (PBS). Several final concentrations of protease were surveyed to identify the optimal concentration for each protein of interest. For IpaB, 1:80,000 worked best; for IpaD, 1:160,000 was best. Ten µl of 3x SDS-PAGE sample buffer and 1 µl of 1.5 M DTT were added to pre-labeled tubes and placed in the thermocycler on the "hot-kill" cycle (which is an infinite hold at 99° C). This way, 20 µl samples can be taken from a single source reaction and stopped immediately. Monomeric and oligomeric IpaB were diluted to 6 µM in PBS and incubated for 10 min at room temperature with 4.4 µg/µl of liposomes or an equivalent volume of buffer. Protease was added to the specified final dilution and mixed. 20 µl samples were removed from the digestion at the specified time points and immediately added to boiling SDS-PAGE sample buffer for 10 min. The samples were separated on a 12% polyacrylamide gel and stained with Coomassie R250. After destaining, the gels were imaged first on an Alpha Imager and then equilibrated with pure water and imaged on an Odyssey infrared imager (LI-COR, Lincoln, NE) using the 700 nm channel and a focus offset of 0.5 mm to obtain high-resolution images.

Liposome Preparation (Chapters I, II, and III). All lipids were purchased from Avanti Polar Lipids (Alabaster, AL) and maintained in chloroform at 25 mg/ml at -20° C. For specific recipes and notes regarding lipid storage (for recipes see Appendix A). Lipids in chloroform were used within 6 months, after which they were replaced. Lipid formulations contained 66.5 mol% DOPC (1,2-dioleoyl-sn-glycero-3-phosphocholine), 23.5 mol % DOPG (1,2-dioleoyl-sn-glycero-3-[phosphor-rac-(1-glycerol)]), and 10 mol% cholesterol. Lipids dissolved in chloroform were combined in a 1.5 ml tube and were dried using a gentle nitrogen stream. Films were then completely dehydrated using a vacuum centrifuge (SpeedVac), using the "medium" drying rate

for 3 hr. The lipid films were then rehydrated for 30 min in a volume of PBS to bring the lipid concentration to 8.7 mg/ml. Rehydrated lipid films were sonicated using a probe sonicator 3-9x (depending on the rehydration volume) for 10 sec on intensity 2, or placed in the sonicator bath for 30-60 min. The multilamellar liposome suspensions were then extruded by 20 passes through a 100-nm pore-sized membrane (GE Healthcare, Pittsburgh, PA) using an Avanti Mini-extruder (Avanti Polar Lipids). Liposomes were stored at 4° C until use.

Liposome Flotation Assay (Chapter II). 65% sucrose was prepared and sterile filtered prior to beginning the experiment. The concentration of sucrose was verified by measuring the refractive index. Monomeric or oligomeric IpaB was used at a concentration of 0.4 mg/ml. Proteins were incubated at room temperature for 15 min. with 4.4 mg/ml liposomes or an equal volume of PBS. Sucrose was added to a final concentration of 30% and 190 ul of this was added to the bottom of an 11 mm x 30 mm ultracentrifuge tube. One ml of 20% sucrose was layered on top of the 30% sucrose layer, and then 150 µl of PBS was layered on top. The tubes were then balanced to within 1 mg of each other by adding PBS to the top layer. Tubes matched by empty weight were used to minimize adjustments. The tubes were spun in an Ultima TL (Beckman-Coulter, Indianapolis, IN) using the TLS-55 rotor at 54,000 RPM (210,000 x *g*) at 4°C for 1 hr. The acceleration rate was set to 3 and the deceleration rate was set to 0. Both the ultracentrifuge and the TLS-55 rotor were pre-chilled to 4°C. The top 150 µl fraction was collected with a micropipet, and the bottom fraction was collected by carefully puncturing the bottom of the tube with a 21-gauge needle. Fractions were collected from the middle layer after the bottom fraction was collected. Fractions were run on 12% gels and stained with Oriole.

Proteolysis followed by flotation and trichloroacetic acid (TCA) precipitation (Chapter II). To further define which parts of IpaB's sequence interact with liposomes, IpaB was proteolytically cleaved into large domain-sized products. These products were then used in liposome flotation analysis and concentrated by precipitation with TCA. In a total volume of 250

µl, monomeric IpaB was diluted to 12 µM in PBS. Subtilisin (3.13 µl of 1:1000 working stock) was added and the reaction incubated 30 sec. at room temperature. The protease inhibitor 4-(2-Aminoethyl)benzenesulfonyl fluoride hydrochloride (AEBSF; 50 µl of 100 mM working stock) was added to the reaction, vortexed immediately, and placed on ice for 10 min. AEBSF does not immediately stop the proteolytic digestion, therefore, this incubation on ice helps to slow the digestion while AEBSF binds. Liposomes (180 µl of 8.7 mg/ml stock) were combined with 70 µl of the inhibited proteolytic reaction and incubated at room temperature for 10 min. Sucrose was added to a final [sucrose] of 30%, and the entire volume was layered onto the bottom of an 11 mm x 30 mm ultracentrifuge tube. One ml of 20% sucrose was layered on top of the 30% sucrose, and topped with 200 µl PBS. The sucrose cushions were spun in an ultracentrifuge as described above in "Liposome Flotation Assay." One 200 µl sample was taken from the top of the cushion using a micropipet, and the bottom fraction (~0.5 ml) was collected as described above. Most of the 20% sucrose cushion contained no protein, except for the final ~200 µl (the portion of the 20% layer that was closest to the PBS layer). This part of the 20% sucrose layer (referred to as "middle") contains residual top layer components that were not collected by pipetting. The top and middle fractions were not pooled, even though they appeared to contain similar products.

To obtain useful amounts of protein for mass spectrometric (MS) analysis, it was necessary to concentrate the products recovered from the flotation by trichloroacetic acid (TCA) precipitation. This is a modified version of the standard Picking lab TCA precipitation. Top, middle, and bottom fractions from separate ultracentrifuge tubes were pooled to obtain three "master" pools: top, middle, and bottom. One ml aliquots of the pools were dispensed into 1.5 ml microcentrifuge tubes on ice, and 100% TCA was added to the samples at a final concentration of 10%. The samples were incubated for at least 1 hr. on ice, and then spun in a refrigerated tabletop microcentrifuge at 17,000 x *g* for 30 min. The supernatant was discarded, and the samples were washed with 5% TCA followed by centrifugation at 17,000 x *g* for 15 min. The pellets were next

washed with ice-cold acetone twice at 17,000 x *g* for 15 min. The tubes were then inverted to dry, and were resuspended in a minimal volume of 3x SDS-PAGE sample buffer. The top fractions formed a compact, white pellet at the bottom of the tube (lipids), and this pellet sometimes still contained a small amount of TCA, causing the pH indicator in the sample buffer to turn from blue to yellow. In these cases, small volumes of dilute NaOH were added to the samples, along with additional 3x SDS-PAGE sample buffer. A small amount of 10% SDS was added to help dissolve the compact white pellet.

Protein Purification (Chapters I and II). Bacteria were pelleted by centrifugation at 5000 RPM in a Sorvall F9-4x1000y for 20 min. The bacteria were resuspended on ice in 100 ml of 1x His-tag binding buffer per liter of clarified culture. The bacteria were lysed by a single pass through a Microfluidics M110L microfluidizer at 100 PSI external pressure and the resulting lysate was clarified by centrifugation at 22,000 x *g* for 30 min. The soluble fraction was retained and purified using immobilized metal-affinity chromatography (IMAC) on a custom AKTA explorer fast-protein liquid chromatography (FPLC) system (GE Healthcare). Protein-containing fractions were evaluated by SDS-PAGE. The most pure fractions were collected and concentrated to 5-20 ml, depending on the starting culture volume. To further purify the IpaB/IpgC complex away from degradation products and impurities, the concentrated protein was buffer-exchanged into hydrophobic interaction buffer A (See Appendix A for recipes) using pre-packed PD-10 buffer exchange columns (GE Healthcare) following the manufacturer's protocol. The eluate was 0.45 µm filtered and further purified by hydrophobic interaction chromatography (HIC) using a 5 ml butyl-hp column (GE Healthcare). The proteins were eluted from the butyl column by a 20 column-volume gradient of HIC buffer "B," which contains no ammonium sulfate (20 mM $NaPO_4$, pH 7.0). The elution gradient target concentration of buffer B was 80%. Peak fractions were analyzed by SDS-PAGE and relevant fractions were pooled, concentrated, and dialyzed into 1x binding buffer for separation from the chaperone.

Separation of the translocator/chaperone complex using mild detergents. Incubation with mild, non-ionic detergents is necessary to release IpaB from IpgC.[144,157] We have previously shown that incubation with N,N-dimethyldodecylamine N-oxide (LDAO) or n-octyl-oligo-oxyethylene (OPOE) gives rise to distinct oligomeric states of IpaB, namely a monomer and a tetramer, respectively. In this work, IpaB possesses a His-tag and IpgC does not, thus allowing IpgC to be washed away while IpaB is retained on an IMAC column. The highly-purified IpaB/IpgC complex in 1x binding buffer was split into two populations and bound to separate IMAC columns. One column was washed with 30 column volumes (CV's) of 1x binding buffer with 0.1% LDAO and the other column was washed with 30 CV's of 1x binding buffer with 2% OPOE. After washing, the columns were sealed and incubated at 4°C with rocking for one hr. The columns were washed and incubated a total of three times with the detergent-containing binding buffer, and then the concentrations of LDAO and OPOE were reduced to 0.05% and 0.5%, respectively, for the final wash. IpaB was then eluted using 1x elution buffer with either 0.05% LDAO or 0.5% OPOE. The eluted protein was analyzed by SDS-PAGE to verify that the chaperone was not present. Protein was dialyzed into 1x PBS with either 0.05% LDAO or 0.5% OPOE and stored at 4° C until used.

Gentamicin-Protection Assay (Chapters I and III). Confluent HeLa cell layers were used to seed 24-well plates 24 hr. prior to inoculation with bacteria. *ipaB* mutant strains were streaked onto trypticase soy agar containing 0.025% Congo red and 100 µg/ml ampicillin one day prior to the assay. Five isolated colonies were inoculated into 10 ml of trypticase soy broth containing 100 µg/ml ampicillin and 50 µg/ml kanamycin. Cultures were grown to an A_{600} of ~0.5. While the cultures are growing, the HeLa cells were washed with serum-free MEM with 0.45% glucose to remove antibiotics. Three µl of bacteria were added to the HeLa cells and the 24-well plate was centrifuged at room temperature at 2000 x *g* for 5 min. The centrifugation step facilitates contact between the HeLa cells and the bacteria. The bacteria were incubated with the HeLa cells for 30

min at 37°C. The media was aspirated and the cells washed 3x with MEM containing 5% calf serum and 50 µg/ml gentamicin, and then incubated for 2 hr in the gentamicin-containing media. After the 2-hr incubation, the cells were washed with MEM-glucose and then overlaid with 0.5% agar to lyse the cells, followed by an overlay with 2x LB agar. The 24-well plates were incubated overnight at 37°C and colonies representing invasive bacteria were counted.

Contact-Mediated Hemolysis: *ipaB* mutants were grown overnight on TSA-CR and inoculated into 10 ml of trypticase soy broth containing 100 µg/ml ampicillin and 50 µg/ml kanamycin. The bacteria were grown to an A_{600} of 0.5, pelleted at 3000 x *g*, and resuspended with 200 µl phosphate-buffered saline (PBS). Three ml defibrinated sheep blood (Colorado Serum, CO) was diluted with 40 ml PBS and centrifuged to collect the red blood cells (RBCs). RBCs were resuspended in 3 ml PBS and 50 µl/well distributed to a 96-well plate. A 50 µl aliquot of each mutant strain was added to each of three wells, and then the 96-well plate was centrifuged at 2200 x *g* for 15 min at room temperature. The plate was incubated at 37°C for 1 hr. The bacteria were sheared from the RBCs by vigorously resuspending the pellet in each well with 100 µl of ice-cold PBS. The plate was again centrifuged at 2200 x *g* for 15 min at 10°C. 100 µl of the supernatant from each well was transferred to a fresh well and the released hemoglobin measured by the absorbance at 545 nm using a Spectramax M5 plate reader (Molecular Devices, Sunnyvale, CA).

Overnight Secretion followed by Western blot analysis: A 10 ml culture of each *ipaB* mutant was grown as above, except the culture was incubated overnight. Bacteria were pelleted by centrifugation at 3000 x *g* and the supernatant was transferred to a 30 ml Corex centrifuge tube on ice. The bacterial pellet was resuspended in 1 ml of water and frozen. One ml of 100% TCA was mixed into the bacterial supernatant, followed by a one hr. incubation on ice. The samples were then spun at 11,800 x g for 15 min. The samples were washed with ice-cold 5% TCA and centrifuged as above. Next, the samples were washed twice with ice-cold acetone. After the final wash, the Corex tubes were inverted and the acetone completely evaporated. Once dry, the pellets

were resuspended with 400 µl PBS plus 200 µl 3x SDS-PAGE sample buffer plus 20 µl 1.5 M DTT. For quantitative purposes, the secreted proteins were analyzed by Western blot. Proteins were transferred to a polyvinylidene difluoride (PVDF) membrane using a Bio-Rad semi-dry blotter (15V, 37 min.). Membranes were blocked with Odyssey blocking buffer (LiCor, Lincoln, NE) diluted 1:1 with PBS for 1 hr. at room temperature while gently shaking. Then membranes were incubated overnight with IgG purified from rabbit anti-sera directed against IpaB, IpaC, and IpaD, diluted (1:1000) in blocking buffer prepared as above. The membranes were washed three times with PBS containing 0.05% Tween-20 to remove excess primary antibody. Alexa-Fluor 680 goat α-rabbit was diluted (1:10,000) as above. The secondary antibody was allowed one hr. to interact with the primary antibody-labeled membranes. Finally, the membranes were washed as above and then imaged on an Odyssey Infrared imager (LiCor).

Fluorescence Labeling of IpaB. To facilitate optimal labeling, IpaB was concentrated to at least 2 mg/ml prior to labeling. Monomeric or oligomeric IpaB was dialyzed into labeling buffer (see Appendix A) plus 5 mM Tris[2-carboxyethyl] phosphine (TCEP) pH: 7.0 and with either 0.05% LDAO or 0.5% OPOE overnight to reduce Cys residues for labeling. The TCEP concentration was adjusted to 1 mM by dialysis immediately before labeling. IpaB was removed from dialysis, 0.45 µm filtered and the concentration determined by absorbance at 280 nm. Enough fluorescein-5-maleimide (FM; Molecular Probes, Eugene, OR) to provide at least a 10-fold molar excess of FM:IpaB was dissolved in a minimal amount of dimethylformamide (DMF). 4 mg of IpaB was aliquoted to a small test tube, along with a 0.25 in. stir bar. The following steps were performed at room temperature while stirring. FM was added dropwise to IpaB and the test tube was purged with N_2 for 10 min to remove molecular oxygen. The labeling reaction was then sealed with paraffin paper and incubated for 2 hr. Free dye was removed from IpaB using an IMAC column. Binding buffer (8x) was added to the labeling reaction to equilibrate the protein with the IMAC. FM-labeled IpaB (FM-IpaB) was then bound to the IMAC and washed with at least 250 ml of

binding buffer plus either 0.05% LDAO or 0.5% OPOE and eluted as above. Peak fractions were pooled, concentrated to 2.5 ml and then buffer exchanged into 1x PBS with either 0.05% LDAO or 0.5% OPOE.

Concentrations were determined for the FM-labeled proteins using UV-Vis absorbance spectroscopy. The A_{280} must be corrected to account for the absorbance of light at 280 nm by the fluorescent probe. The A_{280} and A_{494} of FM-labeled proteins were collected. The A_{280} was corrected using the following equation:

Equation 6: $A_{280\ Observed} - (CF * A_{494}) = A_{280\ Actual}$

Where CF (CF = 0.3 for FM) is the correction factor, $A_{280\ Observed}$ is the experimentally determined absorbance at 280 nm, A_{494} is the experimentally determined absorbance at 494 nm, and $A_{280\ Actual}$ is the absorbance at 280 nm corrected for FM absorbance. $A_{280\ Actual}$ was used to calculate the protein concentration using the Beer-Lambert Law.

Equation 7: $A = \varepsilon cl$

Where A represents the absorbance value, ε represents the molar extinction coefficient, c represents the molar concentration, and l is the path length of the cuvette (1 cm).

The degree of labeling (DOL) was calculated using the following equation:

Equation 8: FM concentration (M) / Protein concentration (M) * 100 = DOL (%)

Fluorescence Quenching of fluorescein-labeled IpaB with potassium iodide. Emission spectra were collected using a Jobin-Yvon FluoroMax-4 spectrofluorometer (Edison, NJ). Samples were excited with 493 nm light using 5 nm slits. Emission was detected from 500-560 nm with 2.5 nm slits and an integration time of 0.1 sec. Fluorescein maleimide-labeled IpaB (FM-IpaB) was diluted into PBS with or without 0.15 mg/ml of liposomes to a final volume of 600 µl. The first

scan of each sample was in the absence of potassium iodide (KI), and then KI (KI stock = 4 M) was titrated 10 µl at a time into the sample, mixed thoroughly, and scanned again. F_o/F values were determined from the spectra using the observed emission maximum (E_{max}) of 518 nm. F_o/F values were plotted as a function of iodide concentration using an x,y scatter plot in Origin Pro 9.0 (OriginLab Corp., Northampton, MA). All subsequent analyses were done in Origin Pro 9.0. The Stern-Volmer equation (Equation 3) was fit to the data.[205]

Equation 3: $F_o/F = 1 + K_{SV}[\mathrm{KI}]$

F_0 is the fluorescence intensity at 515 nm prior to the addition of KI, and F is the fluorescence intensity at 515 nm after adding the specified concentration of KI. The Stern-Volmer quenching constant, K_{SV}, is equal to the slope and was calculated by Origin Pro 9.0.

Calculation of the Protection Index (PI). A protection index was calculated by the following equation as a means to visualize differences in the availability of a particular residue as a result of either oligomer formation or liposome interaction.[163]

Equation 4: $K_{SV}^{\ \mathrm{Monomer}} / K_{SV}^{\ \mathrm{Tetramer}}$ = Protection Index (PI)

We also calculated a protection index to determine how the solvent accessibility of residues was affected by the presence or absence of liposomes. This is the ratio of the $K_{SV}^{\ -\mathrm{Vesicles}}$ to the $K_{SV}^{\ +\mathrm{Vesicles}}$ (Equation 5).

Equation 5: $K_{SV}^{\ -\mathrm{Vesicles}} / K_{SV}^{\ +\mathrm{Vesicles}}$ = Protection Index (PI)

The PI's were plotted as column charts in Origin Pro with error bars representing the standard deviation.

.

REFERENCES

1. Cohen D, Green M, Block C, Slepon R, Ambar R, Wasserman SS, Levine MM. Reduction of transmission of shigellosis by control of houseflies (Musca domestica). Lancet 1991;337(8748):993-7.
2. Lindsay SW, Lindsay TC, Duprez J, Hall MJ, Kwambana BA, Jawara M, Nurudeen IU, Sallah N, Wyatt N, D'Alessandro U and others. Chrysomya putoria, a putative vector of diarrheal diseases. PLoS Negl Trop Dis 2012;6(11):e1895.
3. Hale TL KG. *Shigella*. In: S B, editor. Medical Microbiology. 4th ed. Galveston, TX: University of Texas Medical Branch at Galveston; 1996.
4. CDC. CfDCaP. National *Shigella* Surveillance Overview. In: US Department of Health and Human Services C, editor2011.
5. DuPont HL, Levine MM, Hornick RB, Formal SB. Inoculum size in shigellosis and implications for expected mode of transmission. J Infect Dis 1989;159(6):1126-8.
6. Mounier J, Vasselon T, Hellio R, Lesourd M, Sansonetti PJ. *Shigella* flexneri enters human colonic Caco-2 epithelial cells through the basolateral pole. Infect Immun 1992;60(1):237-48.
7. Bernardini ML, Mounier J, d'Hauteville H, Coquis-Rondon M, Sansonetti PJ. Identification of icsA, a plasmid locus of *Shigella flexneri* that governs bacterial intra- and intercellular spread through interaction with F-actin. Proc Natl Acad Sci U S A 1989;86(10):3867-71.
8. Sansonetti PJ. Pathogenesis of shigellosis: from molecular and cellular biology of epithelial cell invasion to tissue inflammation and vaccine development. Jpn J Med Sci Biol 1998;51 Suppl:S69-80.
9. Koneman E. Color Atlas and Textbook of Diagnostic Microbiology. New York: Lippincott-Raven Publishers; 1997.
10. Bergan J, Dyve Lingelem AB, Simm R, Skotland T, Sandvig K. Shiga toxins. Toxicon 2012;60(6):1085-107.
11. Luis M de la Maza MTP, Janet T Shigei, Ellena M Peterson. Color Atlas of Medical Bacteriology. ASM Press; 2004.
12. Saeed A, Abd H, Edvinsson B, Sandstrom G. Acanthamoeba castellanii an environmental host for *Shigella* dysenteriae and *Shigella* sonnei. Arch Microbiol 2009;191(1):83-8.
13. Nizeyi JB, Innocent RB, Erume J, Kalema GR, Cranfield MR, Graczyk TK. Campylobacteriosis, salmonellosis, and shigellosis in free-ranging human-habituated mountain gorillas of Uganda. J Wildl Dis 2001;37(2):239-44.

.

14. Bovee L, Whelan J, Sonder GJ, van Dam AP, van den Hoek A. Risk factors for secondary transmission of *Shigella* infection within households: implications for current prevention policy. BMC Infect Dis 2012;12:347.
15. Hossain MA, Hasan KZ, Albert MJ. *Shigella* carriers among non-diarrhoeal children in an endemic area of shigellosis in Bangladesh. Trop Geogr Med 1994;46(1):40-2.
16. Hale TL. Genetic basis of virulence in *Shigella* species. Microbiol Rev 1991;55(2):206-24.
17. Watkins HM. Some attributes of virulence in *Shigella*. Ann N Y Acad Sci 1960;88:1167-86.
18. Knight CL, Surawicz CM. Clostridium difficile Infection. Med Clin North Am 2013;97(4):523-36, ix.
19. Kweon MN. Shigellosis: the current status of vaccine development. Curr Opin Infect Dis 2008;21(3):313-8.
20. 2013 Diarrhoeal disease. World Health Organization <http://www.who.int/mediacentre/factsheets/fs330/en/index.html>.
21. Bardhan P, Faruque AS, Naheed A, Sack DA. Decrease in shigellosis-related deaths without *Shigella* spp.-specific interventions, Asia. Emerg Infect Dis 2010;16(11):1718-23.
22. Kotloff KL, Winickoff JP, Ivanoff B, Clemens JD, Swerdlow DL, Sansonetti PJ, Adak GK, Levine MM. Global burden of *Shigella* infections: implications for vaccine development and implementation of control strategies. Bull World Health Organ 1999;77(8):651-66.
23. Chang Z, Lu S, Chen L, Jin Q, Yang J. Causative species and serotypes of shigellosis in mainland China: systematic review and meta-analysis. PLoS One 2012;7(12):e52515.
24. von Seidlein L, Kim DR, Ali M, Lee H, Wang X, Thiem VD, Canh do G, Chaicumpa W, Agtini MD, Hossain A and others. A multicentre study of *Shigella* diarrhoea in six Asian countries: disease burden, clinical manifestations, and microbiology. PLoS Med 2006;3(9):e353.
25. Seol SY, Kim YT, Jeong YS, Oh JY, Kang HY, Moon DC, Kim J, Lee YC, Cho DT, Lee JC. Molecular characterization of antimicrobial resistance in *Shigella* sonnei isolates in Korea. J Med Microbiol 2006;55(Pt 7):871-7.
26. Wei HL, Wang YW, Li CC, Tung SK, Chiou CS. Epidemiology and evolution of genotype and antimicrobial resistance of an imported *Shigella* sonnei clone circulating in central Taiwan. Diagn Microbiol Infect Dis 2007;58(4):469-75.
27. Pickering LK, Evans DG, DuPont HL, Vollet JJ, 3rd, Evans DJ, Jr. Diarrhea caused by *Shigella*, rotavirus, and Giardia in day-care centers: prospective study. J Pediatr 1981;99(1):51-6.
28. Mahoney FJ, Farley TA, Burbank DF, Leslie NH, McFarland LM. Evaluation of an intervention program for the control of an outbreak of shigellosis among institutionalized persons. J Infect Dis 1993;168(5):1177-80.
29. Sharp TW, Thornton SA, Wallace MR, Defraites RF, Sanchez JL, Batchelor RA, Rozmajzl PJ, Hanson RK, Echeverria P, Kapikian AZ and others. Diarrheal disease among military personnel during Operation Restore Hope, Somalia, 1992-1993. Am J Trop Med Hyg 1995;52(2):188-93.
30. Ross AGP, Olds GR, Cripps AW, Farrar JJ, McManus DP. Enteropathogens and Chronic Illness in Returning Travelers. New England Journal of Medicine 2013;368(19):1817-1825.
31. Koster FT, Curlin GC, Aziz KM, Haque A. Synergistic impact of measles and diarrhoea on nutrition and mortality in Bangladesh. Bull World Health Organ 1981;59(6):901-8.
32. Mathur R, Mathur YN, Verma SD. An outbreak of shigellosis in central India: higher death rate in post-measles shigellosis. J Diarrhoeal Dis Res 1989;7(1-2):28-9.

33. Kotloff KL, Nataro JP, Blackwelder WC, Nasrin D, Farag TH, Panchalingam S, Wu Y, Sow SO, Sur D, Breiman RF and others. Burden and aetiology of diarrhoeal disease in infants and young children in developing countries (the Global Enteric Multicenter Study, GEMS): a prospective, case-control study. Lancet 2013;382(9888):209-22.
34. Butler T. Haemolytic uraemic syndrome during shigellosis. Trans R Soc Trop Med Hyg 2012;106(7):395-9.
35. Modell B, Berry RJ, Boyle CA, Christianson A, Darlison M, Dolk H, Howson CP, Mastroiacovo P, Mossey P, Rankin J. Global regional and national causes of child mortality. Lancet 2012;380(9853):1556; author reply 1556-7.
36. Fischer Walker CL, Perin J, Aryee MJ, Boschi-Pinto C, Black RE. Diarrhea incidence in low- and middle-income countries in 1990 and 2010: a systematic review. BMC Public Health 2012;12:220.
37. Checkley W, Buckley G, Gilman RH, Assis AM, Guerrant RL, Morris SS, Molbak K, Valentiner-Branth P, Lanata CF, Black RE. Multi-country analysis of the effects of diarrhoea on childhood stunting. Int J Epidemiol 2008;37(4):816-30.
38. Schmidt WP, Cairncross S, Barreto ML, Clasen T, Genser B. Recent diarrhoeal illness and risk of lower respiratory infections in children under the age of 5 years. Int J Epidemiol 2009;38(3):766-72.
39. Ashraf S, Huque MH, Kenah E, Agboatwalla M, Luby SP. Effect of recent diarrhoeal episodes on risk of pneumonia in children under the age of 5 years in Karachi, Pakistan. Int J Epidemiol 2013;42(1):194-200.
40. VanDerslice J, Briscoe J. Environmental interventions in developing countries: interactions and their implications. Am J Epidemiol 1995;141(2):135-44.
41. Bhattacharya D, Bhattacharya H, Thamizhmani R, Sayi DS, Reesu R, Anwesh M, Kartick C, Bharadwaj AP, Singhania M, Sugunan AP and others. Shigellosis in Bay of Bengal Islands, India: clinical and seasonal patterns, surveillance of antibiotic susceptibility patterns, and molecular characterization of multidrug-resistant *Shigella* strains isolated during a 6-year period from 2006 to 2011. Eur J Clin Microbiol Infect Dis 2013.
42. Gu B, Cao Y, Pan S, Zhuang L, Yu R, Peng Z, Qian H, Wei Y, Zhao L, Liu G and others. Comparison of the prevalence and changing resistance to nalidixic acid and ciprofloxacin of *Shigella* between Europe-America and Asia-Africa from 1998 to 2009. Int J Antimicrob Agents 2012;40(1):9-17.
43. Ke X, Gu B, Pan S, Tong M. Epidemiology and molecular mechanism of integron-mediated antibiotic resistance in *Shigella*. Arch Microbiol 2011;193(11):767-74.
44. DeLappe N, O'Halloran F, Fanning S, Corbett-Feeney G, Cheasty T, Cormican M. Antimicrobial resistance and genetic diversity of *Shigella* sonnei isolates from western Ireland, an area of low incidence of infection. J Clin Microbiol 2003;41(5):1919-24.
45. Mammina C, Pontello M, Dal Vecchio A, Nastasi A. Identification of *Shigella* sonnei biotype g isolates carrying class 2 integrons in Italy (2001 to 2003). J Clin Microbiol 2005;43(5):2467-70.
46. Notes from the field: Outbreak of infections caused by *Shigella* sonnei with decreased susceptibility to azithromycin--Los Angeles, California, 2012. MMWR Morb Mortal Wkly Rep 2013;62(9):171.
47. McDonnell J, Dallman T, Atkin S, Turbitt DA, Connor TR, Grant KA, Thomson NR, Jenkins C. Retrospective analysis of whole genome sequencing compared to prospective typing data in further informing the epidemiological investigation of an outbreak of *Shigella* sonnei in the UK. Epidemiol Infect 2013;141(12):2568-75.
48. Borg ML, Modi A, Tostmann A, Gobin M, Cartwright J, Quigley C, Crook P, Boxall N, Paul J, Cheasty T and others. Ongoing outbreak of *Shigella* flexneri serotype 3a in men

who have sex with men in England and Wales, data from 2009-2011. Euro Surveill 2012;17(13).
49. Okame M, Adachi E, Sato H, Shimizu S, Kikuchi T, Miyazaki N, Koga M, Nakamura H, Suzuki M, Oyaizu N and others. *Shigella* sonnei outbreak among men who have sex with men in Tokyo. Jpn J Infect Dis 2012;65(3):277-8.
50. Khan WA, Griffiths JK, Bennish ML. Gastrointestinal and extra-intestinal manifestations of childhood shigellosis in a region where all four species of *Shigella* are endemic. PLoS One 2013;8(5):e64097.
51. Tzipori S, Sheoran A, Akiyoshi D, Donohue-Rolfe A, Trachtman H. Antibody therapy in the management of shiga toxin-induced hemolytic uremic syndrome. Clin Microbiol Rev 2004;17(4):926-41, table of contents.
52. Gould LH, Demma L, Jones TF, Hurd S, Vugia DJ, Smith K, Shiferaw B, Segler S, Palmer A, Zansky S and others. Hemolytic uremic syndrome and death in persons with Escherichia coli O157:H7 infection, foodborne diseases active surveillance network sites, 2000-2006. Clin Infect Dis 2009;49(10):1480-5.
53. Bin Saeed AA, El Bushra HE, Al-Hamdan NA. Does treatment of bloody diarrhea due to *Shigella* dysenteriae type 1 with ampicillin precipitate hemolytic uremic syndrome? Emerg Infect Dis 1995;1(4):134-7.
54. Al-Qarawi S, Fontaine RE, Al-Qahtani MS. An outbreak of hemolytic uremic syndrome associated with antibiotic treatment of hospital inpatients for dysentery. Emerg Infect Dis 1995;1(4):138-40.
55. Vinh H, Anh VT, Anh ND, Campbell JI, Hoang NV, Nga TV, Nhu NT, Minh PV, Thuy CT, Duy PT and others. A multi-center randomized trial to assess the efficacy of gatifloxacin versus ciprofloxacin for the treatment of shigellosis in Vietnamese children. PLoS Negl Trop Dis 2011;5(8):e1264.
56. Hannu T, Mattila L, Siitonen A, Leirisalo-Repo M. Reactive arthritis attributable to *Shigella* infection: a clinical and epidemiological nationwide study. Ann Rheum Dis 2005;64(4):594-8.
57. Connor BA, Riddle MS. Post-infectious sequelae of travelers' diarrhea. J Travel Med 2013;20(5):303-12.
58. Morse HG, Rate RG, Bonnell MD, Kuberski TT. Reiter's syndrome in a five-year-old girl. Arthritis Rheum 1980;23(8):960-1.
59. Simon DG, Kaslow RA, Rosenbaum J, Kaye RL, Calin A. Reiter's syndrome following epidemic shigellosis. J Rheumatol 1981;8(6):969-73.
60. Lauhio A, Lahdevirta J, Janes R, Kontiainen S, Repo H. Reactive arthritis associated with *Shigella* sonnei infection. Arthritis Rheum 1988;31(9):1190-3.
61. Chen M, Delpech V, O'Sullivan B, Donovan B. *Shigella* sonnei: another cause of sexually acquired reactive arthritis. Int J STD AIDS 2002;13(2):135-6.
62. Schiellerup P, Krogfelt KA, Locht H. A comparison of self-reported joint symptoms following infection with different enteric pathogens: effect of HLA-B27. J Rheumatol 2008;35(3):480-7.
63. Connor BA. Sequelae of traveler's diarrhea: focus on postinfectious irritable bowel syndrome. Clin Infect Dis 2005;41 Suppl 8:S577-86.
64. Borgaonkar MR, Ford DC, Marshall JK, Churchill E, Collins SM. The incidence of irritable bowel syndrome among community subjects with previous acute enteric infection. Dig Dis Sci 2006;51(5):1026-32.
65. McKendrick MW, Read NW. Irritable bowel syndrome--post salmonella infection. J Infect 1994;29(1):1-3.
66. Spiller R, Garsed K. Postinfectious irritable bowel syndrome. Gastroenterology 2009;136(6):1979-88.

67. Gwee KA, Graham JC, McKendrick MW, Collins SM, Marshall JS, Walters SJ, Read NW. Psychometric scores and persistence of irritable bowel after infectious diarrhoea. Lancet 1996;347(8995):150-3.
68. Bashashati M, Rezaei N, Bashashati H, Shafieyoun A, Daryani NE, Sharkey KA, Storr M. Cytokine gene polymorphisms are associated with irritable bowel syndrome: a systematic review and meta-analysis. Neurogastroenterol Motil 2012;24(12):1102-e566.
69. Sansonetti PJ, Kopecko DJ, Formal SB. Involvement of a plasmid in the invasive ability of *Shigella flexneri*. Infect Immun 1982;35(3):852-60.
70. Buchrieser C, Glaser P, Rusniok C, Nedjari H, D'Hauteville H, Kunst F, Sansonetti P, Parsot C. The virulence plasmid pWR100 and the repertoire of proteins secreted by the type III secretion apparatus of *Shigella* flexneri. Mol Microbiol 2000;38(4):760-71.
71. Venkatesan MM, Goldberg MB, Rose DJ, Grotbeck EJ, Burland V, Blattner FR. Complete DNA sequence and analysis of the large virulence plasmid of *Shigella* flexneri. Infect Immun 2001;69(5):3271-85.
72. Schroeder GN, Hilbi H. Molecular pathogenesis of *Shigella* spp.: controlling host cell signaling, invasion, and death by type III secretion. Clin Microbiol Rev 2008;21(1):134-56.
73. Sasakawa C, Kamata K, Sakai T, Makino S, Yamada M, Okada N, Yoshikawa M. Virulence-associated genetic regions comprising 31 kilobases of the 230-kilobase plasmid in *Shigella flexneri 2a*. J Bacteriol 1988;170(6):2480-4.
74. Sasakawa C, Komatsu K, Tobe T, Suzuki T, Yoshikawa M. Eight genes in region 5 that form an operon are essential for invasion of epithelial cells by *Shigella flexneri 2a*. J Bacteriol 1993;175(8):2334-46.
75. Maurelli AT, Baudry B, d'Hauteville H, Hale TL, Sansonetti PJ. Cloning of plasmid DNA sequences involved in invasion of HeLa cells by *Shigella flexneri*. Infect Immun 1985;49(1):164-71.
76. Tobe T, Nagai S, Okada N, Adler B, Yoshikawa M, Sasakawa C. Temperature-regulated expression of invasion genes in *Shigella* flexneri is controlled through the transcriptional activation of the virB gene on the large plasmid. Mol Microbiol 1991;5(4):887-93.
77. Mavris M, Page AL, Tournebize R, Demers B, Sansonetti P, Parsot C. Regulation of transcription by the activity of the *Shigella flexneri* type III secretion apparatus. Mol Microbiol 2002;43(6):1543-53.
78. Blocker A, Gounon P, Larquet E, Niebuhr K, Cabiaux V, Parsot C, Sansonetti P. The tripartite type III secreton of *Shigella flexneri* inserts IpaB and IpaC into host membranes. J Cell Biol 1999;147(3):683-93.
79. Hilbi H, Moss JE, Hersh D, Chen Y, Arondel J, Banerjee S, Flavell RA, Yuan J, Sansonetti PJ, Zychlinsky A. *Shigella*-induced apoptosis is dependent on caspase-1 which binds to IpaB. J Biol Chem 1998;273(49):32895-900.
80. Tran Van Nhieu G, Caron E, Hall A, Sansonetti PJ. IpaC induces actin polymerization and filopodia formation during *Shigella* entry into epithelial cells. Embo J 1999;18(12):3249-62.
81. Menard R, Sansonetti P, Parsot C. The secretion of the *Shigella flexneri* Ipa invasins is activated by epithelial cells and controlled by IpaB and IpaD. Embo J 1994;13(22):5293-302.
82. Menard R, Sansonetti PJ, Parsot C. Nonpolar mutagenesis of the ipa genes defines IpaB, IpaC, and IpaD as effectors of *Shigella flexneri* entry into epithelial cells. J Bacteriol 1993;175(18):5899-906.
83. Stensrud KF, Adam PR, La Mar CD, Olive AJ, Lushington GH, Sudharsan R, Shelton NL, Givens RS, Picking WL, Picking WD. Deoxycholate interacts with IpaD of *Shigella flexneri* in inducing the recruitment of IpaB to the type III secretion apparatus needle tip. J Biol Chem 2008;283(27):18646-54.

84. Olive AJ, Kenjale R, Espina M, Moore DS, Picking WL, Picking WD. Bile salts stimulate recruitment of IpaB to the *Shigella flexneri* surface, where it colocalizes with IpaD at the tip of the type III secretion needle. Infect Immun 2007;75(5):2626-9.
85. Venkatesan MM, Buysse JM, Oaks EV. Surface presentation of *Shigella* flexneri invasion plasmid antigens requires the products of the spa locus. J Bacteriol 1992;174(6):1990-2001.
86. Hromockyj AE, Maurelli AT. Identification of *Shigella* invasion genes by isolation of temperature-regulated inv::lacZ operon fusions. Infect Immun 1989;57(10):2963-70.
87. Adler B, Sasakawa C, Tobe T, Makino S, Komatsu K, Yoshikawa M. A dual transcriptional activation system for the 230 kb plasmid genes coding for virulence-associated antigens of *Shigella flexneri*. Mol Microbiol 1989;3(5):627-35.
88. Kane CD, Schuch R, Day WA, Jr., Maurelli AT. MxiE regulates intracellular expression of factors secreted by the *Shigella* flexneri 2a type III secretion system. J Bacteriol 2002;184(16):4409-19.
89. Page AL, Ohayon H, Sansonetti PJ, Parsot C. The secreted IpaB and IpaC invasins and their cytoplasmic chaperone IpgC are required for intercellular dissemination of *Shigella flexneri*. Cell Microbiol 1999;1(2):183-93.
90. Page AL, Sansonetti P, Parsot C. Spa15 of *Shigella flexneri*, a third type of chaperone in the type III secretion pathway. Mol Microbiol 2002;43(6):1533-42.
91. Parsot C, Hamiaux C, Page AL. The various and varying roles of specific chaperones in type III secretion systems. Curr Opin Microbiol 2003;6(1):7-14.
92. Pilonieta MC, Munson GP. The chaperone IpgC copurifies with the virulence regulator MxiE. J Bacteriol 2008;190(6):2249-51.
93. Parsot C, Ageron E, Penno C, Mavris M, Jamoussi K, d'Hauteville H, Sansonetti P, Demers B. A secreted anti-activator, OspD1, and its chaperone, Spa15, are involved in the control of transcription by the type III secretion apparatus activity in *Shigella* flexneri. Mol Microbiol 2005;56(6):1627-35.
94. Skoudy A, Mounier J, Aruffo A, Ohayon H, Gounon P, Sansonetti P, Tran Van Nhieu G. CD44 binds to the *Shigella* IpaB protein and participates in bacterial invasion of epithelial cells. Cell Microbiol 2000;2(1):19-33.
95. Watarai M, Funato S, Sasakawa C. Interaction of Ipa proteins of *Shigella* flexneri with alpha5beta1 integrin promotes entry of the bacteria into mammalian cells. J Exp Med 1996;183(3):991-9.
96. Lafont F, Tran Van Nhieu G, Hanada K, Sansonetti P, van der Goot FG. Initial steps of *Shigella* infection depend on the cholesterol/sphingolipid raft-mediated CD44-IpaB interaction. Embo J 2002;21(17):4449-57.
97. Handa Y, Suzuki M, Ohya K, Iwai H, Ishijima N, Koleske AJ, Fukui Y, Sasakawa C. *Shigella* IpgB1 promotes bacterial entry through the ELMO-Dock180 machinery. Nat Cell Biol 2007;9(1):121-8.
98. Alto NM, Shao F, Lazar CS, Brost RL, Chua G, Mattoo S, McMahon SA, Ghosh P, Hughes TR, Boone C and others. Identification of a bacterial type III effector family with G protein mimicry functions. Cell 2006;124(1):133-45.
99. Yoshida S, Katayama E, Kuwae A, Mimuro H, Suzuki T, Sasakawa C. *Shigella* deliver an effector protein to trigger host microtubule destabilization, which promotes Rac1 activity and efficient bacterial internalization. Embo J 2002;21(12):2923-35.
100. Niebuhr K, Giuriato S, Pedron T, Philpott DJ, Gaits F, Sable J, Sheetz MP, Parsot C, Sansonetti PJ, Payrastre B. Conversion of PtdIns(4,5)P(2) into PtdIns(5)P by the *S. flexneri* effector IpgD reorganizes host cell morphology. Embo J 2002;21(19):5069-78.
101. Bourdet-Sicard R, Rudiger M, Jockusch BM, Gounon P, Sansonetti PJ, Nhieu GT. Binding of the *Shigella* protein IpaA to vinculin induces F-actin depolymerization. Embo J 1999;18(21):5853-62.

102. Ramarao N, Le Clainche C, Izard T, Bourdet-Sicard R, Ageron E, Sansonetti PJ, Carlier MF, Tran Van Nhieu G. Capping of actin filaments by vinculin activated by the *Shigella* IpaA carboxyl-terminal domain. FEBS Lett 2007;581(5):853-7.
103. Sansonetti PJ, Arondel J, Cantey JR, Prevost MC, Huerre M. Infection of rabbit Peyer's patches by *Shigella* flexneri: effect of adhesive or invasive bacterial phenotypes on follicle-associated epithelium. Infect Immun 1996;64(7):2752-64.
104. Wassef JS, Keren DF, Mailloux JL. Role of M cells in initial antigen uptake and in ulcer formation in the rabbit intestinal loop model of shigellosis. Infect Immun 1989;57(3):858-63.
105. Chen Y, Smith MR, Thirumalai K, Zychlinsky A. A bacterial invasin induces macrophage apoptosis by binding directly to ICE. EMBO J 1996;15(15):3853-60.
106. Zychlinsky A, Kenny B, Menard R, Prevost MC, Holland IB, Sansonetti PJ. IpaB mediates macrophage apoptosis induced by *Shigella flexneri*. Mol Microbiol 1994;11(4):619-27.
107. Sansonetti PJ, Phalipon A, Arondel J, Thirumalai K, Banerjee S, Akira S, Takeda K, Zychlinsky A. Caspase-1 activation of IL-1beta and IL-18 are essential for *Shigella flexneri*-induced inflammation. Immunity 2000;12(5):581-90.
108. Clerc PL, Ryter A, Mounier J, Sansonetti PJ. Plasmid-mediated early killing of eucaryotic cells by *Shigella* flexneri as studied by infection of J774 macrophages. Infect Immun 1987;55(3):521-7.
109. Barzu S, Benjelloun-Touimi Z, Phalipon A, Sansonetti P, Parsot C. Functional analysis of the *Shigella flexneri* IpaC invasin by insertional mutagenesis. Infect Immun 1997;65(5):1599-605.
110. High N, Mounier J, Prevost MC, Sansonetti PJ. IpaB of *Shigella flexneri* causes entry into epithelial cells and escape from the phagocytic vacuole. Embo J 1992;11(5):1991-9.
111. Picking WL, Nishioka H, Hearn PD, Baxter MA, Harrington AT, Blocker A, Picking WD. IpaD of *Shigella flexneri* is independently required for regulation of Ipa protein secretion and efficient insertion of IpaB and IpaC into host membranes. Infect Immun 2005;73(3):1432-40.
112. Fernandez-Prada CM, Hoover DL, Tall BD, Hartman AB, Kopelowitz J, Venkatesan MM. *Shigella* flexneri IpaH(7.8) facilitates escape of virulent bacteria from the endocytic vacuoles of mouse and human macrophages. Infect Immun 2000;68(6):3608-19.
113. Pendaries C, Tronchere H, Arbibe L, Mounier J, Gozani O, Cantley L, Fry MJ, Gaits-Iacovoni F, Sansonetti PJ, Payrastre B. PtdIns5P activates the host cell PI3-kinase/Akt pathway during *Shigella* flexneri infection. EMBO J 2006;25(5):1024-34.
114. Clark CS, Maurelli AT. *Shigella* flexneri inhibits staurosporine-induced apoptosis in epithelial cells. Infect Immun 2007;75(5):2531-9.
115. Kramer RW, Slagowski NL, Eze NA, Giddings KS, Morrison MF, Siggers KA, Starnbach MN, Lesser CF. Yeast functional genomic screens lead to identification of a role for a bacterial effector in innate immunity regulation. PLoS Pathog 2007;3(2):e21.
116. Li H, Xu H, Zhou Y, Zhang J, Long C, Li S, Chen S, Zhou JM, Shao F. The phosphothreonine lyase activity of a bacterial type III effector family. Science 2007;315(5814):1000-3.
117. Arbibe L, Kim DW, Batsche E, Pedron T, Mateescu B, Muchardt C, Parsot C, Sansonetti PJ. An injected bacterial effector targets chromatin access for transcription factor NF-kappaB to alter transcription of host genes involved in immune responses. Nat Immunol 2007;8(1):47-56.
118. Kim DW, Lenzen G, Page AL, Legrain P, Sansonetti PJ, Parsot C. The *Shigella* flexneri effector OspG interferes with innate immune responses by targeting ubiquitin-conjugating enzymes. Proc Natl Acad Sci U S A 2005;102(39):14046-51.

119. Rohde JR, Breitkreutz A, Chenal A, Sansonetti PJ, Parsot C. Type III secretion effectors of the IpaH family are E3 ubiquitin ligases. Cell Host Microbe 2007;1(1):77-83.
120. Yoshida S, Handa Y, Suzuki T, Ogawa M, Suzuki M, Tamai A, Abe A, Katayama E, Sasakawa C. Microtubule-severing activity of *Shigella* is pivotal for intercellular spreading. Science 2006;314(5801):985-9.
121. Goldberg MB, Barzu O, Parsot C, Sansonetti PJ. Unipolar localization and ATPase activity of IcsA, a *Shigella flexneri* protein involved in intracellular movement. Infect Agents Dis 1993;2(4):210-1.
122. Goldberg MB, Theriot JA. *Shigella* flexneri surface protein IcsA is sufficient to direct actin-based motility. Proc Natl Acad Sci U S A 1995;92(14):6572-6.
123. Rathman M, de Lanerolle P, Ohayon H, Gounon P, Sansonetti P. Myosin light chain kinase plays an essential role in S. flexneri dissemination. J Cell Sci 2000;113 Pt 19:3375-86.
124. Schuch R, Sandlin RC, Maurelli AT. A system for identifying post-invasion functions of invasion genes: requirements for the Mxi-Spa type III secretion pathway of *Shigella* flexneri in intercellular dissemination. Mol Microbiol 1999;34(4):675-89.
125. Calderwood SB, Auclair F, Donohue-Rolfe A, Keusch GT, Mekalanos JJ. Nucleotide sequence of the Shiga-like toxin genes of Escherichia coli. Proc Natl Acad Sci U S A 1987;84(13):4364-8.
126. Takao T, Tanabe T, Hong YM, Shimonishi Y, Kurazono H, Yutsudo T, Sasakawa C, Yoshikawa M, Takeda Y. Identity of molecular structure of Shiga-like toxin I (VT1) from *Escherichia coli* O157:H7 with that of Shiga toxin. Microb Pathog 1988;5(5):57-69.
127. Fraser ME, Chernaia MM, Kozlov YV, James MN. Crystal structure of the holotoxin from *Shigella* dysenteriae at 2.5 A resolution. Nat Struct Biol 1994;1(1):59-64.
128. Stein PE, Boodhoo A, Tyrrell GJ, Brunton JL, Read RJ. Crystal structure of the cell-binding B oligomer of verotoxin-1 from E. coli. Nature 1992;355(6362):748-50.
129. Lindberg AA, Brown JE, Stromberg N, Westling-Ryd M, Schultz JE, Karlsson KA. Identification of the carbohydrate receptor for Shiga toxin produced by *Shigella* dysenteriae type 1. J Biol Chem 1987;262(4):1779-85.
130. Garred O, van Deurs B, Sandvig K. Furin-induced cleavage and activation of Shiga toxin. J Biol Chem 1995;270(18):10817-21.
131. Saxena SK, O'Brien AD, Ackerman EJ. Shiga toxin, Shiga-like toxin II variant, and ricin are all single-site RNA N-glycosidases of 28 S RNA when microinjected into Xenopus oocytes. J Biol Chem 1989;264(1):596-601.
132. Tesh VL. Induction of apoptosis by Shiga toxins. Future Microbiol 2010;5(3):431-53.
133. Brigotti M, Tazzari PL, Ravanelli E, Carnicelli D, Rocchi L, Arfilli V, Scavia G, Minelli F, Ricci F, Pagliaro P and others. Clinical relevance of shiga toxin concentrations in the blood of patients with hemolytic uremic syndrome. Pediatr Infect Dis J 2011;30(6):486-90.
134. Faherty CS, Harper JM, Shea-Donohue T, Barry EM, Kaper JB, Fasano A, Nataro JP. Chromosomal and plasmid-encoded factors of *Shigella* flexneri induce secretogenic activity ex vivo. PLoS One 2012;7(11):e49980.
135. Fasano A, Noriega FR, Maneval DR, Jr., Chanasongcram S, Russell R, Guandalini S, Levine MM. *Shigella* enterotoxin 1: an enterotoxin of *Shigella* flexneri 2a active in rabbit small intestine in vivo and in vitro. J Clin Invest 1995;95(6):2853-61.
136. Yavzori M, Cohen D, Orr N. Prevalence of the genes for *Shigella* enterotoxins 1 and 2 among clinical isolates of *Shigella* in Israel. Epidemiol Infect 2002;128(3):533-5.
137. Niyogi SK, Vargas M, Vila J. Prevalence of the sat, set and sen genes among diverse serotypes of *Shigella* flexneri strains isolated from patients with acute diarrhoea. Clin Microbiol Infect 2004;10(6):574-6.

138. Nataro JP, Seriwatana J, Fasano A, Maneval DR, Guers LD, Noriega F, Dubovsky F, Levine MM, Morris JG, Jr. Identification and cloning of a novel plasmid-encoded enterotoxin of enteroinvasive Escherichia coli and *Shigella* strains. Infect Immun 1995;63(12):4721-8.
139. Roy S, Thanasekaran K, Dutta Roy AR, Sehgal SC. Distribution of *Shigella* enterotoxin genes and secreted autotransporter toxin gene among diverse species and serotypes of *Shigella* isolated from Andaman Islands, India. Trop Med Int Health 2006;11(11):1694-8.
140. Farfan MJ, Toro CS, Barry EM, Nataro JP. *Shigella* enterotoxin-2 is a type III effector that participates in *Shigella*-induced interleukin 8 secretion by epithelial cells. FEMS Immunol Med Microbiol 2011;61(3):332-9.
141. Ruiz-Perez F, Wahid R, Faherty CS, Kolappaswamy K, Rodriguez L, Santiago A, Murphy E, Cross A, Sztein MB, Nataro JP. Serine protease autotransporters from *Shigella* flexneri and pathogenic Escherichia coli target a broad range of leukocyte glycoproteins. Proc Natl Acad Sci U S A 2011;108(31):12881-6.
142. Harrington SM, Sheikh J, Henderson IR, Ruiz-Perez F, Cohen PS, Nataro JP. The Pic protease of enteroaggregative Escherichia coli promotes intestinal colonization and growth in the presence of mucin. Infect Immun 2009;77(6):2465-73.
143. Kotloff KL, Pasetti MF, Barry EM, Nataro JP, Wasserman SS, Sztein MB, Picking WD, Levine MM. Deletion in the *Shigella* enterotoxin genes further attenuates *Shigella* flexneri 2a bearing guanine auxotrophy in a phase 1 trial of CVD 1204 and CVD 1208. J Infect Dis 2004;190(10):1745-54.
144. Birket SE, Harrington AT, Espina M, Smith ND, Terry CM, Darboe N, Markham AP, Middaugh CR, Picking WL, Picking WD. Preparation and characterization of translocator/chaperone complexes and their component proteins from *Shigella flexneri*. Biochemistry 2007;46(27):8128-37.
145. Lunelli M, Lokareddy RK, Zychlinsky A, Kolbe M. IpaB-IpgC interaction defines binding motif for type III secretion translocator. Proc Natl Acad Sci U S A 2009;106(24):9661-6.
146. Barta ML, Zhang L, Picking WL, Geisbrecht BV. Evidence for alternative quaternary structure in a bacterial Type III secretion system chaperone. BMC Struct Biol 2010;10:21.
147. Job V, Mattei PJ, Lemaire D, Attree I, Dessen A. Structural basis of chaperone recognition of type III secretion system minor translocator proteins. J Biol Chem 2010;285(30):23224-32.
148. Bongrand C, Sansonetti PJ, Parsot C. Characterization of the promoter, MxiE box and 5' UTR of genes controlled by the activity of the type III secretion apparatus in *Shigella* flexneri. PLoS One 2012;7(3):e32862.
149. Lokareddy RK, Lunelli M, Eilers B, Wolter V, Kolbe M. Combination of two separate binding domains defines stoichiometry between type III secretion system chaperone IpgC and translocator protein IpaB. J Biol Chem 2010;285(51):39965-75.
150. Barta ML, Dickenson NE, Patil M, Keightley A, Wyckoff GJ, Picking WD, Picking WL, Geisbrecht BV. The structures of coiled-coil domains from type III secretion system translocators reveal homology to pore-forming toxins. J Mol Biol 2012;417(5):395-405.
151. Adam PR, Patil MK, Dickenson NE, Choudhari S, Barta M, Geisbrecht BV, Picking WL, Picking WD. Binding Affects the Tertiary and Quaternary Structures of the *Shigella* Translocator Protein IpaB and Its Chaperone IpgC. Biochemistry 2012;51(19):4062-4071.
152. Wiener M, Freymann D, Ghosh P, Stroud RM. Crystal structure of colicin Ia. Nature 1997;385(6615):461-4.
153. Soelaiman S, Jakes K, Wu N, Li C, Shoham M. Crystal structure of colicin E3: implications for cell entry and ribosome inactivation. Mol Cell 2001;8(5):1053-62.

154. Lakowicz JR. Principles of Fluorescence Spectroscopy. New York: Plenum Press; 1983.
155. Buttner CR, Sorg I, Cornelis GR, Heinz DW, Niemann HH. Structure of the Yersinia enterocolitica type III secretion translocator chaperone SycD. J Mol Biol 2008;375(4):997-1012.
156. Villamil Giraldo AM, Lopez Medus M, Gonzalez Lebrero M, Pagano RS, Labriola CA, Landolfo L, Delfino JM, Parodi AJ, Caramelo JJ. The structure of calreticulin C-terminal domain is modulated by physiological variations of calcium concentration. J Biol Chem 2010;285(7):4544-53.
157. Dickenson NE, Choudhari SP, Adam PR, Kramer RM, Joshi SB, Middaugh CR, Picking WL, Picking WD. Oligomeric states of the *Shigella* translocator protein IpaB provide structural insights into formation of the type III secretion translocon. Protein Sci 2013;22(5):614-27.
158. Senerovic L, Tsunoda SP, Goosmann C, Brinkmann V, Zychlinsky A, Meissner F, Kolbe M. Spontaneous formation of IpaB ion channels in host cell membranes reveals how *Shigella* induces pyroptosis in macrophages. Cell Death Dis 2012;3:e384.
159. Akeda Y, Galan JE. Chaperone release and unfolding of substrates in type III secretion. Nature 2005;437(7060):911-5.
160. Guichon A, Hersh D, Smith MR, Zychlinsky A. Structure-function analysis of the *Shigella* virulence factor IpaB. J Bacteriol 2001;183(4):1269-76.
161. Harrington AT, Hearn PD, Picking WL, Barker JR, Wessel A, Picking WD. Structural characterization of the N terminus of IpaC from *Shigella flexneri*. Infect Immun 2003;71(3):1255-64.
162. Harrington A, Darboe N, Kenjale R, Picking WL, Middaugh CR, Birket S, Picking WD. Characterization of the Interaction of Single Tryptophan Containing Mutants of IpaC from *Shigella flexneri* with Phospholipid Membranes. Biochemistry 2006;45(2):626-36.
163. Nalefski EA, Falke JJ. Location of the Membrane-Docking Face on the Ca2+-Activated C2 Domain of Cytosolic Phospholipase A2†. Biochemistry 1998;37(51):17642-17650.
164. Roehrich AD, Martinez-Argudo I, Johnson S, Blocker AJ, Veenendaal AK. The extreme C-terminus of *Shigella* IpaB is required for regulation of T3SS secretion, needle-tip composition and binding. Infect Immun 2010.
165. Epler CR, Dickenson NE, Bullitt E, Picking WL. Ultrastructural analysis of IpaD at the tip of the nascent MxiH type III secretion apparatus of *Shigella flexneri*. J Mol Biol 2012;420(1-2):29-39.
166. Hume PJ, McGhie EJ, Hayward RD, Koronakis V. The purified *Shigella* IpaB and *Salmonella* SipB translocators share biochemical properties and membrane topology. Mol Microbiol 2003;49(2):425-39.
167. Zakharov SD, Kotova EA, Antonenko YN, Cramer WA. On the role of lipid in colicin pore formation. Biochim Biophys Acta 2004;1666(1-2):239-49.
168. Greig SL, Radjainia M, Mitra AK. Oligomeric structure of colicin ia channel in lipid bilayer membranes. J Biol Chem 2009;284(24):16126-34.
169. Lindeberg M, Cunnac S, Collmer A. Pseudomonas syringae type III effector repertoires: last words in endless arguments. Trends in Microbiology 2012;20(4):199-208.
170. Block A, Alfano JR. Plant targets for Pseudomonas syringae type III effectors: virulence targets or guarded decoys? Curr Opin Microbiol 2011;14(1):39-46.
171. Baltrus DA, Nishimura MT, Romanchuk A, Chang JH, Mukhtar MS, Cherkis K, Roach J, Grant SR, Jones CD, Dangl JL. Dynamic evolution of pathogenicity revealed by sequencing and comparative genomics of 19 Pseudomonas syringae isolates. PLoS Pathog 2011;7(7):e1002132.
172. Kvitko BH, Ramos AR, Morello JE, Oh HS, Collmer A. Identification of harpins in Pseudomonas syringae pv. tomato DC3000, which are functionally similar to HrpK1 in

promoting translocation of type III secretion system effectors. J Bacteriol 2007;189(22):8059-72.
173. Lindeberg M, Stavrinides J, Chang JH, Alfano JR, Collmer A, Dangl JL, Greenberg JT, Mansfield JW, Guttman DS. Proposed guidelines for a unified nomenclature and phylogenetic analysis of type III Hop effector proteins in the plant pathogen Pseudomonas syringae. Mol Plant Microbe Interact 2005;18(4):275-82.
174. Charkowski AO, Alfano JR, Preston G, Yuan J, He SY, Collmer A. The Pseudomonas syringae pv. tomato HrpW protein has domains similar to harpins and pectate lyases and can elicit the plant hypersensitive response and bind to pectate. J Bacteriol 1998;180(19):5211-7.
175. Preston G, Huang HC, He SY, Collmer A. The HrpZ proteins of Pseudomonas syringae pvs. syringae, glycinea, and tomato are encoded by an operon containing Yersinia ysc homologs and elicit the hypersensitive response in tomato but not soybean. Mol Plant Microbe Interact 1995;8(5):717-32.
176. Ferreira AO, Myers CR, Gordon JS, Martin GB, Vencato M, Collmer A, Wehling MD, Alfano JR, Moreno-Hagelsieb G, Lamboy WF and others. Whole-genome expression profiling defines the HrpL regulon of Pseudomonas syringae pv. tomato DC3000, allows de novo reconstruction of the Hrp cis clement, and identifies novel coregulated genes. Mol Plant Microbe Interact 2006;19(11):1167-79.
177. Lee J, Klusener B, Tsiamis G, Stevens C, Neyt C, Tampakaki AP, Panopoulos NJ, Noller J, Weiler EW, Cornelis GR and others. HrpZ(Psph) from the plant pathogen Pseudomonas syringae pv. phaseolicola binds to lipid bilayers and forms an ion-conducting pore in vitro. Proc Natl Acad Sci U S A 2001;98(1):289-94.
178. Oh HS, Kvitko BH, Morello JE, Collmer A. Pseudomonas syringae lytic transglycosylases coregulated with the type III secretion system contribute to the translocation of effector proteins into plant cells. J Bacteriol 2007;189(22):8277-89.
179. Oh HS, Park DH, Collmer A. Components of the Pseudomonas syringae type III secretion system can suppress and may elicit plant innate immunity. Mol Plant Microbe Interact 2010;23(6):727-39.
180. Espina M, Olive AJ, Kenjale R, Moore DS, Ausar SF, Kaminski RW, Oaks EV, Middaugh CR, Picking WD, Picking WL. IpaD Localizes to the Tip of the Type III Secretion System Needle of *Shigella flexneri*. Infect Immun 2006;74(8):4391-400.
181. Bannantine JP, Lingle CK, Stabel JR, Ramyar KX, Garcia BL, Raeber AJ, Schacher P, Kapur V, Geisbrecht BV. MAP1272c encodes an NlpC/P60 protein, an antigen detected in cattle with Johne's disease. Clin Vaccine Immunol 2012;19(7):1083-92.
182. Dennis MM, Antognoli MC, Garry FB, Hirst HL, Lombard JE, Gould DH, Salman MD. Association of severity of enteric granulomatous inflammation with disseminated Mycobacterium avium subspecies paratuberculosis infection and antemortem test results for paratuberculosis in dairy cows. Vet Microbiol 2008;131(1-2):154-63.
183. Raizman EA, Fetrow JP, Wells SJ. Loss of income from cows shedding Mycobacterium avium subspecies paratuberculosis prior to calving compared with cows not shedding the organism on two Minnesota dairy farms. J Dairy Sci 2009;92(10):4929-36.
184. Aramini JM, Rossi P, Huang YJ, Zhao L, Jiang M, Maglaqui M, Xiao R, Locke J, Nair R, Rost B and others. Solution NMR structure of the NlpC/P60 domain of lipoprotein Spr from Escherichia coli: structural evidence for a novel cysteine peptidase catalytic triad. Biochemistry 2008;47(37):9715-7.
185. Rabsch W, Tschape H, Baumler AJ. Non-typhoidal salmonellosis: emerging problems. Microbes Infect 2001;3(3):237-47.
186. Crawford RW, Rosales-Reyes R, Ramirez-Aguilar Mde L, Chapa-Azuela O, Alpuche-Aranda C, Gunn JS. Gallstones play a significant role in Salmonella spp. gallbladder colonization and carriage. Proc Natl Acad Sci U S A 2010;107(9):4353-8.

187. Moest TP, Meresse S. Salmonella T3SSs: successful mission of the secret(ion) agents. Curr Opin Microbiol 2013;16(1):38-44.
188. Aussel L, Zhao W, Hebrard M, Guilhon AA, Viala JP, Henri S, Chasson L, Gorvel JP, Barras F, Meresse S. Salmonella detoxifying enzymes are sufficient to cope with the host oxidative burst. Mol Microbiol 2011;80(3):628-40.
189. Ellermeier JR, Slauch JM. Adaptation to the host environment: regulation of the SPI1 type III secretion system in Salmonella enterica serovar Typhimurium. Curr Opin Microbiol 2007;10(1):24-9.
190. Gunn JS. Mechanisms of bacterial resistance and response to bile. Microbes Infect 2000;2(8):907-13.
191. Prouty AM, Gunn JS. *Salmonella enterica* serovar typhimurium invasion is repressed in the presence of bile. Infect Immun 2000;68(12):6763-9.
192. Prouty AM, Brodsky IE, Manos J, Belas R, Falkow S, Gunn JS. Transcriptional regulation of *Salmonella enterica* serovar Typhimurium genes by bile. FEMS Immunol Med Microbiol 2004;41(2):177-85.
193. Kaniga K, Trollinger D, Galan JE. Identification of two targets of the type III protein secretion system encoded by the inv and spa loci of *Salmonella typhimurium* that have homology to the *Shigella* IpaD and IpaA proteins. J Bacteriol 1995;177(24):7078-85.
194. Pope LM, Reed KE, Payne SM. Increased protein secretion and adherence to HeLa cells by *Shigella* spp. following growth in the presence of bile salts. Infect Immun 1995;63(9):3642-8.
195. Johnson S, Roversi P, Espina M, Deane JE, Birket S, Picking WD, Blocker A, Picking WL, Lea SM. Expression, limited proteolysis and preliminary crystallographic analysis of IpaD, a component of the *Shigella flexneri* type III secretion system. Acta Crystallograph Sect F Struct Biol Cryst Commun 2006;62(Pt 9):865-8.
196. Barta ML, Guragain M, Adam P, Dickenson NE, Patil M, Geisbrecht BV, Picking WL, Picking WD. Identification of the bile salt binding site on IpaD from *Shigella flexneri* and the influence of ligand binding on IpaD structure. Proteins 2012;80(3):935-45.
197. Johnson S, Roversi P, Espina M, Olive A, Deane JE, Birket S, Field T, Picking WD, Blocker AJ, Galyov EE and others. Self-chaperoning of the Type III Secretion System Needle Tip Proteins IpaD and BipD. J Biol Chem 2007;282(6):4035-44.
198. Dickenson NE, Zhang L, Epler CR, Adam PR, Picking WL, Picking WD. Conformational Changes in IpaD from *Shigella flexneri* upon Binding Bile Salts Provide Insight into the Second Step of Type III Secretion. Biochemistry 2010.
199. Oaks EV, Picking WD, Picking WL. Antibody response of monkeys to invasion plasmid antigen D after infection with *Shigella spp*. Clin Diagn Lab Immunol 1996;3(2):242-5.
200. Collazo CM, Zierler MK, Galan JE. Functional analysis of the Salmonella typhimurium invasion genes invl and invJ and identification of a target of the protein secretion apparatus encoded in the inv locus. Mol Microbiol 1995;15(1):25-38.
201. Hayward RD, Hume PJ, McGhie EJ, Koronakis V. A Salmonella SipB-derived polypeptide blocks the 'trigger' mechanism of bacterial entry into eukaryotic cells. Mol Microbiol 2002;45(6):1715-27.
202. Sakai T, Sasakawa C, Makino S, Kamata K, Yoshikawa M. Molecular cloning of a genetic determinant for Congo red binding ability which is essential for the virulence of *Shigella* flexneri. Infect Immun 1986;51(2):476-82.
203. Geisbrecht BV, Bouyain S, Pop M. An optimized system for expression and purification of secreted bacterial proteins. Protein Expr Purif 2006;46(1):23-32.
204. Granier S, Kim S, Shafer AM, Ratnala VR, Fung JJ, Zare RN, Kobilka B. Structure and conformational changes in the C-terminal domain of the beta2-adrenoceptor: insights from fluorescence resonance energy transfer studies. J Biol Chem 2007;282(18):13895-905.

205. Stern O, Volmer M. On the quenching-time of fluorescence Physik. Zeitschr. 1919;20:183-188.

APPENDICES

Appendix A: Recipes

Buffers:

Agarose gel for DNA electrophoresis

25 ml 1X TAE
15 µl 6 mM Ethidium bromide
0.3 g agarose (electrophoresis grade)

1X TAE (running buffer for agarose gel electrophoresis)

4.84g Tris
1.142ml Glacial acetic acid
2ml 0.5 M EDTA
Q.S. to 1 L

Hydrophobic Interaction Chromatography (HIC) Buffer A

20 mM $NaPO_4$
1M ammonium sulfate
pH: 7.0

HIC Buffer B

20 mM $NaPO_4$
pH: 7.0

IMAC Binding Buffer

20 mM Tris-HCl
500 mM NaCl
5mM imidazole
pH: 7.9

IMAC Charge Buffer

50 mM $NiSO_4$

IMAC Elution Buffer

20 mM Tris-HCl
500 mM NaCl
400 mM imidazole
pH: 7.9

IMAC Strip Buffer

20 mM Tris-HCl
500 mM NaCl
100 mM EDTA
pH: 7.9

IMAC Wash Buffer

20 mM Tris-HCl
500 mM NaCl
60 mM imidazole
pH: 7.9

Phosphate-Buffered Saline (PBS)

130 mM NaCl
10 mM Na_2HPO_4
1.5 mM K_2HPO_4
3 mM KCl

12% SDS-PAGE Separating Gel (Sufficient for two gels)

3.00 ml diH20
2.50 ml 1.5 M Tris-HCl, pH 8.8
100 µl 10% (w/v) SDS
4.00 ml 29:1% (w/v) acrylamide:bisacrylamide
0.15 ml 10% (w/v) ammonium persulfate (APS)
10 µl N,N,N′,N′-Tetramethylethylenediamine (TEMED)

15% SDS-PAGE Separating Gel (Sufficient for two gels)

2.50 ml diH20
2.50 ml 1.5 M Tris-HCl, pH 8.8
100 µl 10% (w/v) SDS
5.00 ml 29:1% (w/v) acrylamide:bisacrylamide
0.15 ml 10% (w/v) APS
10 µl TEMED

5% SDS-PAGE Stacking Gel (Sufficient for two gels)

2.85 ml diH2O
1.25 ml 0.5 M Tris-HCl, pH 6.8
50.0 µl 10% (w/v) SDS
1.00 ml 29:1% (w/v) acrylamide:bisacrylamide
0.2ml 10% (w/v) APS
15µl TEMED

Maleimide-Labeling buffer:

To prepare proteins to be labeled with sulfhydryl-reactive dyes.

50 mM 4-(2-Hydroxyethyl)piperazine-1-ethanesulfonic acid (HEPES)
150 mM NaCl
5 mM Tris(2-carboxyethyl)phosphine hydrochloride (TCEP)
pH: 7.0

SDS-PAGE destain

5% (v/v) methanol
7.5% (v/v) glacial acetic acid

SDS-PAGE running buffer

2.42g Tris
14.41g glycine
1.0g SDS
Q.S. to 1 L

SDS-PAGE stain

0.1% (w/v) Coomassie Brilliant Blue R-250
5% (v/v) methanol
7.5% (v/v) glacial acetic acid

Solution A

8.0g NaCl
0.4g KCl
0.5g $NaHCO_3$
1.0g glucose
Q.S. to 1 L and filter sterilize.

<u>Media:</u>

20x NPS (1L):

(NPS = 100 mM PO_4, 25 mM SO_4, 50 mM NH_4, 100 mM Na, 50 mM K)
In a graduated cylinder, combine (in the below sequence) and stir until dissolved:
800 ml nanopure H_2O
66 g $(NH_4)_2SO_4$
136 g KH_2PO_4
142 g Na_2HPO_4
Q.S. to 1 L

Congo Red agar

37g Tryptic soy agar
0.03% Congo Red
Q.S. to 1 L

Luria-Bertani (LB) Broth

25.0 g LB broth (ready-made mix)
Q.S. to 1 L

LB Agar

37.0 g LB agar (ready-made mix)
Q.S. to 1 L

Dulbecco's Modified Eagle Medium (DMEM)

9.53g DMEM
2.2g $NaHCO_3$
Q.S. to 1 L and filter sterilize

DMEM plus Calf Serum (CS)

9.53g DMEM
2.2g $NaHCO_3$
100ml calf serum
Q.S. to 1 L and filter sterilize

DMEM plus CS plus Gentamycin

9.53g DMEM
2.2g $NaHCO_3$
100ml calf serum
50mg gentamycin
Q.S. to 1 L and filter sterilize

DMEM plus Glucose

9.53g DMEM
2.2g $NaHCO_3$
4.5g glucose
Q.S. to 1 L and filter sterilize

Minimal Medium:

This bacterial growth medium provides a non-inducing, lactose-free environment and is excellent for starter (10 ml) cultures for protein expression.

9.25 ml sterile H_2O
20 µl 1 M $MgSO_4$
125 µl 40% glucose
100 µl 25% aspartate
500 µl 20x NPS

Terrific broth (TB):

To prepare 1L of TB, combine 900 ml of tryptone-yeast (Component A) with 100 ml of TB salts (Component B). Components A and B must be prepared and sterilized separately. If combined prior to autoclave sterilization, the salts will precipitate.

<u>Component A (tryptone-yeast):</u>

12 g Tryptone
24 g Yeast extract
4 ml Glycerol
900 ml nanopure H_2O

<u>Component B (TB Salts):</u>

Combine the following in ~600 ml of nanopure H_2O:
125.41 g K_2HPO_4
23.12 g KH_2PO_4

Q.S. to 1 L

Tryptic Soy Agar (TSA)
37g TSA (ready-made mix)
Q.S. to 1 L

Tryptic Soy Broth (TSB)
25g TSB (ready-made mix)
Q.S. to 1 L

Other:

Liposomes:
66.5 mol% DOPC, 23.5 mol % DOPG, 10 mol% CHOL

Lipid	1x	2x	4x
DOPC	36.6 µl	73.2 µl	146.4 µl
DOPG	13.12 µl	26.24 µl	52.5 µl
Cholesterol	2.71 µl	5.42 µl	10.84 µl

Resuspension volumes (final lipid concentration = 8.735 mg/ml):
1x: 150 µl
2x: 300 µl
4x: 600 µl

Notes:

- All lipids, except for cholesterol (see below), were purchased from Avanti Polar Lipids (Alabaster, AL) as 25 mg/ml chloroform preparations.
- Cholesterol was purchased from Sigma-Aldrich.
- Upon receipt, lipids were removed from glass ampoules, aliquoted into 2 ml amber glass vials with screw-top Teflon-lined lids and stored at -20° C.
- 1x lipid films were used for making SRB-filled liposomes.
- 2x and 4x films were prepared when large volumes of liposomes were needed, such as for the quenching experiments in Chapter II or liposome flotation assays.

Protease Inhibitor

- Dissolve 4-(2-Aminoethyl)-benzenesulfonylfluoride hydrochloride (AEBSF) in nanopure water at a concentration of 100 mM.
- Store 200 µl aliquots at -20° C.
- AEBSF aliquots were thawed immediately prior to use at room temperature. It is not advisable to thaw AEBSF at higher temperatures, because AEBSF's t1/2 decreases steeply with increasing temperature.

Appendix B: Primer Sequences

To make C19S – Use BsrGI
B75f – GAG AGA GAG TGT ACA GAG CTT GGA GCA AAT ACT
B76r- GAG AGA GAG TGT ACA AGT CAA TAT TTT GGC AAG AG

To make S58C– Use BsrGI
B77f - GAG AGA GAG TGT ACA TCA AAT ATA TTA ATC CCT GAA
B78r - GAG AGA GAG TGT ACA GTG TGC ATT AGT TGT ATT AAT

To make S107C – Use BssHII
B79f – GAG AGA GAG GCG CGC CAG CAA AAA AAC CTA GAA TT
B80r - GAG AGA GAG GCG CGC CTG TTG CTG GCA CTT CCA AGC AGT AAT TTT A

To make S149C – Use AflII
B81f – GAG AGA GAG CTT AAG AAC GCA GAT TGT AAA ATA AAA GAC CTA GAA AAT
B82r – GAG AGA GAG CTT AAG TTT ATT AAT TTG TTT TTC ATA GT

To make S237C – Use BsrGI
B83f – GAG AGA GAG TGT ACA CAG CAG AAA TCA TTA AC
B84r – GAG AGA GAG TGT ACA TAG CTG TTC AGC AGA TG

To make A254C- Use BsrGI
B85f – GAG AGA GAG TGT ACA TTT ATT CAA CTA GTT GGA
B86r – GAG AGA GAG TGT ACA CAT CAA TTG AGT AAC ACT G

To make A353C- Use BsrGI
B87f – GAG AGA GAG TGT ACA GGC AAT TCC TTC ATG GA
B88r – GAG AGA GAG TGT ACA TGC TTG TAC TAT AGC ATC

To make A420C- Use BsrGI
B89f – GAG AGA GAG TGT ACA GTT GGT AAA CAG GCA G
B90r – GAG AGA GAG TGT ACA TAC GAG AAC GAC TGC TG

To make S486C- Use BsrGI
B91f – GAG AGA GAG TGT ACA CAT TTA AAC CAA GCA GT
B92r – GAG AGA GAG TGT ACA AAT AAT TTG TTT GGA TAT TAC T

To make A502C- Use BsrGI
B93f – GAG AGA GAG TGT ACA CAA GCG GGA GGA AGT
B94r – GAG AGA GAG TGT ACA AGA GTT AAC ACT TTC TCC T

To make S520C- Use BsrGI
B95f – GAG AGA GAG TGT ACA AAT CTA GCA GAC CTG AC
B96r – GAG AGA GAG TGT ACA CGC GCT GTT CTG GAA A

Primers used to insert TEV sites. The underlined bases indicate the sequence encoding the TEV site.

To insert a TEV site prior to residue 58.

B302F- PO4 TAT TTC CAA GGA TCA ACT TCA AAT ATA TTA ATC
B303R- PO4 AAG ATT TTC GAG TGC ATT AGT TGT ATT AA

To insert a TEV site prior to residue 82. **Bold T** in B304F's TEV site is a silent mutation in the wobble position to reduce hairpin

B304F- PO4 TAT TT**T** CAA GGA TTA ATT GGA AAC CTT ATT CAA A
B305R- PO4 AAG ATT TTC AAG CGT TAG TTG GGA ACT T

To insert a TEV site prior to residue 190. Note: the **bold T** in B306F is a substitution for C in the wobble position to reduce hairpin.

B306F- PO4 TAT TTC CAA GGA GA**T** GCA GCA GTT AAA GAC
B307R- PO4 AAG ATT TTC TTT TTT GAT AGT GAG TTG TAT T

To insert a TEV site prior to residue 220.

B308F- PO4 TAT TTC CAA GGA GAA ATA GAC TCT TTT TCT GCA
B309R- PO4 AAG ATT TTC TTT TTC GAG TTG CAT TGA TTT

To insert a TEV site prior to residue 312: Note: the **bold bases** in B310F and B313R are substitutions in the wobble position to reduce hairpin.

B310F- PO4 TAT TT**T** CA**G** GGA ATA CTT GGG GCA CTT TTA A (52°)
B311R- PO4 AAG ATT TTC TTT CCC AAC ACA ACC CAT T (54°)

To insert a TEV site prior to residue 495:

B312F- PO4 TAT TTC CAA GGA GGA GAA AGT GTT AAC TCT G (54°)
B313R- PO4 AAG ATT TTC TAA TAA AAC TGC TTG GT**A** TAA A (54°)
To make IpaB 11-312:

B314F- GAG AGA GAG CAT ATG TTT CCT CTT GCC AAA ATA TT
Use B293R for reverse.

To make IpaB 11-357:

Use B314F for forward.
B315R- GAG AGA GAG GGA TCC TCA GGA ATT GCC GGT CGC T

To make IpaB 11-390:

Use B314F for forward.
B316R- GAG AGA GAG GGA TCC TCA GCC CAA GCC TTC GAG CA

To make IpaB 11-495:

Use B314F and B292R

VITA

Philip Robert Adam

Candidate for the Degree of

Doctor of Philosophy

Thesis: INVESTIGATION OF THE PROTEIN-PROTEIN AND PROTEIN-LIPID INTERACTIONS OF IPAB FROM *SHIGELLA FLEXNERI*

Major Field: Microbiology and Molecular Genetics

Biographical:

Education:

Completed the requirements for the Doctor of Philosophy in Microbiology and Molecular Genetics at Oklahoma State University, Stillwater, Oklahoma in May, 2014.

Completed the requirements for the Bachelor of Science in Microbiology at University of Kansas, Lawrence, KS in May, 2009.

Experience and Selected Awards:

Five accepted peer-reviewed manuscripts (two first-author)
Thirteen awards for excellence in research, presentation, or academics
Six presentations at national professional meetings
Fourteen presentations at regional/local professional meetings

Graduate Research Assistant at Oklahoma State University 2009-2014
Grula Distinguished Graduate Fellowship, 2013

Undergraduate Research Assistant at University of Kansas 2007-2009
Del and Carol Shankel Biomedical Scholarship, 2008
Lance S. Foster Outstanding Junior in Biology Award, 2008
K-INBRE Summer Scholar, State of Kansas, 2008

Professional Memberships:

American Society for Microbiology
American Society for Microbiology Missouri Valley Branch